CALIFORNIA STATE POLYTECHNIC UNIVERSITY, POMONA
THESIS ELECTRONIC SIGNATURE PAGE

Submitted: Term Summer   Year 2021
Bronco ID: 010612719
Email Address: bjhouse@cpp.edu

THESIS INFORMATION

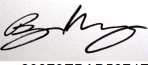|	
THESIS TITLE	Stratigraphic Investigation and Provenance Interpretations of the mid-Tertiary
AUTHOR	Brianna House
PROGRAM	Geology, M.S.

SIGNATURES

Bryan P. Murray
_____
Committee Chair Name
Thesis Committee Chair
_____
Position
Geology
_____
Department

_____
Organization

DocuSigned by:
20873EBAB5874F6...   8/18/2021
_____
Signature
bpmurray@cpp.edu
_____
Email

Jonathan A. Nourse
_____
Committee Member 2 Name
Committee Chair Member
_____
Position
Geology
_____
Department

_____
Organization

DocuSigned by:
Jonathan A. Nourse
562E96F6E80E44B...   8/18/2021
_____
Signature
janourse@cpp.edu
_____
Email

Jeff Marshall
_____
Committee Member 3 Name
Committee Chair Member
_____
Position
Geology
_____
Department

_____
Organization

DocuSigned by:
Jeff Marshall
5CA674BC5B574FA...   8/18/2021
_____
Signature
marshall@cpp.edu
_____
Email

Upload Thesis Attachment:

Revised August 2020,
Graduate Studies Office

STRATIGRAPHIC INVESTIGATION AND PROVENANCE

INTERPRETATIONS OF THE MID-TERTIARY SOLEDAD ROJO

FORMATION IN THE SOUTHERN BASIN AND RANGE PROVINCE,

WESTERN PALO VERDE MOUNTAINS, SOUTHEASTERN CALIFORNIA

A Thesis

Presented to the

Faculty of

California State Polytechnic University, Pomona

In Partial Fulfillment

of the requirements for the degree

Master of Science

In

Geology

By

Brianna House

2021

SIGNATURE PAGE

THESIS:

STRATIGRAPHIC INVESTIGATIONS AND PROVENANCE INTERPRETATIONS OF THE MID-TERTIARYSOLEDAD ROJO FORMATION IN THE BASINAND RANGE PROVINCE, WESTERN PALO VERDE MOUNTAINS, SOUTHEASTERN CALIFORNIA

AUTHOR:

Brianna J. House

DATE SUBMITTED:

Summer 2021

Department of Geological Sciences

Dr. Bryan P. Murray
Thesis Committee Chair
Geological Sciences

_____

Dr. Jonathon Nourse
Geological Sciences

_____

Dr. Jeff Marshall
Geological Sciences

_____

ACKNOWLEDGMENTS

ABSTRACT

New stratigraphic and paleocurrent data from the Soledad Rojo formation, a red conglomeratic sandstone unit in the western Palo Verde Mountains of southeastern California, illustrate the evolution of a basin that was formed during mid-Tertiary crustal extension. The Soledad Rojo formation is subdivided into three distinct lithofacies: (1) Unit R, the lower unit of alluvial fan deposits that include trough cross bedding, varying colored red beds with coarse grained granule/pebble conglomeratic lithic arkose sandstones interbedded with matrix- and clast-supported, moderately to poorly sorted cobble conglomerates with subangular-subrounded metaplutonic and volcanic clasts; (2) the middle unit, Unit BT, is a fluvial cobble-boulder conglomerate that is buff colored, clast-supported, and imbricated with rounded to subrounded, moderately well sorted metaplutonic clasts; and (3) Unit L, the upper unit of alluvial fan deposits that is composed of light gray to tan colored conglomeratic lithic arkose with interbedded clast-supported pebble conglomerate containing subangular to subrounded metaplutonic and volcanic clasts. Each subunit showcases variable lithofacies and clast compositions that display changes in sediment provenance and depositional environments during the history of the basin formation. Preliminary stratigraphic and structural interpretations infer that deposition occurred in a synextensional basin of a moderate energy alluvial/fluvial system derived from nearby sediment sources, such as the Black Hills and Palo Verde Mountains. Provenance interpretations of the conglomerates and sandstones within the Soledad Rojo formation are supported by clast count data, thin section point-counting and hand sample textural and compositional analyses, all of which suggest a relatively short

distance of sediment transportation after erosion from the local mountainous regions that consist of rocks with volcanic and metaplutonic compositions.

Paleocurrent analysis further suggests that the Soledad Rojo formation was derived from local exposures, with individual clast imbrications suggesting SE-and NE-directed paleo-flow directions, inferring the majority of the sediment source is generally to the northwest and southwest. Although the timing and deposition of the three subunits in the Soledad Rojo formation is difficult to constrain, recent ^{40}Ar/^{39}Ar and U-Pb detrital zircon geochronological dating in the basin indicates rock fragments within the red-bed unit were deposited during the late Oligocene to early Miocene (ca. 23.5 to 25 Ma) age for the Soledad Rojo formation.

TABLE OF CONTENTS

LIST OF TABLES

LIST OF FIGURES

CHAPTER 1: Introduction

The Soledad Rojo formation, an informal name proposed by Elliot and Marshall (2011), is a red conglomeratic sandstone unit located between the Black Hills and Palo Verde Mountains of southeastern California (Figures 1 and 2). This study area is located within the southern Basin and Range Province of western North America, where regional extensional deformation and magmatism occurred during the late Oligocene to early Miocene from approximately 28 Ma to 14 million years ago (Irwin 1991) (Figure 1). Preliminary work by Murray and Al-kaabi (Murray 2018 and Al-kaabi 2021) subdivided the Soledad Rojo formation into three distinct subunits, each containing variances in lithofacies and clast compositions that suggested possible changes in sediment provenance and depositional environments during the development of the basin. This previous research suggested that the northeast-striking, moderately east dipping unit was deposited in the late Oligocene to early Miocene (ca. 24 Ma) during regional mid-Tertiary extension in a proximal-medial alluvial fan/braided fluvial system that formed in a normal fault-bounded basin (Figure 3) (Murray et al, 2019).

Although this study site is located within the Palo Verde Mining District, an area of Imperial County known for barite prospecting, and near the well-known Hauser Geode Beds to the north-east, the depositional history, provenance, and tectonic setting of the Soledad Rojo formation basin are poorly understood. In addition, this study area is also proposed to be adjacent to the path of the ancestral Colorado River (Sherrod and Tosdal, 1991), but the influence of this river system on the deposition of the Soledad Rojo formation is unknown.

The focus of this research project is to investigate the textural and compositional characteristics of the Soledad Rojo formation basin to determine the depositional processes, sedimentary environments, and provenance source rock of the three distinct subunits. To better understand this isolated basin within lower Basin and Range, questions regarding depositional history included: (1) What are the paleoflow directions of sediment drainage into the Soledad Rojo formation? (2) Are there changes in paleoflow direction in the basin that suggest multiple sources? (3) Can the sediment sources of the Soledad Rojo formation be identified as local or distal? (4) How do paleoflow directions, sediment sources and tectonics affect the distribution of lithofacies in the basin? and (5) How does the Soledad Rojo formation relate to the underlying and overlying rocks? Two stratigraphic columns, one each covering an edge of the basin, were constructed to illustrate a sedimentary log record of the basin to represent the average grain size and clast type of the conglomeratic sandstone units. In addition, a generalized paleoflow direction for deposition from paleocurrent clast imbrication measurements were taken throughout. Most sediment deposits from within the Soledad Rojo formation are interpreted to have been derived from either local mountain ranges or from distal sources. Based on the sedimentological research, this study proposes the Soledad Rojo formation was formed in alternating alluvial and fluvial debris flow events. The clast information provided aids in the identification of the sediments entering the basin from all directions.
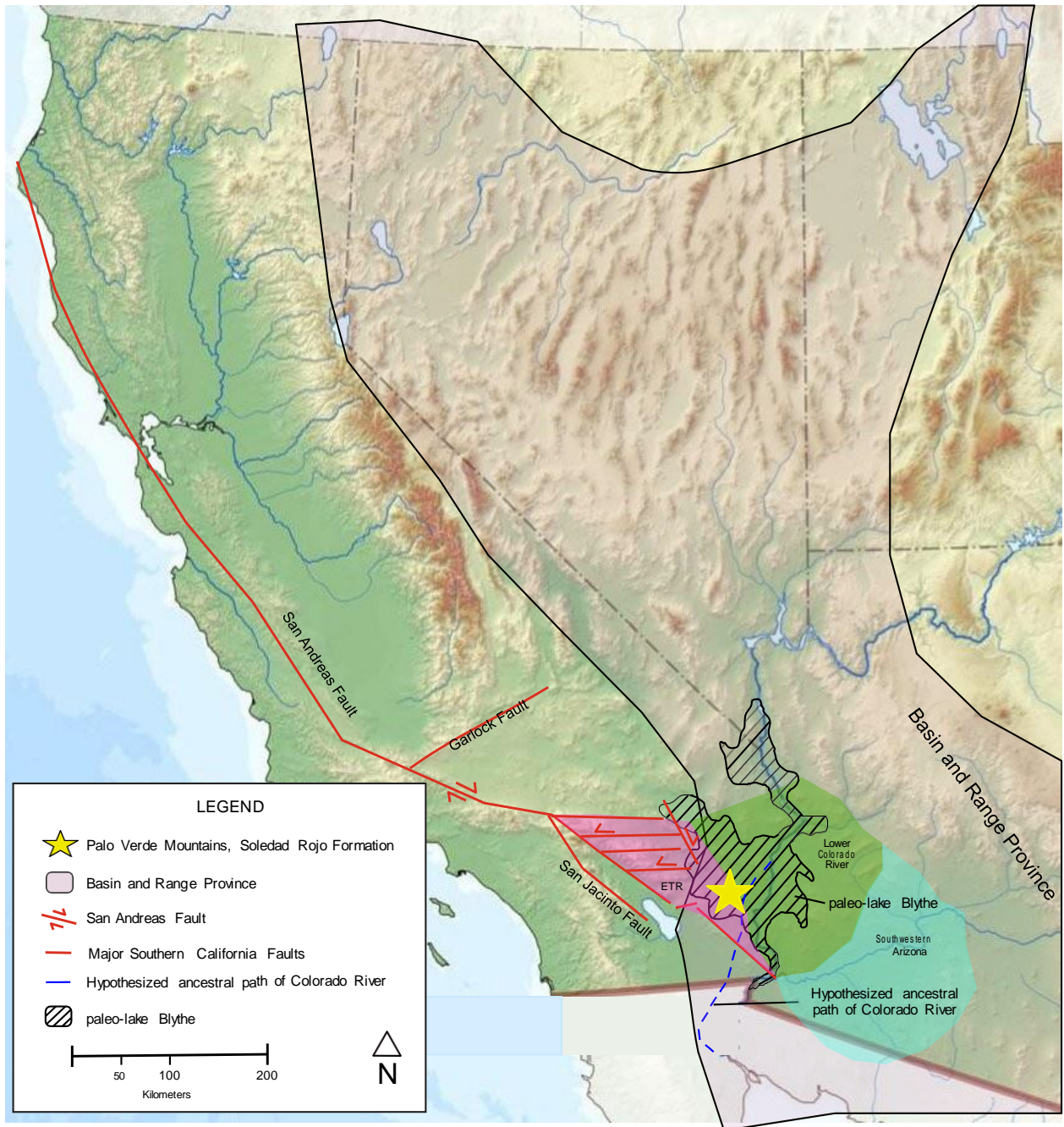
Figure 1. Location of Palo Verde Mountains in southeast California (yellow star) within the Basin and Range (light pink overlay). Three zones of the Basin and Range include the Lower Colorado River (green overlay), Southwestern Arizona (blue overlay) and the Eastern Transverse Ranges (dark pink overlay). The location of major transform faults, including the San Andreas Fault, Garlock Fault, and San Jacinto Fault, are indicated by red lines. The location of the hypothesized ancestral path of the Colorado River, shown in a dotted blue line, compared to the current path of the Colorado River is shown. (modified from Sherrod and Tosdal, 1991). The location of the Blythe paleo-lake that flooded the Lower Colorado River into the location of the Soledad rojo formation is indicated by striped overlay (after House et al. (2008). The Eastern Transverse Ranges (dark pink overlay) is a location that experienced clockwise transrotation such that potential sources SW of the San Andreas Fault restores farther southeast (after Bennet, 2016 and Langenheim, 2009)

3
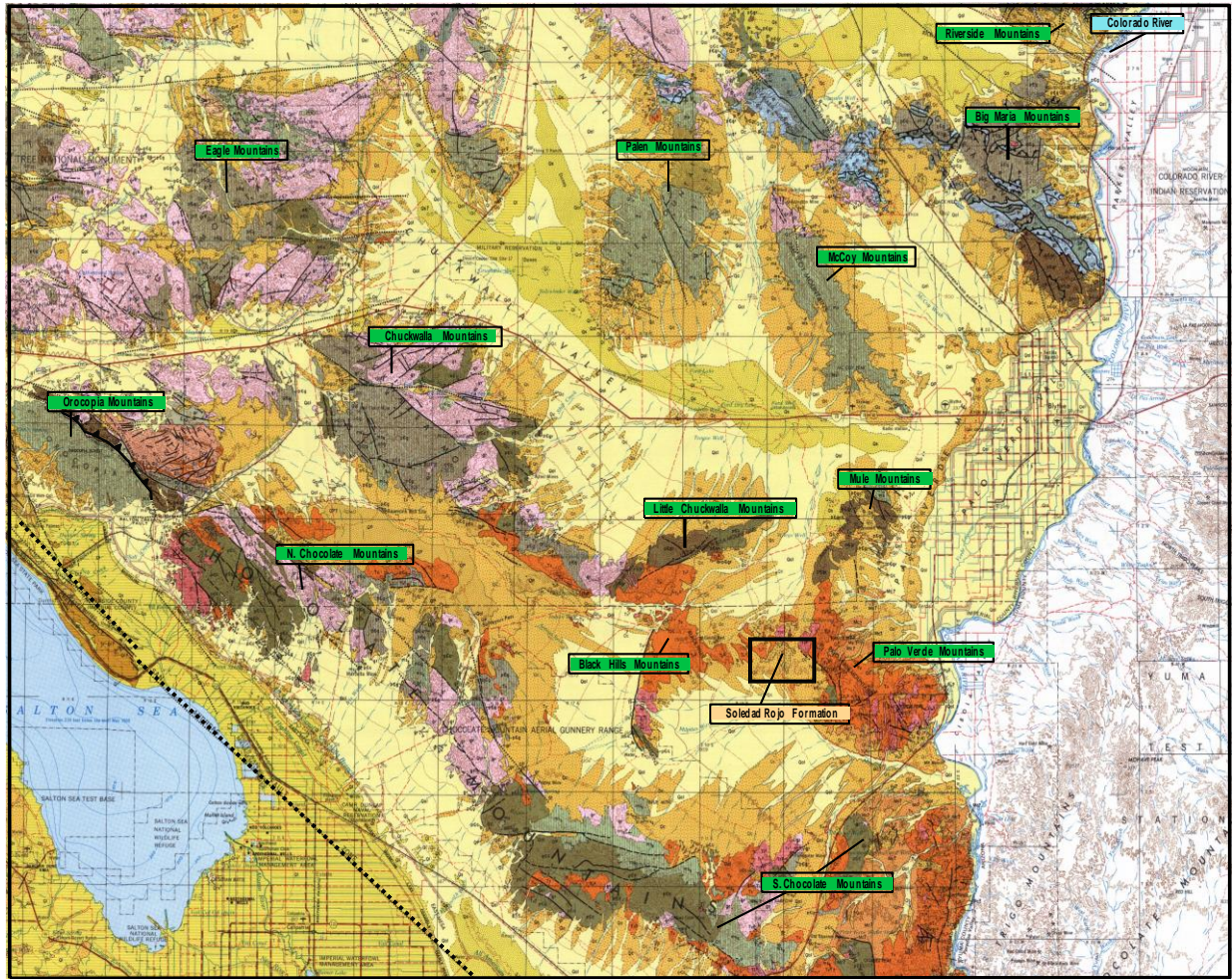
Figure 2. Geologic map of the research site in southeastern California (black box, orange label). Surrounding mountain ranges are labeled in green. (after Jennings, (1967).

Legend

Qal	Alluvium	....	San Andreas Fault
Qc	Pleistocene Nonmarine	▲▲▲	Orocopia Thrust
QP	Plio-Pleistocene Nonmarine	▭	Soledad Rojo Formation location
Mc	Undivided Miocene Nonmarine		
Tv	Tertiary Volcanics		N ▲
Ti	Tertiary Intrusive		
Tc	Tertiary Nonmarine		
pCc	Precambrian Igneous and Metamorphic Complex		
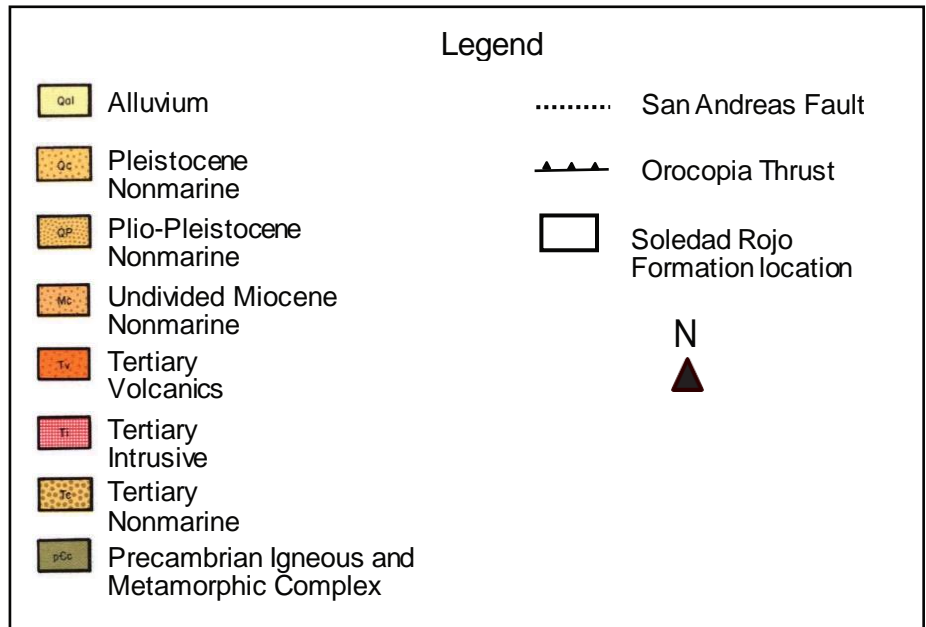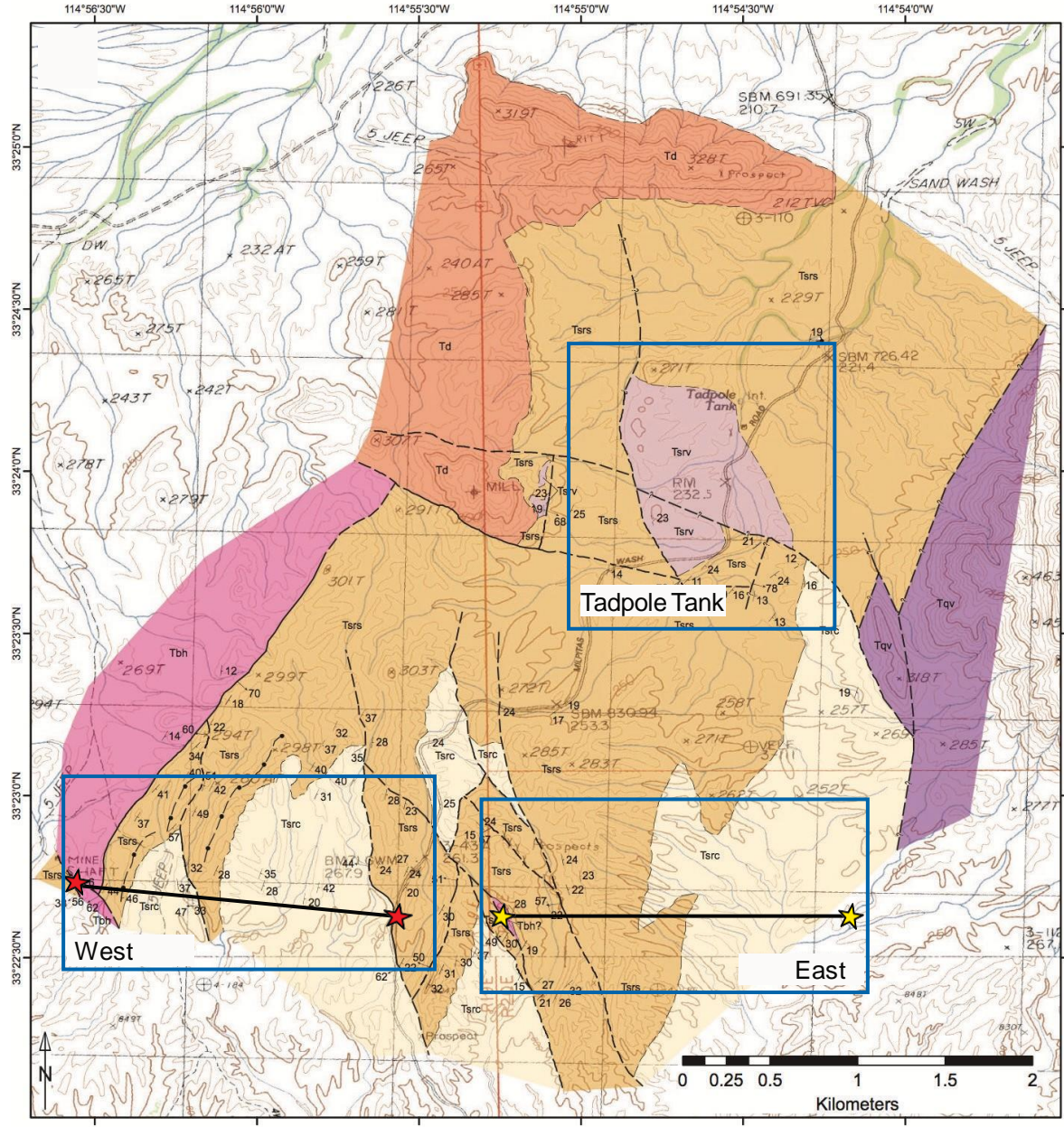
Figure 3. Geologic map of Soledad Rojo formation showing the new research locations that include the Western stratigraphic column, Eastern stratigraphic column and Tadpole Tank, all boxed in blue.(after Murray and Al- kaabi, 2018)

Legend

Td	"Mill" dacitic intrusion (late Oligocene -early Miocene)
Tsrc	Upper Soledad Rojo fm., light gray conglomerate/sandstone
Tsrs	Lower/mid Soledad Rojo fm., orange-red sandstone/conglomerate
Tsrv	Basal Soledad Rojo fm., mafic lava & silicic tuff
Tbh	Tuff of Black Hills & underlying volcanic rocks (late Oligocene)
Tqv	Quechan Volcanics (late Oligocene)
——	Fault (certain)
– –	Fault (approximately located)

N

CHAPTER 2: Geologic Setting

The Palo Verde Mountains are located adjacent to the Colorado River in southeastern California, within the southern Basin and Range Province of the western North America (Figures 1 and 2). This area is at a transitional zone between the tectonic regimes of the strike-slip motions of the San Andreas Fault, which encompasses the majority of southern California, and the extensional tectonics of the Basin and Range Province (Figure 1). In the late Tertiary (Neogene Period), approximately 20 million years ago, this region on the margin of southwestern North America was in the process of changing from a subduction margin to a transform margin which promoted tectonic extension, subsidence, and infilling of the basins during the late Oligocene and Quaternary periods (Brown, 1991, Bennett et al., 2016. Faulds, 2001). Prior to extension, the early Tertiary (Paleogene Period), was a time of tectonic inactivity with gradual erosion of the former Cordilleran thrust belt locally (Irwin, 1991, Faulds, 2001).

The timing of extension in the southern Basin and Range varies from 28 Ma to 14 Ma, with the age of extension generally migrating from the southwest to the northwest of the southwestern United States. During that time period, volcanism consisting of ignimbrite flare ups and uplifted metamorphic core complexes migrated through what is now southeastern California. Extension, more specifically in the southern Basin and Range Province, was dominated by the formation of large-offset normal faults that formed the metamorphic core complexes found today regionally (McQuarrie and Wernicke, 2005). Armstrong and Ward (1991) suggests volcanism in the region is anticipated to have overlapped with extension in time but likely peaked slightly earlier than the highest rates of extension, suggesting thermal softening of the lithosphere pior

might have initiated the onset of rapid core-complex extension when magmatism effectively burnt the bridge (the post-Laramide magmatic gap) which bonded the Cordillera to North America (Armstrong and Ward (1991). As the extension moved north, as did the magmatism throughout the entire Basin and Range (Faulds, 2001).

This region of the Basin and Range province is a meeting point between three zones of the Basin and Range: The Lower Colorado River portion, the Eastern TransverseRanges and the Southwestern Arizona portion (Figure 1) (Bennett et al., 2016, Langenheim et al., 2009). The Palo Verde Mountains and Soledad Rojo formation are south of the Eastern Transverse Ranges, which have exposed igneous and metamorphic crystalline basement rocks. The Eastern Transverse Ranges crustal block was rotated clockwise in response to dextral shear and transrotation within the San Andreas Fault zones (Langenheim, 2009), later identified to be similar to those in the San Gabriel Mountains to the northeast. North of the Eastern Transverse Ranges, the Eastern California Shear Zone dominates the Mojave tectonic regimes (Figure 1), leading to basins south of the shear zone to later being filled with Pliocene and Quaternary deposits after transtensional and northwest transrotational deformation occurred along the San Andreas Fault (Bennett et al, 2016). It has been proposed that as volcanism peaked during extension, this led to thick volcanic sections accumulating in many of the half-grabens until calming during the late Miocene, allowing for thick sections of alluvial fans to be accumulated in large basins around 6 Ma (Faulds, 2001).

The Soledad Rojo formation contains a variety of volcanic and meta-plutonic rocks consisting of, but not limited to: tuffs, granites, muscovite schists, as well as biotite and augen rich gneisses (Figure 2). Seismic reflection profiles, interpreted by Morris

(1993), observations suggest that the basins in this region are characterized to have high-angle normal faults forming half-graben tilted blocks with changing dips throughout, indicating progressive growth-fault deformation of the basin units (Figure 4a). These strong reflective layers are separated by transparent seismic areas, thus leading to Tertiary filling of basins with sedimentary and volcanic rocks similar to the surrounding mountains of the Milpitas wash (Morris, 1993) (Figure 4a). Preliminary work by Murray (2019) suggests that the northeast-striking, moderately east dipping Soledad Rojo formation was deposited in the late Oligocene to early Miocene (ca. 24 Ma) (Figure 3). The Oligocene volcanic Black Hills Tuff bounds the western basin of the Milpitas Wash Road with a northeast striking, steep southeast dipping normal fault, hypothesized to be a faulted unconformity. On the eastern edge of the Soledad Rojo formation, east of Milpitas Wash Road, the late Oligocene - Miocene metaplutonic Palo Verde Mountains bounds the formation with a poorly exposed northeast striking, northwest dipping normal fault. The tectonic observations completed by Murray (2019), confirming with Morris (1993), shows evidence of a half graben tectonic framework, with both normal faulted mountains bounding the basin displaying uplifted footwall tectonics, with the Soledad Rojo formation displaying subsidence hangingwall tectonics overall (Figure 4b).

Research of the drainage basin in the Palo Verde Mountains notes that prior to 6 million years ago, a paleo-lake existed in what is now Blythe and may have contributed to the spillover drainage in this area millions of years after deposition of the Soledad Rojo formation occurred (Sherrod and Tosdal, 1991, Bennett et al., 2016). This possibility serves as subtle importance, as the research from this paper and field site locations are directly split between the Milpitas Wash Road, which runs north-south dividing the study area, and the resulting stratigraphic columns created run west-east of this wash. Reconstructions of the area confirms the Palo Verde Mountains moved northwesterly from tectonic movements in the last 11 Ma after deposition of the Soledad Rojo, leading to the possibility of river drainage and sediment transportation into the basin due to the subsidence (Bennett et al., 2016).
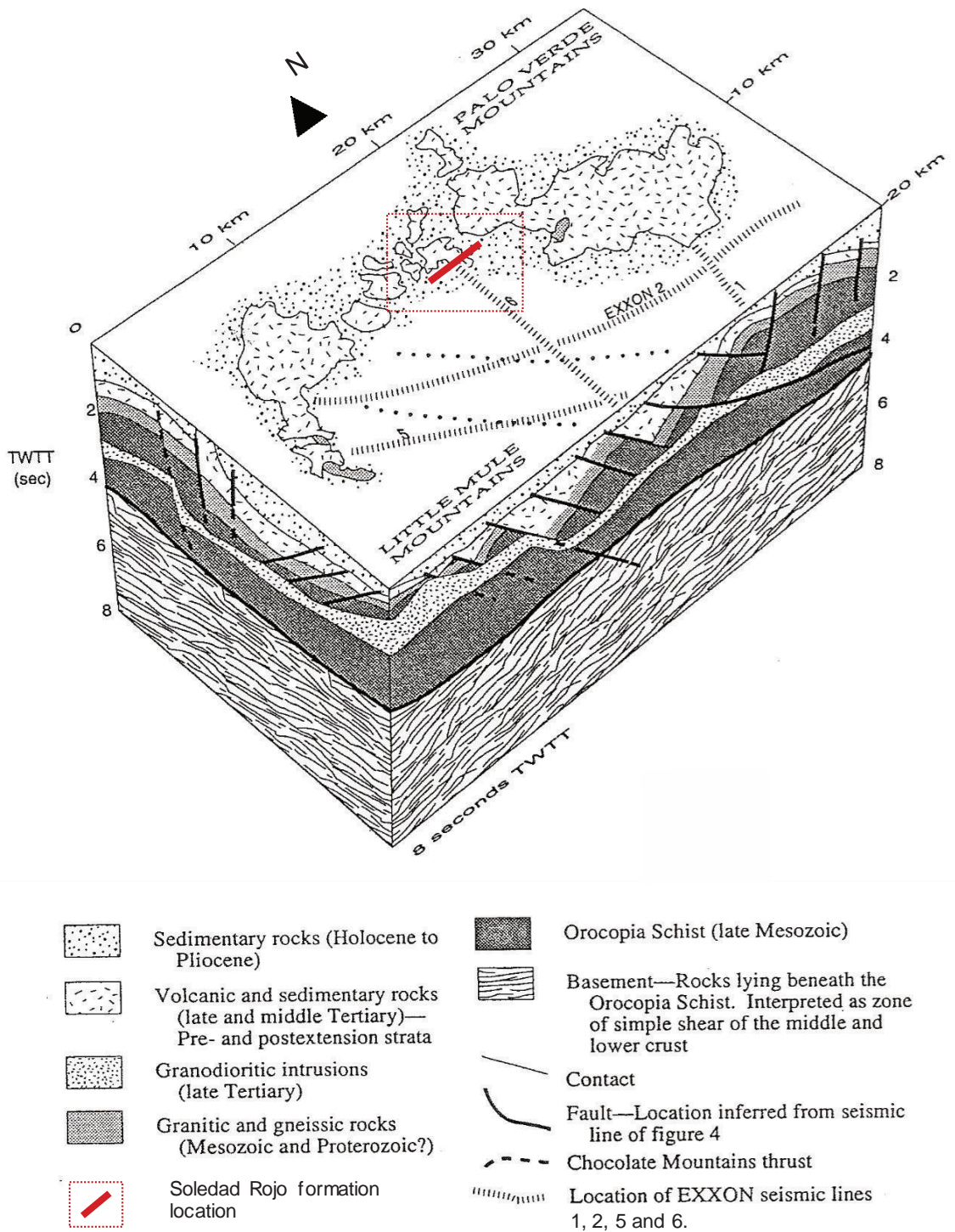
Figure 4a. Seismic 3-dimensional interpretive profile displaying half-graben tilted block geometry of the basin between Palo Verde Mountains and Little Mule Mountains. Location of Soledad Rojo fm. research site and stratigraphic columns intersect at the top of seismic profile 6, and run in the same general direction of seismic profile 2 heading east, boxed in red. Stratigraphic columns trending west to east highlighted with the red line. (after from Morris, 1993).
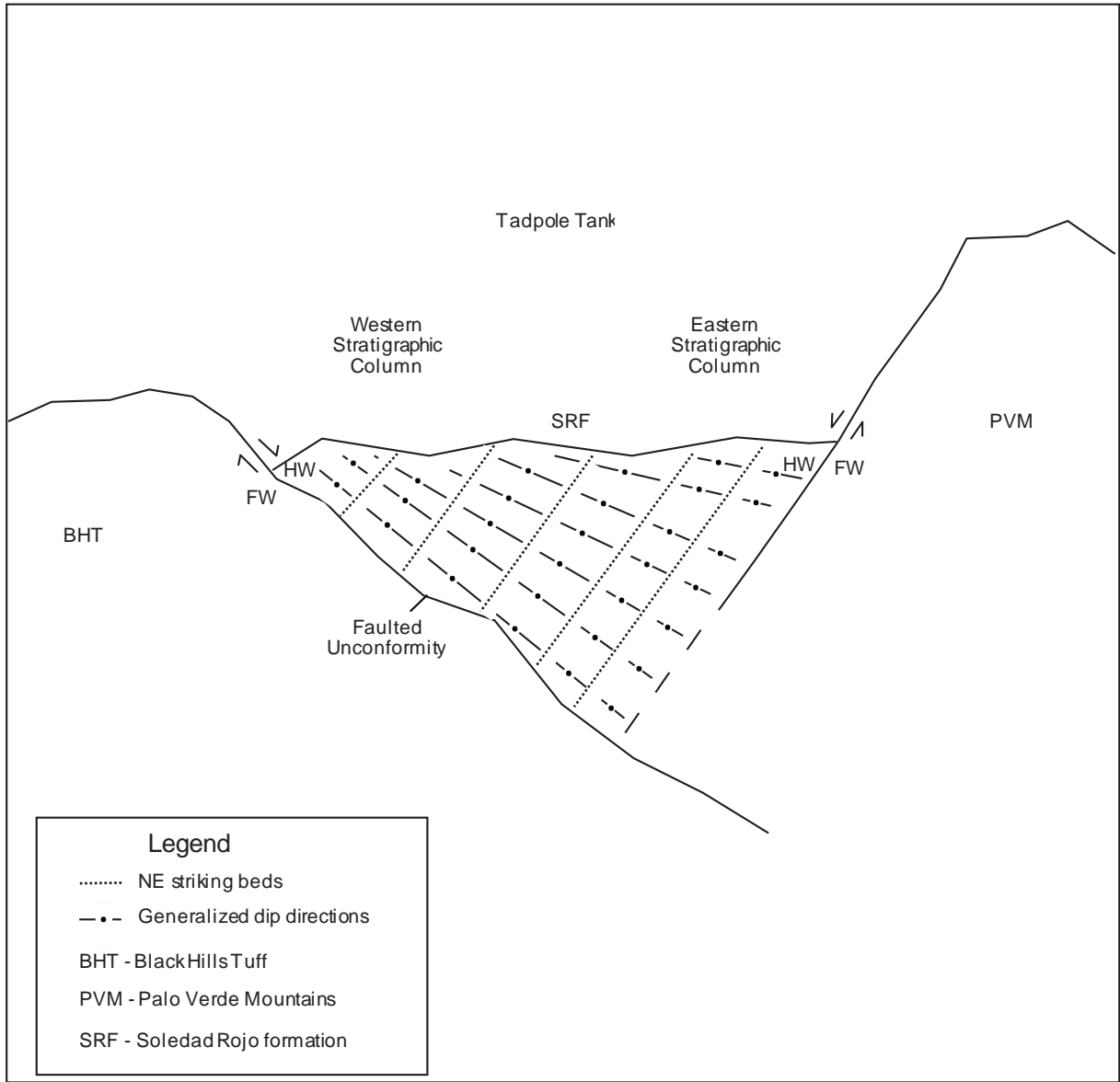
Figure 4b. Generalized schematic drawing of tectonic framework of the Soledad Rojo fm basin. Normal faults bounding each side of the Soledad Rojo formation, or SRF, by the Black Hills Tuff, referenced as BHT, and Palo Verde Mountains, referenced as PVM. Tectonically, the BHT is the acting footwall, FW, and the SRF is the hanging wall (HW), as well as the PVM also acting as the FW, leading the SRF becoming a half-graben basin. The faulted unconformity on the western stratigraphic side of SRF infers a southeast provenance, as well as steeper dips overall in the west by the BHT and becoming more shallow heading east towards PVM on the eastern stratigraphic column, shown in striped lines. Generalized NE strikes of SRF shown in lines. Tadpole Tank is located to the north approximately 5km into the page.

CHAPTER 3: Methods

A provenance analysis was conducted for this research by using conglomerate clast counts, paleocurrent indicators and sandstone modal compositions collectively. Two stratigraphic columns measured in the Soledad Rojo formation for this study provided the basis for the following descriptions of sedimentary lithofacies and interpretations of depositional processes (Figure 5 and Figure 7). The two stratigraphic sections were measured in different parts of the study area to examine any spatial variations within the basin: one column west and east sides of Milpitas Wash Road in the south and also an analysis at Tadpole Tank in the north (Figure 3, Figure 5). Using a Brunton compass and a Jacob's Staff, the stratigraphic columns were made to measure the bed thickness by placing the staff along the bed plane at the base of the beds wanting to measure, aligned at a right angle with the bedding and sighted down-dip perpendicular to strike of the beds (Appendix C.28). As shown in Figure 5, mapping of the basin led to the rough division between the various subunits along both stratigraphic columns and were distinguished while in the field on a geologic map (Table 1). Bedding boundaries and lithological subdivisions were based on color and clast size variances. Previous mapping completed through Cal Poly Pomona (Murray et al., 2018) (Figure 3) verified multiple normal faults that run through the study area and were used for this study.

A variety of sedimentological parameters were investigated while measuring these sections to interpret how the lithologic subunits of the formation were deposited and where the sediment originated from, which collectively included 22 clast counts stations, 220 paleocurrent measurements and 17 hand sample descriptions; in addition,

point counting analyses were performed on three sandstone thin sections from the Tadpole Tank region (Figure 5, Figure 6).

The Western stratigraphic column (Figures 5-7), starts ~ 1 km west of Milpitas Wash Road and runs east towards the road, runs ~380 meters east towards Milpitas Wash Road showcasing gently rolling hills topography cutting through stream washes and climbing outcrop peaks. The Eastern Stratigraphic Column (Figure 5-7), starts ~0.5 km east of Milpitas Wash Road at an underlying pink ignimbrite and continues east towards the Palo Verde Mountains. The eastern stratigraphic column runs ~390 meters east towards the Palo Verde mountains and showcases a subtle, rolling hills topography that cuts through drainage washes and former mining prospect locations. The Tadpole Tank region (Figure 5) is not directly included in the western and eastern stratigraphic columns, but is the location of a small slot canyon carved into the Soledad Rojo formation that displays excellent stratigraphic features along the canyon walls (Figure 11e). The Tadpole Tank region in the Soledad Rojo formation is a highly active site for water collection and fluvial flow processes during heavy rain and flash flooding events. On multiple research attempts, access into the Tadpole Tank canyon was not accessible, with heavy water discharge from seasonal rains creating ephemeral pools.

Paleocurrent measurements from individual imbricated clasts, as well as imbricated clasts that were grouped adjacently, were taken concurrently with the conglomerate clast counts to determine paleoflow directions from alluvial/fluvial processes that occurred throughout the basin during deposition (Figures 12-16). For each clast count, an average of 20 strike and dip measurements of imbricated clasts were taken using a Brunton compass (Tables 8-12). To determine paleoflow directions, the strike and

dip planar measurements of the imbricated clasts were input into Stereonet 11

(Allmendinger et al., 2012; Cardozo and Allmendinger, 2012) that were then converted

using the program into their corresponding poles to bedding plans; since imbricated clasts

dip upstream, the trend of the pole to plane was used to determine the direction of

paleoflow for each clast. Further rotation of the poles using Stereonet 11 was to correct

tectonic tilt and to restore all data to original horizontality. Rose diagrams and mean

vector directions for the imbrications were also calculated using Stereonet 11 to provide

the average paleoflow direction for each clast count. Results of the paleocurrent analysis

are presented in the corresponding sections below, with details of individual clast

imbrication measurements provided in Appendix A.

Conglomerate clast counts consisted of the lithologic identification of clasts larger

than 2mm for each count location, for a total of 22 clast counts taken, with 10 stations on

the western stratigraphic column, 9 stations on the eastern stratigraphic column and 3

stations for Tadpole Tank (Figures 16-17, Tables 2-6, Appendix C.24). Due to extensive

desert varnish in the study area, outcrops for clast counting were selected based on

availability and had identifiable clasts not covered in varnish. For each clast count,

selected outcrops were counted using a 2 x 2- foot fishing net with a 2-inch grid spacing

to reduce sampling bias towards more prominent larger clasts and to avoid double

counting of individual clasts, with an average count of 30 identifiable clasts per outcrop.

The clast counts results were used to calculate relative frequency for different clast

compositions, the frequency distribution of grain sizes (i.e., degree of sorting) and

corresponding phi sizes, the average composition for each clast count, as well as a

comparison analysis of measured paleoflow directions and grain sizes throughout the

14

basin (Figure 25). Conglomerate clast count data for the different stratigraphic units were compared and recorded on Microsoft Excel. Clast sizes are listed in millimeters using the Wentworth grain scale for maximum measurements. The results of the conglomerate clast counts are presented in the corresponding sections below, with details of each clast count presented in Appendix A and Appendix B.

A total of 17 hand samples were collected from the three study localities across the basin for qualitative analyses of the textural and compositional characteristics of the deposits (Table 7, Figures 8-11). Each hand sample was closely examined, noting the different sizes and compositions of the grains, as well as the average colors of both the matrix and lithic clasts present. Observing the samples with a hand lens, the degree of sorting, clast sizes, roundness and mineral compositions were analyzed, using these factors to infer sediment transportation processes and maturity. Clast roundness showcases the measure of sharpness of a grain's angular edges and corners, with increased roundness representing a great distance traveled, however, the time it takes for edges to smooth is relative based on individual rock types, hardness, and the transportation method. Results and compositions of the 17 hand samples from the western and eastern stratigraphic columns, as well as the Tadpole Tank region, are presented in the corresponding sections below and compared to compositions derived from clast count analysis (Figures 26-27).

Alongside the hand samples, a compositional analysis from three thin sections that had previously been made of the orange-red sandstone (ORSS) layer from the Tadpole Tank region (Figure 5) were counted on a Pelcon Point Counter provided by Cal Poly Pomona, followed by the completion of two QFL diagrams, a QmFLt diagram, and

LmLvLs diagram to determine clast type specifics and provenance categories (Figures

28-29). For each thin section, 500 points were counted using the Gazzi-Dickinson method

of point counting (Dickinson, 1970, Ingersoll et al 1984). Nine categories of grain types

were counted and were used in the data analysis including: monocrystalline quartz,

polycrystalline quartz, potassium feldspar, plagioclase feldspar, sedimentary lithics,

metamorphic lithics, volcanic lithics, muscovite mica, zircons, cement and matrix

percentages, as well as water pore spaces that were encountered during the analysis. The

point count raw data categories and recalculated parameters, such as the QFL, QmFLt,

LmLvLs diagrams, are defined in Tables 13-14.

CHAPTER 4: Sedimentology and Stratigraphy

The Soledad Rojo formation is grouped into three sedimentary units for this study, each with distinct colors, lithofacies and clast compositions that may suggest changes in sediment provenance and depositional environments during the history of the basin (Figure 3, Figure 5, Figure 7). The lower unit of the Soledad Rojo formation, Unit R, is named for its red color. It includes trough cross beds, coarse grains, matrix and clast supported subunits and conglomerates from meta plutonic and volcanic origin (Figure 15). Unit BT, named for its beige tan color, and Unit R, located at the Tadpole Tank area of the basin, are the middle unit and a fluvial deposit. The BT unit is a beige tan colored, clast supported, and imbricated with rounded to subrounded moderately well sorted cobble and boulder conglomerate with metaplutonic clasts (Figure 15). Unit L, named for its light tan color, is a lithic arkose containing subangular to subrounded metaplutonic and volcanic clasts (Figure 14). In the study area, Unit L and Unit R of the Soledad Rojo formation are observed on both sides of Milpitas Wash Road, but are compositionally and texturally different when comparing exposures between the different stratigraphic columns. Unit BT is located on the western portion of Milpitas Wash Road, north of the two stratigraphic columns (Figure 3 and Figure 5). Detailed descriptions of the three research sections, the two stratigraphic column of the Soledad Rojo formation, as well as its subdivisions (Table 1) are provided in this chapter below, in addition to descriptions of volcanic rocks associated with the formation (Figure 6 and Figure 7).

17

Soledad Rojo formation Unit Lithofacies

	Map Unit	Facies Association	Lithology	Collective Thickness (m)	Description
Western Stratigraphic Column	Unit R - BRSS	Conglomerate and interbedded sandstone	Alluvial debris flow conglomeratic sandstone deposits: volcanic and metaplutonic fragments	~160	Brick red; matrix supported, ¼ mm to ½ mm fine to medium angular to subangular sandy matrix. Clasts are subangular to subrounded pebble to small cobbles gravel at 5mm to 80mm in size. Clasts consist of sicilic tuffs and metamorphic rocks such as biotite and augen gneisses. Contains white calcite layers throughout.
	Unit R - DRSS	Conglomerate and interbedded sandstone	Alluvial debris flow conglomerate deposits: volcanic fragments	~16	Dark red; matrix and clast supported, 2 mm to 5 mm subrounded fine pebble matrix. Clasts are rounded pebble to cobble clasts up to 200mm in size. Clasts consists of rhyolitic and tuffaceous rock fragments.
	Unit R - ORSS	Conglomerate and interbedded cross-stratified sandstone	Alluvial debris flow conglomeratic sandstone deposits: volcanic and metaplutonic fragments	~30	Orange red; matrix supported, 1 mm to 3 mm subrounded fine pebbled matrix. Clasts are subrounded to rounded medium pebble clasts from 10mm up to 25mm in size. Clasts consist of unidentified volcanics, biotite gneisses and muscovite schists. Contains white calcite layers throughout.
	Unit R - VRSS	Conglomerate and interbedded sandstone	Alluvial debris flow conglomeratic sandstone deposits: volcanic and metaplutonic fragments	~39	Vivid red; matrix supported, 1 mm to 3 mm very coarse sand and fine pebble angular matrix. Clasts are subangular to subrounded medium pebble to cobble clasts at 10mm to 200mm. Clasts consist of biotite and feldspar rich augen gneisses, cherts and wacke rock fragments.
	Unit R - LRSS	Conglomerate and interbedded sandstone	Alluvial debris flow conglomeratic sandstone deposits: volcanic and metaplutonic fragments	~6	Light red; clasts supported, 1 mm to 2 mm fine pebble subangular to subrounded matrix. Clasts are subrounded to rounded medium pebble to cobble clasts at 10mm to 200mm. Clasts consist of unidentified volcanics, wackes, gneisses and tuffaceous rock fragments.
	Unit L	Conglomerate and interbedded sandstone	Alluvial debris flow conglomeratic sandstone deposits: volcanic and metaplutonic fragments	~132	Tan: matrix to clast supported, 1/4 mm to 1 mm fine to coarse sand subrounded to rounded cemented matrix. Clasts are subangular to subrounded fine pebble to coarse pebble clasts at 5mm to 50mm in size. Clasts consists of biotite gneisses and muscovite schists and tuffaceous rock fragments.
Eastern Stratigraphic Column	Unit R - BRSS	Conglomerate and interbedded sandstone	Alluvial debris flow conglomeratic sandstone deposits: metaplutonic fragments	~135	Brick red; matrix supported, 3 mm to 5 mm fine pebble angular to subangular matrix. Clasts are subangular to subrounded medium pebble to small cobble clasts at 10mm to 85mm in size. Clasts consists of biotite gneisses and muscovite schists. Contains white calcite layers throughout.
	Unit R - DRSS	Conglomerate and interbedded sandstone	Alluvial debris flow conglomeratic sandstone deposits: volcanic and metaplutonic fragments	~58.5	Dark red; clast supported, 1 mm to a 2 mm very coarse sand to fine pebble angular to subangular matrix. Clasts are subangular to sub-rounded pebbels to cobbles ranging from 10mm up to 240mm in size. Clasts consists of ignimbrites, biotite gneisses, and muscovite schists. Contains concentrated biotite laminations
	Unit L	Conglomerate and interbedded sandstone	Alluvial debris flow conglomeratic sandstone deposits: volcanic and metaplutonic fragments	~166	Tan: matrix to clast supported, 1/4 mm to 1 mm fine to coarse sand subrounded to rounded matrix. Clasts are subangular to subrounded coarse pebble to small cobble clasts at 20mm to 150mm in size. Clasts consists of ignimbrite, biotite gneisses and muscovite schists.
Tadpole Tank	Unit BT	Conglomerate and interbedded sandstone	Fluvial conglomeratic sandstone: volcanic and metaplutonic fragments	NM	Buff to Beige; clast supported, 3 mm to 5 mm fine pebble subrounded to rounded matrix. Clasts are rounded large pebble to large cobble clasts at 40mm to 240mm in size. Clasts consists of porphyeritic and vessicular volcanic rocks fragments.
	Unit R - ORSS	Conglomerate and interbedded cross-stratified sandstone	Alluvial debris flow conglomeratic sandstone deposits: volcanic and metaplutonic fragments	NM	Orange red; matrix to clast supported, 5 mm subangular, fine pebble matrix. Clasts are medium pebbles to medium at 10mm to 80mm medium cobbles, with the largest size as a small boulder at over 350mm. Clasts consist of unidentified volcanics, basalts, augen gneisses and tuffaceous rock fragments.
				NM - not measured	

Table 1: Lithofacies associations for Soledad Rojo formation.

18

Figures 5. Detailed geologic maps of Soledad Rojo formation (see Figure 3 for locations). (A) Tadpole Tank, (B) Western Stratigraphic Column (red stars) and Eastern Stratigraphic Column (yellow stars). Green dots indicate hand sample locations (Figure 8, Table 2) Yellow triangles represent clast count locations (Figure 7, Tables 6-12).
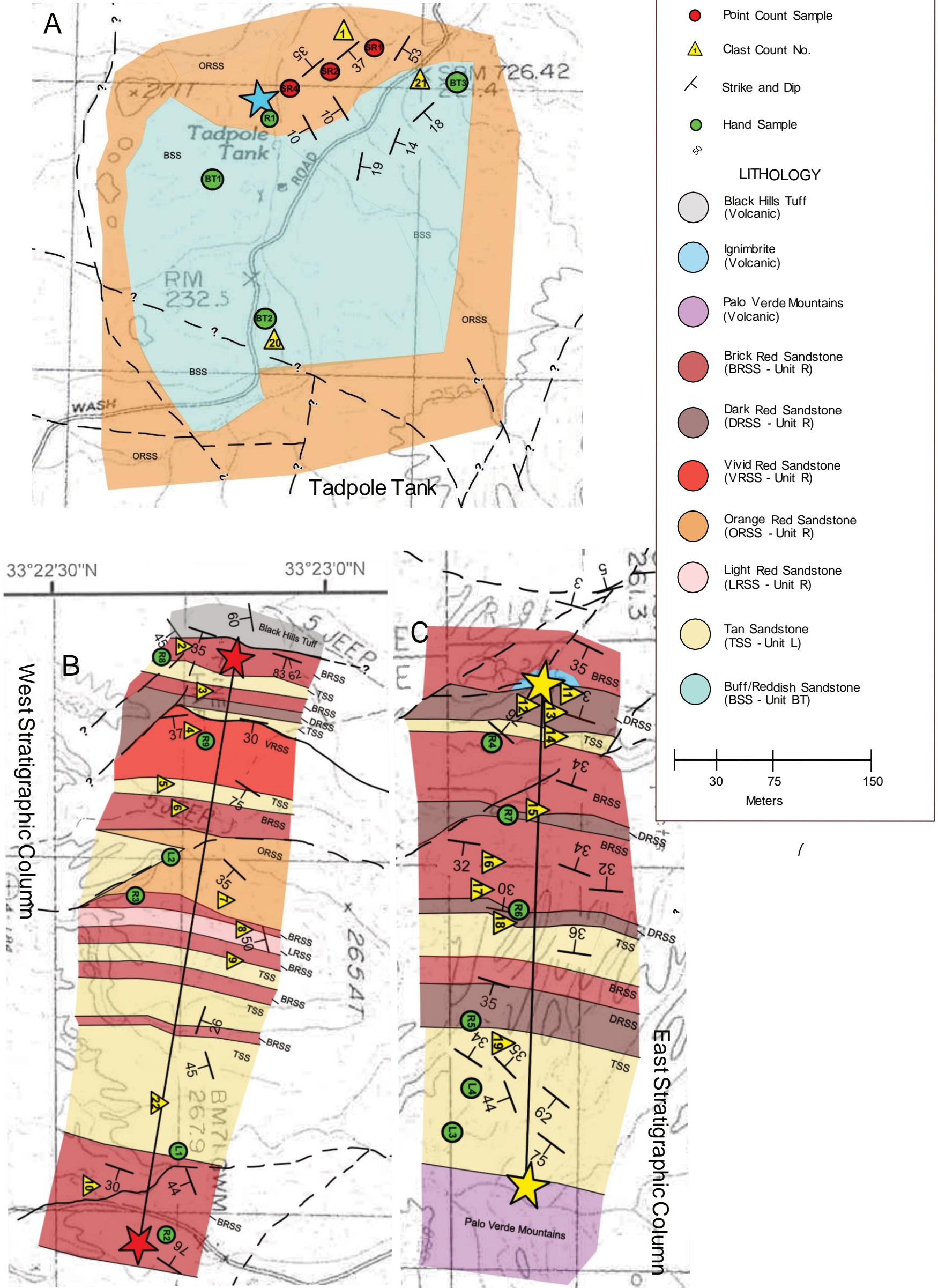
Western and Eastern Stratigraphic Columns: Key

EXPLANATION

LITHOLOGY (lithofacies code)

- TSS - upper Soledad Rojo fm., light tan conglomeratic sandstone (Unit L)
- BRSS - mid/lower Soledad Rojo fm., brick red conglomeratic sandstone (Unit R)
- ORSS - mid/lower Soledad Rojo fm., orange-red conglomeratic sandstone (Unit R)
- VRSS - mid/lower Soledad Rojo fm., very red conglomeratic sandstone (Unit R)
- DRSS - mid/lower Soledad Rojo fm., dark-red conglomeratic sandstone (Unit R)
- LRSS - mid/lower Soledad Rojo fm., light-red conglomeratic sandstone (Unit R)

- Welded Tuff
- Pink Ignimbrite
- Massive sandstone

GRAIN LITHOLOGY

- Cobbles/pebbles, grain supported conglomerate
- Granules/ Very Coarse Sand, matrix supported conglomeratic sandstone
- Coarse Sand, matrix supported conglomeratic sandstone
- Medium/ Fine Sand, matrix supported conglomeratic sandstone
- Very Fine/ Silt / Clay Sand, matrix supported conglomeratic sandstone

GRAIN SIZE

- cl - clay
- s - silt
- vf - very fine sand
- f - fine sand
- m - medium sand
- c - coarse sand
- vc - very coarse sand
- g - granule
- p - pebble
- cb - cobble
- b - boulder

- Clast Count locations
- Mud cracks
- Paleocurrent direction from clast imbrications
- Number of measured clasts
- 40Ar/39Ar date (Murray et al., 2019)
- Faults
- Calcite layers

Vertical scale in meters

20

Western

Eastern

n = 247

n = 221

CONGLOMERATE CLAST COMPOSITION

- Volcanic
- Quartzite
- Augen Gneiss
- Welded Tuff
- Gneiss
- Chert
- Orange-red sandstone (ORSS)
- Brick-red sandstone (BRSS)
- Granodiorite
- Very-red sandstone (VRSS)
- Ignimbrite
- Schist
- Tan sandstone (TSS)
- Dark-red sandstone (DRSS)
- Light-red sandstone (LRSS)
- Wackee
- Green/Black basalt
- Andesite
- Diorite
- Rhyolite
- Pumice
- Gabbro
- Felsic Granite

Figure 6. Western and Eastern stratigraphic column key.
Unit lithology, grain lithology and clast count compositions
included for comparison on stratigraphic columns.
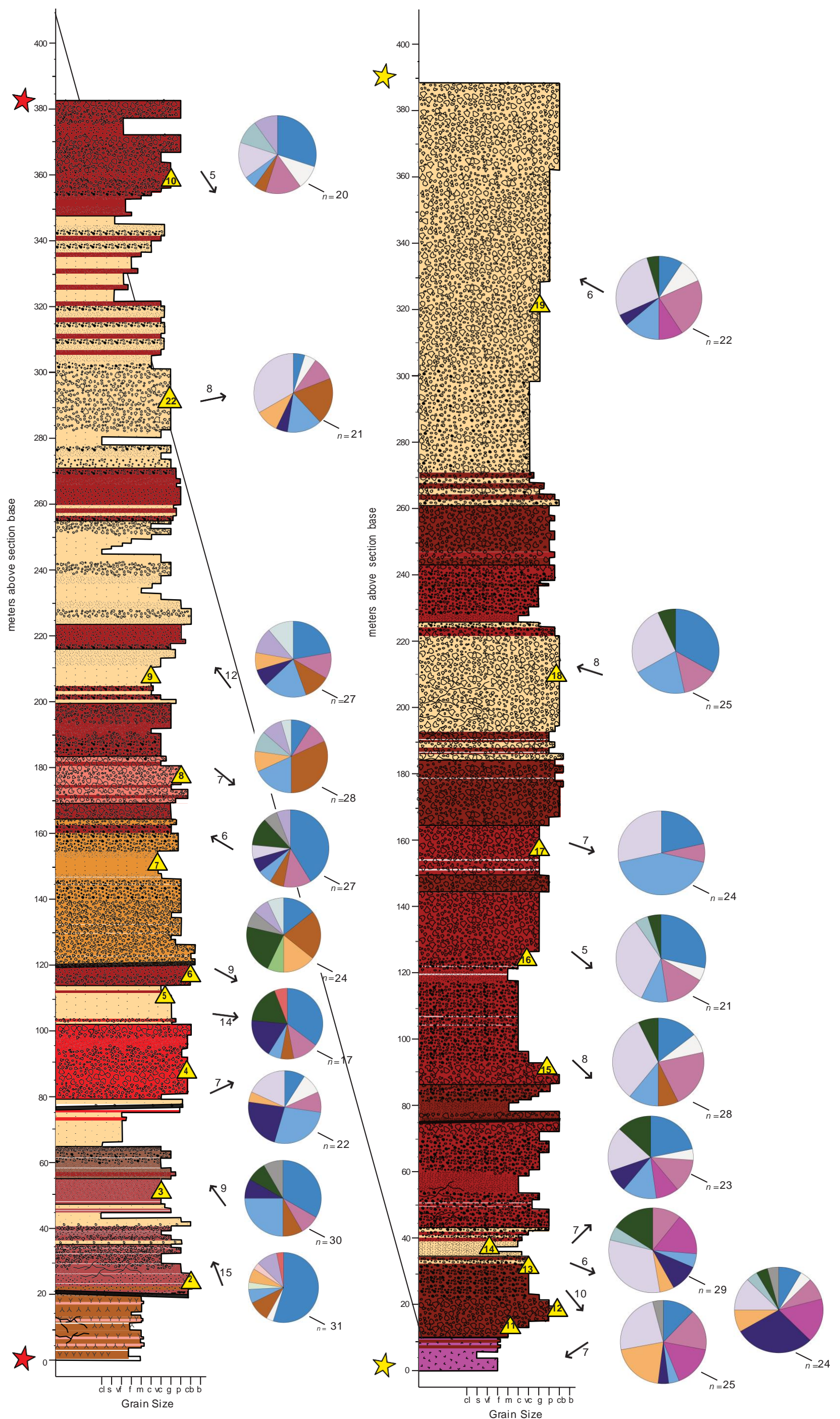
Figure 7. Western (red stars) and Eastern (yellow stars) stratigraphic columns. Numbered clast counts shown in yellow triangles. Arrows and number of clasts represent paleocurrent provenance with determined directions. Pie charts represent composition of clast counts, and number of clasts observed.

21

A.   Underlying Volcanic Rocks

Tuff of Black Hills Mountains

The tuff of the Black Hills Mountains is found in the western most part of the study area in contact with Unit R of the Soledad Rojo formation (Figure 2, Figure 3 and Figure 5, Appendix C). This volcanic rock is a welded ignimbrite that compromises the basal 19.5 meters of the Western stratigraphic column (Figure 7); the base of the ignimbrite is not exposed, however displays a contact fault in the west and is hypothesized to underlie the eastern stratigraphic column. The base of the ignimbrite starts out as a dark gray-reddish color, with vesicular mafic lithics, transitioning upsection from a dark red intermediate material with an increasing quartz content to an alternating series of red, rhyolitic felsic extrusive rock strata layers containing high quartz and an alkali feldspar composition.

Ignimbrite & Palo Verde Mountains

A pink ignimbrite and the Palo Verde Mountains enclose the Eastern stratigraphic column (Figure 2, Figure 3 and Figure 5). The pink ignimbrite compromises the basal 11 meters of the Eastern stratigraphic column (Figure 7); the bedding thickness of the ignimbrite is an example of crude bedding, it is laterally continuous and the base of the formation is not exposed. The ignimbrite is interpreted to be deposited unconformably alongside the Soledad Rojo formation as part of the welded tuff from the Black Hills Mountains. The metaplutonic Palo Verde Mountains are not included in the Eastern stratigraphic column, however contain intrusive and extrusive rocks including basaltic,

22

andesitic, and rhyolitic flows that serve importance to the provenance of conglomerates on that side of Milpitas Wash Road.

B.   Lower member Soledad Rojo formation, Red Sandstone, Unit R (BRSS, DRSS, VRSS, ORSS, LRSS)

The vibrant red, north east - striking, moderately west dipping sandstone unit of the Soledad Rojo formation, referred to as Unit R, displays high ridges along Milpitas Wash Road, and is the reason for the name of the formation (Figure 5). Unit R consists of a red coarse grain lithic arkose that displays north-easterly trough-cross stratification and cut-and-fill channel structures throughout (Figure 15). Unit R collectively made up 248 meters of the Western stratigraphic column, and another 224 meters on the Eastern stratigraphic column (Figures 7). Compositionally, Unit R consists of a crumbly red silty-sand matrix that varies with different reddish hues, especially on the western portion of the study site, interbedded with granule/pebble conglomerates. Unit R is characteristically clast supported throughout the two stratigraphic columns with a matrix that is subangular to subrounded sands and pebbles, alongside moderately poorly sorted cobble sized meta plutonic and volcanic clasts. Rock fragments typically found within Unit R (described in detail in Chapter 6) included basalt, biotite gneiss, augen gneiss, muscovite schist, granitic rocks, quartzite and a high amount of tuffaceous rocks, with slight variations in compositional portions between the western and eastern stratigraphic sections (Table 1, Figures 6-7).

Due to the color variances, Unit R was further divided into several subunits based on different lithological parameters to assist with inferring different smaller scale events

23

of transport and deposition, as well as periods of non-deposition or erosion (Figure 5). These five sub-units include: (1) a brick red conglomeratic sandstone (BRSS), (2) a dark red conglomeratic sandstone (DRSS), (3) a vivid red conglomeratic sandstone (VRSS), (4) an orange-red conglomeratic sandstone (ORSS), and (5) a light red conglomeratic sandstone (LRSS). All of the subunits were identified on the Western stratigraphic column (Figure 7); only the dark red sandstone (DRSS) and the brick red sandstone (BRSS) were observed on the Eastern stratigraphic column (Figure 7).

Unit R (BRSS) - Brick Red Conglomeratic Sandstone

The brick red conglomeratic sandstone of Unit R (BRSS) collectively makes up 160 meters of the overall 248 meters of the red sandstones on the Western stratigraphic column, the largest of the red subunits in the western side of the road (Figure 5). In total, the BRSS brick red conglomeratic sandstone subunit was identified seven times throughout the western stratigraphic column and characteristically had thin white coatings of calcite in the post-depositional cracks of the sedimentary rock (Figure 12, Appendix C.40-42). The western brick red conglomeratic sandstone showcases sedimentary structures such as mud cracks (Appendix C.32) and laminations composed of darker heavier minerals streaked throughout. Similarly, the brick red conglomeratic sandstone of Unit R made up 135 meters of the overall 224 meters of Unit R in the Eastern column (Figure 5). In total, the BRSS subunit was identified three times throughout the Eastern stratigraphic column and is characteristically similar to the BRSS subunit to the western portion site of the research, varying between matrix grain sizes,

24

grain support and overall crumbly texture compared to the western stratigraphic column (Figure 12, Appendix C.58, Appendix C.64).

For the Western stratigraphic column, the brick red conglomeratic sandstone (BRSS) subunit exhibits an upsection increase in grain sizes (Figures 5-7). Towards the bottom of the stratigraphic section, BRSS is matrix supported, composed of a crumbly fine to medium sand angular matrix. Clasts found inside BRSS are subangular to subrounded pebbles starting at 5 mm to 80mm, shown in clast count three, labeled as CC3, and is composed of silicic tuffs and metaplutonic rocks such as biotite and augen gneisses (Table 8, Appendix A, Appendix C.30). Upsection, the brick red conglomeratic sandstone becomes crumblier and less resistant, with the grain sizes of the matrix sizes transitioning to a coarse sand, however the clast sizes stayed similar in size, as shown in clast count seven (Figures 5-7). On the eastern stratigraphic column (Figure 5 and Figure 7), the brick red conglomeratic sandstone is matrix supported and is composed of a unresistant angular fine pebble matrix. Clasts within BRSS on the Eastern stratigraphic column are subangular to subrounded medium pebbles to small cobbles, shown in clast count fifteen, consisting predominantly of metaplutonic rocks such as biotite gneisses and muscovite schists (Table 10). Upsection, the brick red conglomeratic sandstone matrix becomes crumblier and less resistant, similar to the western stratigraphic, however the clast sizes grew larger in size moving east towards the Palo Verde Mountains (Figure 7).

Brick Red Conglomeratic Sandstone Hand Sample Compositions

Hand samples of the brick red conglomeratic sandstone BRSS were taken to compare the change in lithofacies throughout the western and eastern stratigraphic

column, allowing for a better understanding of the depositional dynamics of sediment into the basin. Freshly fractured in the field, three samples of BRSS were taken for upsection observation on the Western stratigraphic column: (1) Unit R - R2, (2) Unit R - R3, (3) and Unit R - R8, and another three from the Eastern stratigraphic column: (1) Unit R - R4, (2) Unit R - R6.1 and (3) Unit R 6.2 (Figure 8).

Hand sample Unit R - R2 was taken on the eastern side of Milpitas wash road, however is still considered part of the continuing western brick red conglomeratic sandstone unit, thus is not included on the eastern stratigraphic column (Figure 8). This sample consists of a finer sand matrix, and is grain supported. The clasts in this hand sample are significantly larger compared to any other sample, and averaged 25mm in size, largest clast at 60mm (Table 2). These rock fragments are angular, moderately sorted clast that are immature to sub-mature in texture, with a desert pavement finish. To compare, a roundness and sphericity hand sample analysis chart was created to visually represent the average change in conglomerate size and shape, as well as investigate the relationship between the two properties of grains when interpreting the various hand samples (Figure 9). Hand sample Unit R - R3, taken near the contact between the orange and brick red sandstone on the Western stratigraphic column, is the least resistant textured red sandstone of all the samples (Figure 8 and Figure 10). This sample consists of a fine to medium sand matrix that is matrix supported and has rounded equant well sorted clasts that are mature in texture, with a slight desert pavement finish.

The clasts in the bright red R3 hand sample averaged 2mm in size, the largest clast at 3mm (Table 2). Hand sample R3 has distinctly finer grains, the brightest red color and seems to have traveled the most distance due to its smaller clast sizes. Hand sample

Unit R - R8 consists of a medium sandy matrix that is matrix supported, has subrounded equant poorly sorted clasts that are submature in texture, with a desert pavement finish (Figure 8). The clasts in the brick red R8 hand sample averaged 5mm in size, the largest clast at 10mm (Table 2).

Taken from the Eastern stratigraphic column (Figure 8) hand sample Unit R - R4 is the same brick red conglomeratic sandstone unit found on the western stratigraphic column. This sample consists of a finer sand matrix, and is grain supported. The clasts in this hand sample averaged 10mm in size, the largest clast at 40mm (Table 2). These rock fragments are angular, very poorly sorted clast that are sub-mature in texture, with a desert pavement finish. Hand sample Unit R - R6 was taken at a contact between a brick red conglomerate sandstone layer (BRSS) and a dark red conglomerate sandstone layer (DRSS). Due to its variability in one location, two samples were taken and both show different grain sizes and textures (Figure 8). Hand sample Unit R - R6.1 has distinctly finer grains and consists of a fine to medium sand matrix that is matrix supported and has sub-angular well sorted clasts that are mature to submature in texture, with a slight desert pavement finish. The clasts in the R6.1 hand sample averaged ½ mm in size, the largest clast at 2mm (Table 2). Hand sample R6.2 has distinctly coarser grains and consists of a fine to medium sand matrix that is grain supported and has sub-angular poorly sorted clasts that are immature in texture, with a slight desert pavement finish. The clasts in hand sample R6.2 averaged ½ mm in size, the largest clast at 20mm (Table 2).

Brick Red Conglomeratic Sandstone Interpretations

On the western stratigraphic column, there is a defined upsection of sediments going eastwards in the direction of faults towards Milpitas Wash Road. It is interpreted that the faults crossing the western stratigraphic column are uplifting Unit R in this general location, creating the crumbly texture that is less resistant continuing east. This uplift and texture change is hypothesized to be causing more alluvial debris flows and higher erosion rates overall in this part of the basin. On the eastern stratigraphic column, conglomerate clasts are similar in sedimentological characteristics as western stratigraphic column; it contains a crumbly, fine angular matrix, with subangular to subrounded grains. However, the eastern stratigraphic column displays larger grains overall and has lithics indicative of metaplutonic sources. Hand samples of the brick red conglomeratic sandstone on the western stratigraphic column display more texturally mature grains (Figure 9) compared to on the eastern stratigraphic column, which is consistent with the crumbly texture outcrops east of Milpitas Wash. It is interpreted that the possibility of the same event occurred within the Soledad Rojo basin during the deposition of the brick red conglomeratic sandstone, leading to the different sources from the east to the west to collect and intermix within the basin.

Unit R (DRSS) - Dark Red Conglomeratic Sandstone

The dark red conglomeratic sandstone subunit of Unit R (DRSS) collectively makes up 16 meters of the overall 248 meters of the Soledad Rojo formation on the western stratigraphic column and in the eastern column collectively makes up 58.5 meters of the overall 224 meters (Figure 5, Figure 7, Appendix C.33, Appendix C.37) and

28

based on stratigraphic relationships are believed to have been concurrently deposited with Unit BT. The dark red conglomeratic sandstone DRSS was identified once on the western stratigraphic column and varied from matrix-supported to grain-supported (Figure 5 and Figure 7); with grain-supported rocks support areas of high topography, whereas matrix-supported rocks are low-lying, inferred to be from differential weathering. The dark red conglomeratic sandstone DRSS was identified four times on the eastern stratigraphic column and is grain supported throughout, with slight variations compared to the western column (Figure 5 and Figure 7.

For the Western stratigraphic column, the matrix supported dark red conglomeratic sandstone DRSS is composed of a fine pebble matrix (Table 2). Clasts found within this DRSS are rounded pebbles to cobbles, shown in clast count six CC6 and contain predominantly tuffaceous and rhyolitic rocks. On the Eastern stratigraphic column (Figure 5 and Figure 7), the dark red conglomeratic sandstone DRSS is composed of fine pebble angular to subangular matrix with a sub-rounded cobble clast, shown in clast counts eleven through thirteen (Table 7 and Figure 13). The clasts observed on the eastern stratigraphic column are composed of volcanic and metamorphic rock fragments including ignimbrites, muscovite schists and biotite gneisses.

Dark Red Conglomeratic Sandstone Hand Sample Compositions

Hand samples of the dark red conglomeratic sandstone DRSS were taken to compare the change in lithofacies throughout eastern stratigraphic column, allowing for a better understanding of the depositional dynamics of sediment into the basin. Freshly fractured in the field, two samples of DRSS were taken for observation: (1) Unit R - R5,

and (2) Unit R - R7 (Figure 8). Hand sample Unit R - R5, from the dark red sandstone DRSS on the Eastern stratigraphic column, was taken westward heading back towards the Milpitas Wash Road, near a contact between Unit R and Unit L. This hand sample is the least resistant textured red conglomerate sandstone of all the samples collected. Hand sample R5 has distinctly finer grains, and is interpreted to be at the location of a possible fault due to the mapped strike and dips, as well as large clast sizes (Figure 5, Figure 8 and Figure 10). The clasts in this hand sample averaged 10mm in size, the largest clast at 20mm. This sample is matrix supported and consists of a medium sand matrix. Clasts are angular to subangular, very poorly sorted and sub-mature in texture, with a desert pavement finish (Table 2). Hand sample Unit R - R7 is matrix to clast supported medium sandy matrix. Similar to Unit - R6.2 of the brick red conglomeratic sandstone of the eastern stratigraphic column, the clasts in this hand sample are larger compared to the other samples and averaged 10mm in size, largest clast at 20mm. These rock fragments are subrounded, poorly sorted, sub-mature in texture, with a desert pavement finish (Table 2, Figure 8).

Dark Red Conglomeratic Sandstone Interpretations

Unlike the dark red conglomerate sandstone DRSS from the western stratigraphic section, this subunit on the eastern stratigraphic column has laminations concentrated, likely derived from the same source of the biotite rich gneisses found in the eastern stratigraphic section, which are also absent from the western section. Upsection in the eastern stratigraphic column, the thickness of the dark red conglomeratic sandstone DRSS subunits starts at 24 meters and thins to 1.5 meters thick as the strat column

30

reaches closer to the Palo Verde Mountains (Figure 7). The dark red conglomeratic sandstone becomes more matrix-supported upsection, interpreted that the DRSS is getting further away from source and has an eastern paleoflow direction. The varying matrix supported low-lying regions to clast supported uplifted sections in this subunit infer a graded bedding deposition, which is characteristic of a decrease in sediment transport energy overtime. Hand samples of the dark red conglomeratic sandstone on the western stratigraphic column display texturally submature grains (Figure 9) compared to on the eastern stratigraphic column which display texturally immature grains, which is consistent with the crumbly texture outcrops east of Milpitas Wash. It is interpreted that the dark red conglomeratic sandstone was formed during a rapid depositional event. Within the Soledad Rojo formation, both options are hypothesized to be possible.

Unit R (VRSS) - Vivid Red Conglomeratic Sandstone

The vivid red conglomeratic sandstone beds (VRSS) of Unit R collectively makes up 39 meters of the overall 248 meters of the red unit in the western column, and are absent from the eastern stratigraphic column (Figure 5 and Figure 7). In total, the vivid red sandstone subunit was identified once on the western stratigraphic column at a faulted contact between a tan conglomerate sandstone layer. This subunit varied from matrix-supported to grain-supported depending on topography, but was inverse to the dark red conglomeratic sandstone subunit; in uplifted regions - with matrix-supported rocks support areas of high topography (Appendix C.34), whereas grain-supported rocks are low-lying. The vivid red conglomerate sandstone VRSS is matrix supported and

31

composed of a fine pebbled white and red angular matrix (Table 2). Clasts found in

VRSS are subangular to subrounded pebbles, shown in clast count four (Appendix A).

Vivid Red Conglomeratic Sandstone Hand Sample Compositions

One sample of the vivid red conglomeratic sandstone VRSS was taken for

upsection observation on the Western stratigraphic column: (1) Unit R - R9 to compare

the change in lithofacies throughout the western and eastern stratigraphic column,

allowing for a better understanding of the depositional dynamics of sediment into the

basin (Figure 8). Hand sample Unit R - R9 consists of a very coarse sand matrix that is

matrix supported and has rounded to subrounded equant poorly sorted clasts that are sub-

mature to mature in texture, with a desert pavement finish. The clasts in the brick red R9

hand sample averaged 10mm in size, the largest clast at 40mm (Table 2).

Vivid Red Conglomeratic Sandstone Interpretations

The vivid red conglomeratic sandstone has a higher amount of metamorphic and

sedimentary debris compared to the corresponding subunits in Unit R on the western

stratigraphic column, containing medium sized cobbles of biotite and feldspar rich augen

gneisses up to 120mm, as well as chert and wacke rock fragments, interpreted as a

possible different source. The hand sample of the vivid red conglomeratic sandstone on

the western stratigraphic column displayed texturally submature grains (Figure 9). It is

interpreted that the varying matrix supported uplifted regions to clast supported low-lying

sections in this subunit infer an inverse graded bedding deposition, which is characteristic

of sediments deposited in debris flows environments, likely during tectonic activity at the

faulted contact. This evidence coincides with the northeasterly paleocurrents that were found and grain size data (Figure 18) inferring this location may be a source of sediment supply locally.

Unit R (ORSS) - Orange Red Conglomeratic Sandstone

The orange-red sandstone (ORSS) unit of the Tadpole Tank region primarily outcropped Milpitas Wash Road and underlies Unit BT further into the canyon fed wash. The orange-red sandstone is distinctly different compared to the brick red and dark red conglomeratic sandstones of Unit R further south due to its locality within the fluvial fed canyon wash path, with one layer of an orange-red subunit identified in the western stratigraphic column and is inferred to have drained south into the Soledad Rojo basin (Figure 5 and Figure 7). This part of Tadpole Tank is averagely composed of a pebble subangular matrix and is primarily clast supported throughout the Tadpole Tank region (Table 1, Appendix C.17-22, Appendix C.38-39). The clasts sizes ranged from medium pebbles to medium cobbles, the largest being a small boulder at over 350mm, and are composed of angular to rounded metaplutonic and volcanic debris such as tuffaceous rocks, as well as biotite and augen gneisses (Table 12).

The orange-red conglomeratic sandstone bed of Unit R (ORSS) is observed in the western stratigraphic column once and collectively makes up 30 meters of the overall Unit R and is absent from the eastern stratigraphic column (Figure 5 and Figure 7). Compared to the brick red conglomerate sandstone in the western stratigraphic column, the orange red conglomeratic sandstone ORSS subunit is characteristically a brighter orange than the main brick red conglomerate sandstone BRSS subunit, as well as contains

different type of conglomerate fragments more closely related to the orange-red arkose and clasts found in Unit R ORSS in the Tadpole Tank region. The orange-red conglomeratic sandstone subunit on the western stratigraphic column is matrix supported and composed of a crumbly fine pebbled subrounded matrix (Table 8). Clasts are subrounded to rounded coarse pebbles up to 25mm (Appendix A). Compositionally, the orange-red conglomeratic sandstone subunit contained volcanic and metamorphic fallout that includes schists and biotite gneisses, as well as post-depositional white layers throughout (Figure 12).

Orange Red Conglomeratic Sandstone Hand Sample Compositions

Hand samples of the orange red conglomeratic sandstone ORSS were taken to compare the change in lithofacies north of the stratigraphic columns, allowing for a better understanding of the depositional dynamics of sediment into the entire basin (Figure 5). Freshly fractured in the field, one sample of ORSS was taken for observation: (1) Unit R - R1. Hand sample Unit R - R1 was taken on top of the large, resistant anvil sandstone outcrop and has a distinct crumbly orange-red texture (Figure 8). It consists of a very coarse sand, is matrix supported and has subrounded, moderately sorted larger clasts that are sub-mature in texture, with the beginning of a desert pavement finish. This hand sample was a very crumbly, non-resistant rock. Rock fragments included large feldspar crystals and quartzite. The clasts in the orange-red R1 hand sample averaged 2mm in size, the largest clast at 4mm. (Table 2).

Orange Red Conglomeratic Sandstone Interpretations

Flash floods and fluvial drainage have led to the erosion of the orange-red sandstone ORSS of Unit R and has resulted in the presentation of a large assortment of conglomerates and sedimentary structures along the canyon walls, further defining the formation of this basin, displayed in clast count one (CC1) (Figure 15). Comparingly, within the 30 meters of this strata layer on the western stratigraphic column, the matrix transitions from matrix supported to grain supported twice and has similar clasts characteristics interpreted as part of fluvial transportation. The hand sample of the orange red conglomeratic sandstone on the western stratigraphic column displayed texturally submature grains (Figure 9). It is interpreted that this subunit originated from the orange-red anvil sandstone structure further north near Tadpole Tank and was transported further south into the basin.

Unit R (LRSS) - Light Red Conglomeratic Sandstone

A thin light red conglomeratic sandstone (LRSS) bed is observed between two larger corresponding tan sandstone layers from Unit L, as well as below the orange-red conglomeratic sandstone Unit R (Figure 5, Figure 7 and Table 8). The light red conglomerate sandstone LRSS collectively made up 6 meters of the overall 248 meters of the Unit R western stratigraphic column and is absent from the eastern stratigraphic column.

Light Red Conglomeratic Sandstone Interpretations

The light red conglomeratic sandstone LRSS is interpreted to be a gradational contact between Unit L and Unit R. However, compared to the other Unit R subunits on the western stratigraphic column, it is still characteristically different and is included as a separate Unit R subunit based on the intermixing of tan and red coarse matrix grains, as well as the amount of wackes, subangular gneisses and tuffaceous rocks present, shown in clast count eight (Appendix A).

C.   Middle member Soledad Rojo formation, Beige Conglomeratic Sandstone, Unit BT (BSS)

Unit BT, the beige conglomeratic sandstone, is at the lowest point of the western side of Milpitas Wash Road in the Tadpole Tank region alongside the northern portion of Unit R ORSS, however Unit BT is not visibly included in the western or eastern stratigraphic columns (Figure 3 and Figure 5). As part of the middle unit in the Soledad Rojo formation, Unit BT is a buff colored clast supported, imbricated with rounded to subrounded, moderately well sorted cobble to boulder conglomerate containing metaplutonic rock fragments and interbedded orange-red lithic arkose (Table 12). Sedimentary structures found along the conglomeratic walls of Unit BT and the orange-red sandstone (ORSS) of Unit R: include channel scours, horizontal bedding, thin granule-pebble conglomeratic lenses, graded bedding, and trough cross bedding (Figure 15, Appendix C.5-16). These structures showcased north-westerly dipping trough-cross stratification. Rock fragments analyzed in clast count twenty and clast count twenty-one of Unit BT display unidentified volcanics, interpreted as porphyritic rock, with varying

36

colors, as well as distinctive ophitic mineral textures characteristic to this part of Tadpole Tank (Figures 17).

Unit BT Hand Sample Compositions

Hand samples of the beige conglomeratic sandstone Unit BT were taken to compare the change in lithofacies north of the stratigraphic columns, allowing for a better understanding of the depositional dynamics of sediment into the entire basin (Figure 5). Freshly fractured in the field, three samples of Unit BT were taken for observation in the Tadpole Tank: (1) Unit BT - BT1, (2) Unit BT - BT2, and (3) Unit BT - BT3 (Table 7).

Hand sample Unit BT - BT1 was taken on the western side of Milpitas Wash Road outside of Tadpole Tank (Figure 8 and Figure 11). At this location, a thin layer of orange-red sandstone pebble sized conglomerates ORSS is mixed in with the lighter Unit BT sandstone (BSS) which includes small cobbles. The clasts in the Unit BT - BT1 hand sample averaged 20mm in size, the largest clast at 25mm (Table 2). Hand sample Unit BT - BT1 showcased finer grains, was matrix supported and contained less clasts compared to hand sample Unit BT - BT2 and hand sample Unit BT - BT3.

Hand sample Unit BT - BT2 was characteristically different and is a lighter buff color (Figure 8). The BT2 hand sample consists of a fine sand matrix that is matrix supported and has rounded to subrounded equant very poorly sorted clasts that are sub-mature in texture, with a desert pavement, eroded finish. The clasts in the BT2 hand sample averaged 1mm in size, the largest clast at 5mm. Hand sample Unit BT - BT3 is a buff, slightly reddish color (Figure 8). The sample consists of a fine sand matrix that is

matrix supported and has rounded to subrounded equant moderately sorted clasts that are sub-mature in texture, with a desert pavement, eroded finish.

Unit BT Interpretations

The location of Unit BT, topographically, is in a depression between small east-west trending tectonics and north-south trending tectonics regionally. As a natural depression, it is interpreted that assorted sediments from multiple sources accumulate in this region until being further transported south of the Tadpole Tank. Synchronously, hand samples Unit BT - BT2 and Unit BT - BT3 display conglomerates that continue to get larger the further east. The hand samples of the beige conglomeratic sandstone in the Tadpole Tank displayed more texturally mature grains when compared to the clasts within the stratigraphic columns (Figure 9). This observation infers the provenance source for the lithics in the beige conglomeratic sandstone are possibly in mountains trending east and has a westward paleoflow direction, agreeing with the paleocurrent data (Figure 18).

D.   Upper member Soledad Rojo formation, Tan Conglomeratic Sandstone, Unit L (TSS)

The uppermost unit of the Soledad Rojo formation, Unit L, is characteristically identifiable due to its lighter color against the vibrant red sandstones in this basin, however it is in more abundance on the eastern stratigraphic column side, observed by the regularity of larger outcrops at the surface. The shallowly dipping (20-25°) Unit L is a tan to light grey conglomeratic lithic arkose that collectively makes up 132 meters of the

overall 380 meters of the western stratigraphic column (Figure 5 and Figure 7), and makes up 166 meters of the overall 390 meters' eastern stratigraphic column side of the study site. The tan conglomeratic sandstone of Unit L is the most distributed and dispersed sandstone throughout the entire Palo Verde Mountain basin and shows evidence to be the most recent layer deposited in the region hypothesized during the Pliocene - Pleistocene (Jennings, 1967). It is moderately resistant to environmental factors on both sides of Milpitas Wash Road due to compaction, desert varnish and future desert pavement taking place, as well as larger cobbles beginning to weather at the surface (Figure 14, Appendix C48-57, Appendix C.65-69). Outcrops that were found overall have been cemented and desert varnished, but were less cemented on the eastern stratigraphic column (Figure 14).

There are observed gradational contacts between the different units. On the western stratigraphic column, starting at the Black Hills Tuff heading east, descriptions of Unit L's tan conglomeratic sandstone start at 4.5 meters of thickness with little to no outcrops and lead into a small wash. This pattern was consistent with the tan conglomeratic sandstone throughout the whole western stratigraphic column, inter-fingering with the subunits of Unit R (Figure 5 and Figure 7) In total, seven tan sandstone layers were recorded on the western stratigraphic column and three layers were recorded on the eastern stratigraphic column. Decent outcrops of this unit, however, were limited on the western side of Milpitas Wash Road, and most are recognized to have been eroded into the basin. Outcrops that were found either have been partially cemented with desert varnish such as in clast count nine, or consisted of a powdery, high clay rich sediment, such as in clast count five, that appeared eroded away with rounded and subrounded

39

matrix grains, making clast identification difficult (Figure 14). Outcrops of Unit L closer to the road heading east changed to a medium/coarse sand matrix but contained little to no clasts and showcased erosion. (Figure 14, Tables 9-11). There were slight variations in colors of Unit L, predominately in rock fragment colors as well as minor variations in sizes and textures of grains.

Unit L Hand Sample Compositions

Hand samples of the tan conglomeratic sandstone Unit L were taken to compare the change in lithofacies between the western and eastern stratigraphic columns, allowing for a better understanding of the depositional dynamics of sediment into the basin (Figure 5). Freshly fractured in the field, two samples of Unit L were taken for observation in the Western stratigraphic column: (1) Unit L - L1, and (2) Unit L - L2, as well as two samples were taken in the Eastern stratigraphic column: (3) Unit L - L3 and (4) Unit L - L4 (Table 2).

Hand sample Unit L - L1 from the western stratigraphic column was taken on the side of Milpitas Wash Road and was noticeably cemented and hard to break (Figure 8 and Figure 11). The sample consists of a coarse sand matrix that is matrix supported and has elongated poorly sorted clast that are sub-mature in texture, with a desert pavement finish. The clasts in the L1 hand sample averaged 8 mm in size, the largest clast at 10mm. Hand sample L2 was found at a contact alongside Unit R westward towards the Black Hills Mountains along the western stratigraphic column (Figure 8 and Figure 11). This sample is clast supported and consists of a very coarse sand matrix. Clasts are subangular to subrounded equant moderately sorted and are sub-mature to mature in texture, with a

40

slight desert pavement finish, however, is powdered compared to hand sample L1 (Figure 11). The clasts in the L2 hand sample averaged 2mm in size, the largest clast at 4mm (Table 2).

Hand sample Unit L - L3 from the eastern stratigraphic column was taken westward heading back towards the Milpitas Wash Road from the Palo Verde Mountains, closest to the mountains (Figure 8 and Figure 11). Similar to sample L1 on the western stratigraphic column, the outcrop of sample L3 was cemented and hard to break. Sample L3 is matrix supported and consists of a medium sand matrix with elongated moderately sorted clast that are sub-mature in texture, with a desert pavement finish (Figure 8). The clasts in the L3 hand sample averaged ½ mm in size, the largest clast at 1mm (Table 2). Hand sample L4 is matrix supported and consists of a medium to fine sand matrix with subrounded equant well sorted clasts that are sub-mature to mature in texture (Figure 11). The clasts in the L4 hand sample averaged 1mm in size, the largest clast at 3mm.

Unit L Interpretations

On the eastern stratigraphic column (Figure 5 and Figure 7), due to there being less faults and less Unit R outcrops, the tan conglomeratic sandstone of Unit L is the more dominant unit going east exhibiting larger matrix grains, showcased in clast count eighteen, as well as larger overall conglomerate clasts, as shown in clast count nineteen. The hand samples of the tan conglomeratic sandstone in both stratigraphic columns displayed a range of texturally submature to mature grains when compared to the other clast types (Figure 9). Unit L showcased variations in sizes and textures of grains, however it is hypothesized that the western and eastern stratigraphic columns in the

41

Soledad Rojo formation came from the same source and depositional event series. A local water drainage braiding through the surface of this tan conglomerate sandstone unit on the eastern side is presumed to be originating from the Palo Verde Mountains, leading to further sediment transporting and entering the basin debris (Appendix C).

Sedimentology and Stratigraphy Interpretations

A sequence is repeated in the facies, alternating between brick red (BRSS), dark red (DRSS) to tan conglomeratic sandstones (Figure 5), interrupted by north-south trending faults while going upsection on the western stratigraphic column, as well as cyclical changes in deposition (Figure 7). This repetition of layers implies the horizontal sequence has been uplifted and tilted slightly, with Unit L the upper sequence, deposited more recently into the basin as an alluvial debris flow, and Unit R, the lower sequence, an older alluvial debris flow that has been uplifted from normal fault extension. Graded bedding throughout the basin varied between small scale planar bedding layers averaging 300mm in size for each series, as well as large scale representative in meters on the western stratigraphic column. The beds are typically normal graded and represent depositional events of moderate strength which led to the deposition of the heavier conglomerate rock fragments first, leaving the finer particles to deposit as the flow decreased regionally.

Comparing hand samples of both the western and eastern stratigraphic columns, there were variations in grain sizes and degree of sorting throughout the Soledad Rojo formation. From the western stratigraphic column, hand sample from Unit L - L1 (Figure 8) has a reddish tint due to its proximity to the brick red sandstone (sample R2) directly

42

to the east and has likely been cemented due to the chemical reactions during fluvial and alluvial drainage between Unit R and Unit L sediments. Conglomerate clast colors on the hand sample from Unit L - L2 range from reds, blues, purples, and greens, indicating they are likely of volcanic descent of the nearby Black Hills Tuff. The conglomerate clasts in hand samples from Unit R - R8 and Unit R - R9 infer they are of volcanic descent from the nearby Black Hills Tuff. At the location of sample R8, there is evidence of highly varnished conglomerates and crumbly loose rock fragments, inferring different weathering processes such as mechanical and chemical altering the outcrops, contributing to grain deposition and travel. Sample R9 conglomerate clasts are very porous, further indicating they are of volcanic descent of the nearby Black Hills Tuff. At the location of hand sample R9, there is evidence of high varnished conglomerates and cemented dense rocks, unlike hand sample R8 that is crumbly.

From the Eastern stratigraphic column, hand sample L3 has larger grains and conglomerate clasts compared to hand sample L4 on the eastern stratigraphic column (Figure 8). At the location of the tan sandstone L4 sample, there is recent evidence of fluvial drainage into the valley, possibly in an alluvial flow path, because of the grains sizes and well sorting compared to hand sample L3. Hand sample L3 is the closest sample heading towards the Palo Verde Mountains and shows indication of travel from the mountain front. The dark red R5 hand sample clasts became larger going east at the last indication of the red sandstone until reaching the Palo Verde mountains. This discovery was inconsistent with the trend of the clasts in Unit R; the conglomerates in Unit R were becoming smaller and more subrounded the further traveled east. The indication of large conglomerates infers a fault, alongside recent uplift in the last segment

43

of Unit R, due to its close proximity near an uplifted mountain front, and fresh deposition of the clasts. Samples R6.1 and R6.2, though at the same location, showcase a suddenly changing environment. Sample R6.1's fine sand matrix and clasts, as well as being well sorted, infers a reworked depositional process, likely a water drainage route that has traveled rock fragments from a higher elevation. Whereas sample R6.2 has a similar matrix, however, it has larger clasts, coinciding the water drainage hypothesis.

The two distinct units in the northern Tadpole Tank region, Unit BT and Unit R ORSS both contained sedimentary structures indicative to intense fluvial activity such as cross stratification and normal graded bedding unlike the other subunits within the Soledad Rojo basin (Figure 15). These types of structures can be interpreted as sediment and water previously had interactions throughout the basin dynamics in the past. Normal graded bedding features can be interpreted as a fluvial environment that experienced a decrease in sediment supply at a point in time, with fining of sediments upsection. Cross stratification structures within Soledad Rojo formation are deposited on inclined surfaces, implying the presence of ancient currents in Tadpole Tank occurred after uplift regionally, such as the flow of a localized river, or a flash flooding event leading to fluvial fed debris flows.

Based on a reconstruction of the different lithofacies throughout the Soledad Rojo formation, the architecture of the alluvial fan displays a facies analysis interpretation using eight models representing different fluvial styles, derived from Mial (Mial, 1985), providing further information on the basin dynamics. Upon closer examination of sediments present throughout the Soledad Rojo formation include: a mixture of massive, matrix supported gravel (Gms) with graded bedding, massive or crudely bedded gravel

44

(Gm) with horizontal bedding and clast imbrication, as well as stratified gravel (Gt) through the indication of trough cross beds. Other observations of ripple marks, indicative of fine to coarse sands (Sr) and fine pebbles (Ss) with the evidence of cross stratification. Only within the Tadpole Tank area and limited areas on the eastern column was silty mud found (Fm) due to the massive matrix bedding in some locations and desiccation cracks found throughout. These classified lithofacies infer Model 1, Model 2, and Model 3 for an alluvial architecture analysis (Mial, 1985) as the presumed fluvial environments (Figure 19).

Model 1 is characteristic of proximal regions regarding alluvial fan environments that have an equal mixture of source weathering rates, as well as rainfall and water transport that occurs, creating an abundance in debris flows into the basin (Figure 19). Model 2 is characteristic of locations in the basin that are further from the source and experience less debris flows regionally (Figure 19). This type of environment is indicative of shallow channels and leads to cut bank erosion. Due to the lower Basin and Range being an extensional basin, debris flows are presumed to occur, leading to gravel flood sheets and longitudinal bars. Model 3 is characteristic of a similar environment of Model 2, however it has larger grain sizes overall and typically has distinct topographic levels with sparse vegetation and active channels, which is proven in Soledad Rojo formation during flooding events (Figure 19). Mixed architecture in a basin is common and occurs when there are multiple fluvial systems at play, interchanging between style changes several or many times within one section (Mial, 1985).

Hand Sample Analysis - Stratigraphic Columns and Tadpole Tank

Western Hand Samples

	Sample #	Clast Grain Size Average (mm)	Clast Phi Size	Clast Roundness	Clast Sphericity	Rock Texture	Sorting	Maturity	Color	Matrix type	Matrix Grain Size (mm)	Matrix Phi Size
Unit L												
	L1	8.0 - 10.0	-2.0	0.3	0.3	ull / Fracture	Well sorted	Submature	Tan/reddish	Matrix supported	1/2 - 1.0	1.0
	L2	2.0 - 4.0	-2.0	0.3	0.7	ull / Fracture	Moderately sorted	Immature	Tan/reddish	Clast supported	1.0 - 2.0	-1.0
Unit R												
	R2	35.0 - 40.0	-5.0	0.3	0.3	ull / Fracture	Poorly sorted	Immature	Brick red	Clast supported	2.0 - 4.0	-2.0
	R3	2.0 - 3.0	-2.0	0.9	0.7	ull / Fracture	Well sorted	Mature	Brick red	Matrix supported	1/8 - 1/2	3.0
	R8	5.0 - 10.0	-2.0	0.5	0.7	ull / Fracture	Moderately sorted	Submature	Brick red	Matrix supported	1/4 - 1/2	2.0
	R9	10.0 - 40.0	-2.0	0.5	0.9	ull / Fracture	Very poorly sorted	Submature	Vivid red	Matrix supported	1/2 - 1.0	-1.0

Eastern Hand Samples

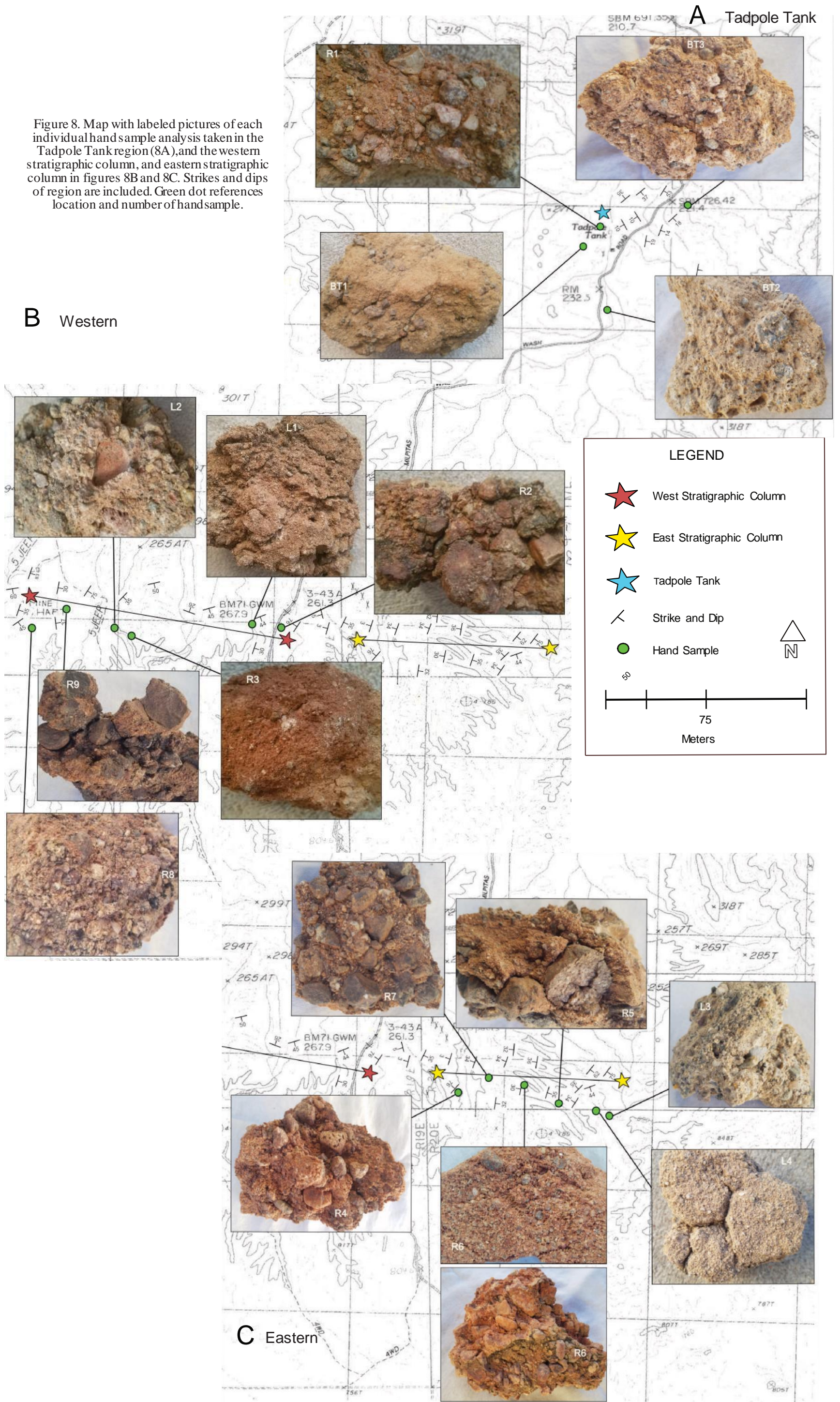|	Sample #	Clast Grain Size Average (mm)	Clast Phi Size	Clast Roundness	Clast Sphericity	Rock Texture	Sorting	Maturity	Color	Matrix type	Matrix Grain Size (mm)	Matrix Phi Size
Unit L												
	L3	2.0 - 10.0	-2.0	0.1	0.7	ull / Fracture	Moderately sorted	Submature	Tan	Matrix supported	1/2 - 1.0	1.0
	L4	1.0 - 3.0	-2.0	0.3	0.9	ull / Fracture	Well sorted	Submature	Tan/reddish	Matrix supported	1/4 - 1/2	2.0
Unit R												
	R4	10.0 - 40.0	-2.0	0.1	0.3	ull / Fracture	Very poorly sorted	Submature	Brick red	Matrix supported	1.0 - 2.0	-1.0
	R5	10.0 - 20.0	-2.0	0.1	0.7	ull / Fracture	Very poorly sorted	Submature	Dark red	Matrix supported	1/4 - 1/2	2.0
	R6.1	1/2 - 2.0	1.0	0.3	0.3	ull / Fracture	Well sorted	Submature	Brick red	Matrix supported	1/4 - 1/2	2.0
	R6.2	1/2 - 20.0	-2.0	0.5	0.3	ull / Fracture	Poorly sorted	Immature	Brick red	Clast supported	1/4 - 1/2	2.0
	R7	10.0 - 20.0	-4.0	0.3	0.9	ull / Fracture	Poorly sorted	Submature	Dark red	Matrix supported	1.0 - 2.0	-1.0

Tadpole Tank Hand Samples

	Sample #	Clast Grain Size Average (mm)	Clast Phi Size	Clast Roundness	Clast Sphericity	Rock Texture	Sorting	Maturity	Color	Matrix type	Matrix Grain Size (mm)	Matrix Phi Size
Unit BT												
	BT1	20.0 - 25.0	-2.0	0.3	0.7	ull / Fracture	Poorly sorted	Submature	Buff	Matrix supported	1/4 - 1/2	2.0
	BT 2	1.0 - 5.0	-2.0	0.5	0.9	ull / Fracture	Very poorly sorted	Submature	Light buff	Matrix supported	1/16 - 1/8	3
	BT3	5.0 - 10.0	-2.0	0.3	0.5	ull / Fracture	Moderately sorted	Submature	Light buff /reddish	Matrix supported	1/4	2.0
Unit R												
	R1	2.0 - 4.0	-2.0	0.5	0.7	ull / Fracture	Very poorly sorted	Submature	Orange red	Matrix supported	1.0 - 2.0	-1.0

Table 2. Rock hand sample analysis from the Western stratigraphic column, Eastern stratigraphic column, and the Tadpole Tank canyon. All samples were freshly fractured in the field.

Figure 8. Map with labeled pictures of each individual hand sample analysis taken in the Tadpole Tank region (8A), and the western stratigraphic column, and eastern stratigraphic column in figures 8B and 8C. Strikes and dips of region are included. Green dot references location and number of hand sample.

Figure 9. Labeled Roundness vs. Sphericity diagrams from hand sample qualitative analysis for western stratigraphic column and eastern stratigraphic column and Tadpole Tank. Samples found in Tadpole Tank had more rounded mature grains. Unit R samples found on the western stratigraphic are more texturally matures compared to the eastern stratigraphic column.
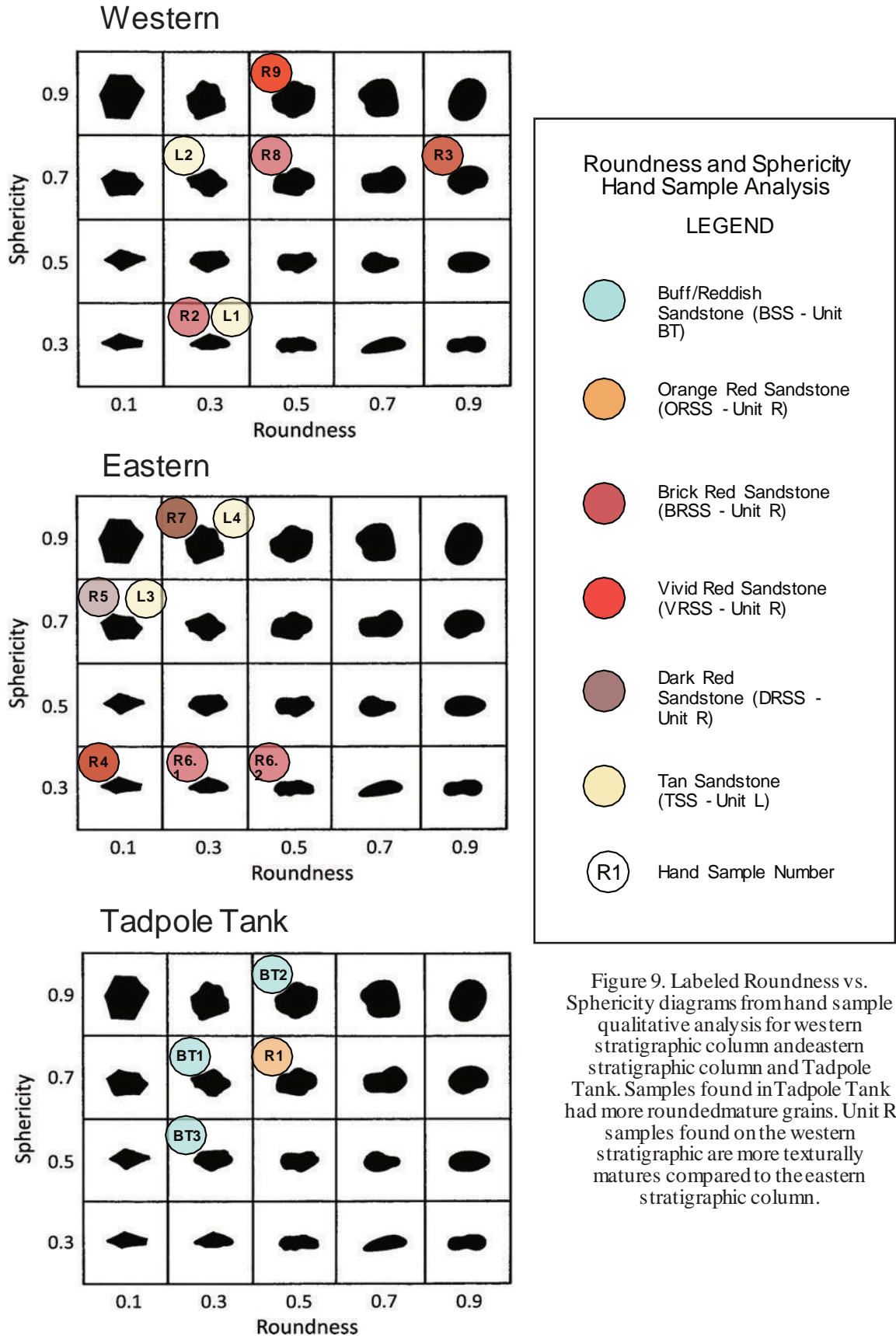
Hand Samples Locations - Unit R

Figure 10a. Hand sample R3 location within brick red sandstone (BRSS) sublayer and is part of the western stratigraphic column. White post-depositional layer (white arrow). Rockchisel for scale. (Left)

Figure 10b. Hand sample R9 location within vivid red sandstone (VRSS) sublayer, part of the west stratigraphic column. Large ripple or cut-and-fill structure (white arrow). Pencil for scale. (Right)

Figure 10c. Hand sample R5. Cemented finer grained matrix brick red sandstone on the eastern stratigraphic column with large cobbles (white arrow). Water bottle forscale. (Right)

Hand Samples Locations - Unit L and Tadpole Tank

Figure 11a. Hand sample L1 location within tan conglomerate sandstone sublayer Unit L and is part of the west stratigraphic column, White arrow showing desert varnish. Sharpie for scale.

Figure 11b. Zoom in on hand sample L2 on tan conglomerate sandstone Unit L. White arrow to show powdery, more rounded rocks. Pen for scale.

Figure 11c. Hand Sample L4 from tan conglomerate sandstone Unit L on the eastern stratigraphic column Showing erosional and trough channels. White arrow shows area of imbricated conglomerate and other sediments below a cut and fill structure. (Left)

Figure 11d. Brecciated rocks cover the surface throughout the beige conglomerate sandstone BT unit in a possible angular unconformity between alluvium in Tadpole Tank, shown with a white arrow. (Left)

Western and Eastern Stratigraphic Columns - Unit R - BRSS, VRSS and ORSS Pictures

Figure 12a. Outcrop of Unit R, Brick red conglomerate sandstone (BRSS) with postdepositional layers (white arrow) between BRSS layers.

Figure 12b Unit R vivid red conglomerate sandstone (VRSS) evidence of exfoliation (white arrow).

Figure 12c. Showing fluvial and erosional processes in orange red conglomerate sandstone (ORSS) of western stratigraphic column, similar to Tadpole Tank. GPS for scale. Shows interbedded conglomerates and sandstones, with gravel lenses present (white arrow).

Western and Eastern Stratigraphic Columns - Unit R - DRSS Pictures

Figure 13a. Ripples on BRSS Unit R outcrop on the eastern stratigraphic column along contact with BRSS and DRSS (white arrow). Water bottle for scale. (Top right)

Figure 13b. Dark red and brick red sandstone gradational layer. Shows ancient trough channels. Unit R crumbly packed matrix outcrop showcasing larger conglomerates and cobbles on the eastern stratigraphic column (white arrow). Water bottle for scale. (Left)

Figure 13c. Unit R dark red sandstone (DRSS) zoom in showing channel troughs (yellow dotted line, white arrow), as well as grain sizes and amount of matrix in unit.

Western and Eastern Stratigraphic Columns - Unit L Pictures

Figure 14a. (Left) Unit L light tan uplifted outcrop that has been oxidized and desert varnished (white arrow); evidence of exfoliation, fracturing and erosion. Grain sizes showcase predominantly matrix.
Brunton compass for scale.

Figure 14b (Right). Outcrop of Unit L, showing powdery consistency of recent layer of mud/fine sand that was deposited in this unit (white arrow). Shows angular/sub-angular grains. Jacob's staff for scale.

Figure 14c (Left). Unit L indication of trough channels. Size and color of clasts noticeable due to large conglomerates (white arrow). Individual clasts have cracks.
Notebook for scale.

Figure 14d (Right). Unit L outcrop showing planar bedding layers that are eroding in a sheet fracture way. White arrow dhows fine grain sediments with no clasts present. Brunton compass for scale.
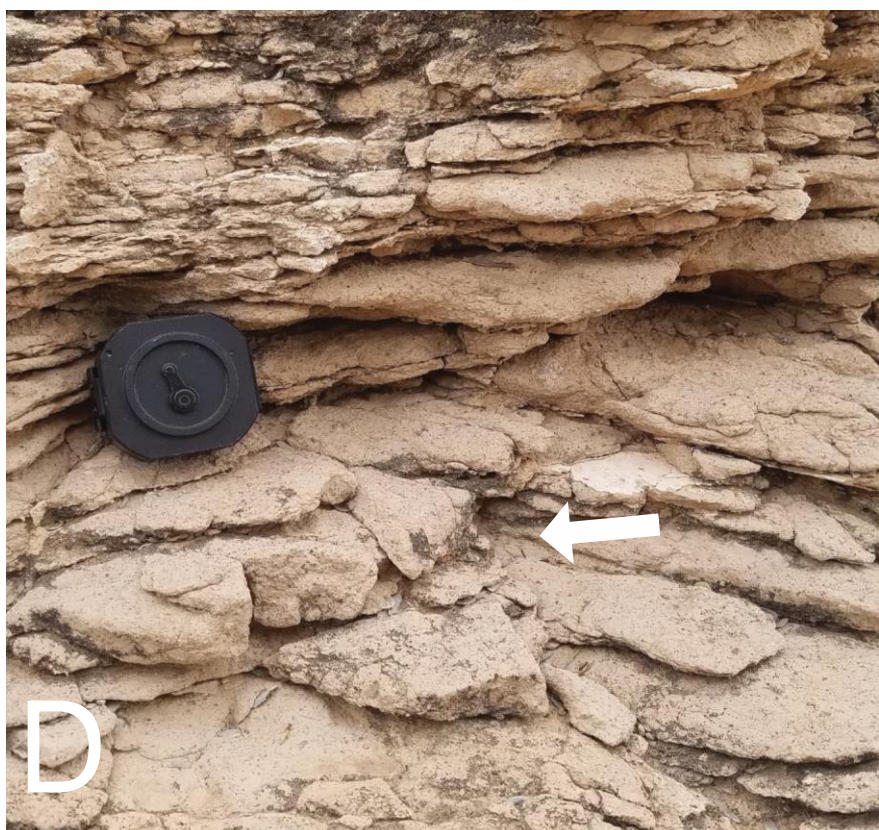
Tadpole Tank Unit BT and Unit R - ORSS Pictures
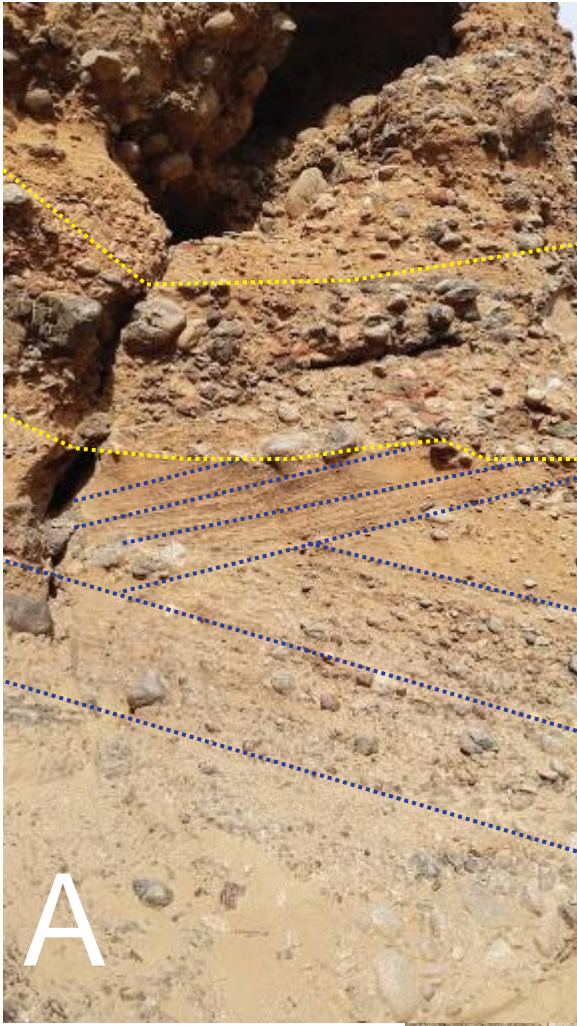
Figure 15a. Unit R Tadpole Tank entrance of canyon fed conglomerate walls. Evidence of different depositional events. (Left)
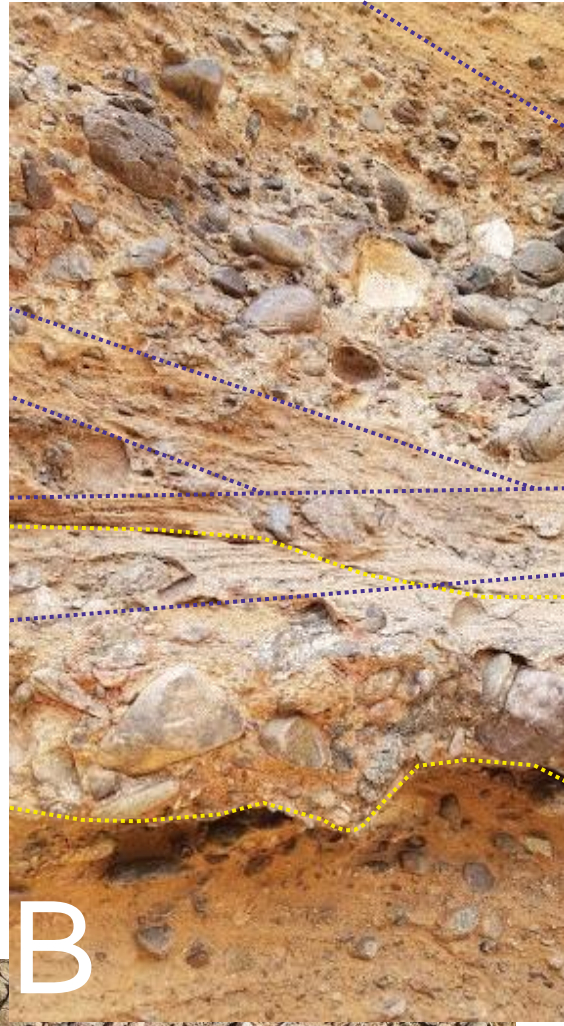
Figure 15b. Unit R Tadpole Tank entrance of canyon fed conglomerate walls. Evidence of erosion, subrounded to rounded clasts and multiple depositional events. (Right)
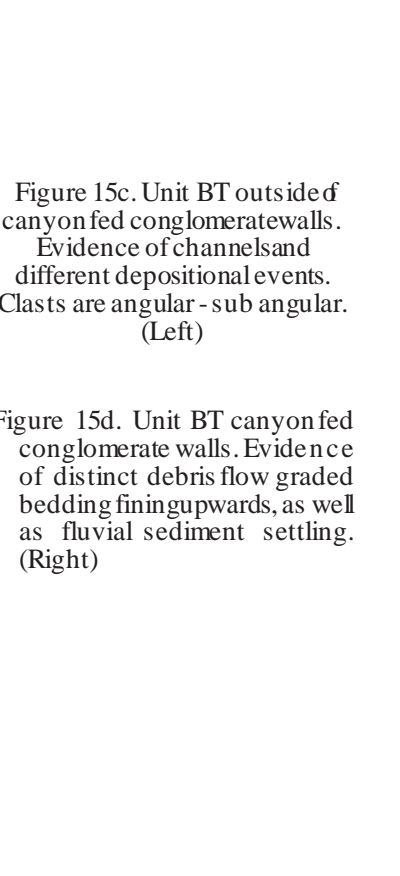
Figure 15c. Unit BT outside of canyon fed conglomerate walls. Evidence of channels and different depositional events. Clasts are angular - sub angular. (Left)
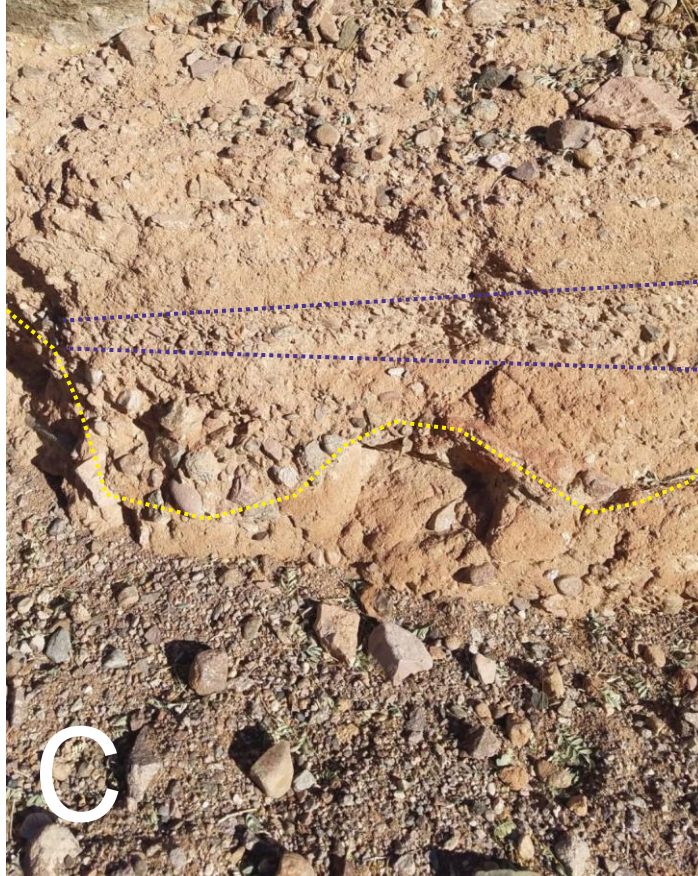
Figure 15d. Unit BT canyon fed conglomerate walls. Evidence of distinct debris flow graded bedding fining upwards, as well as fluvial sediment settling. (Right)
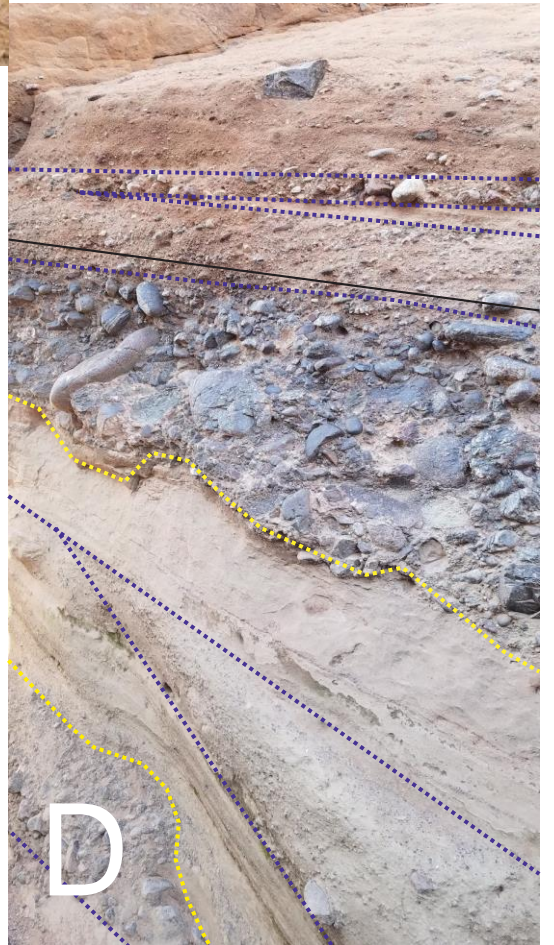
Figure 15e. Unit R orange red sandstone canyon fed conglomerate walls. Shows indication of trough channels, as well as evidence of water during seasonal heavy rains and sediment deposition occurring.

Clast Count Pictures - Stratigraphic Columns

Figure 16a. Clast Count 4 showcasing a bright vivid red matrix (VRSS) outcrop on the west stratigraphic column. Evidence of large cobbles (white arrow). (Left)

Figure 16b. Clast Count 4 with 2 x 2-foot net for counting analysis. (Bottom)

Figure 16c. Clast Count sixteen (CC16) crumbly finer grained brick red sandstone on the eastern stratigraphic column (white arrow). Sub-angular fine pebbled matrix and 10-20mm medium sized pebbles. GPS for scale.

Figure 16d. Unit L, clast count fourteen (CC14) location without net zoom in. Larger conglomerates found on the eastern stratigraphic column (white arrow). (Left)

Figure 16e. Unit L clast count fourteen (CC14) location with net. North arrow for scale and indicating north direction. (Right)

Clast Count Pictures - Tadpole Tank

Figure 17a. Unit R orange red sandstone (ORSS), clast count one (CC1) location in Tadpole Tank without net zoom in. White arrow shows large clast for comparison between A and B. Yellow lines represent fine sediment layer, interpreted as a decrease in transport energy. (Top)

Figure 17b. Unit R ORSS clast count one (CC1) location in Tadpole Tank with net. North arrow for scale.

Figure 17c. Unit BT of Tadpole Tank. Size and color of clasts noticeable due to large conglomerates presumed to be porphyritic rock fragments. Evidence of mafic lava that occurred in the area at one point in depositional history. North arrow for scale.

Grain Size vs. Paleocurrent Imbrication Map

Figure 18. Grain size versus clast imbrication paleocurrent measurements for (A) Tadpole Tank, as well as (B) the western stratigraphic column (red stars) and eastern, stratigraphic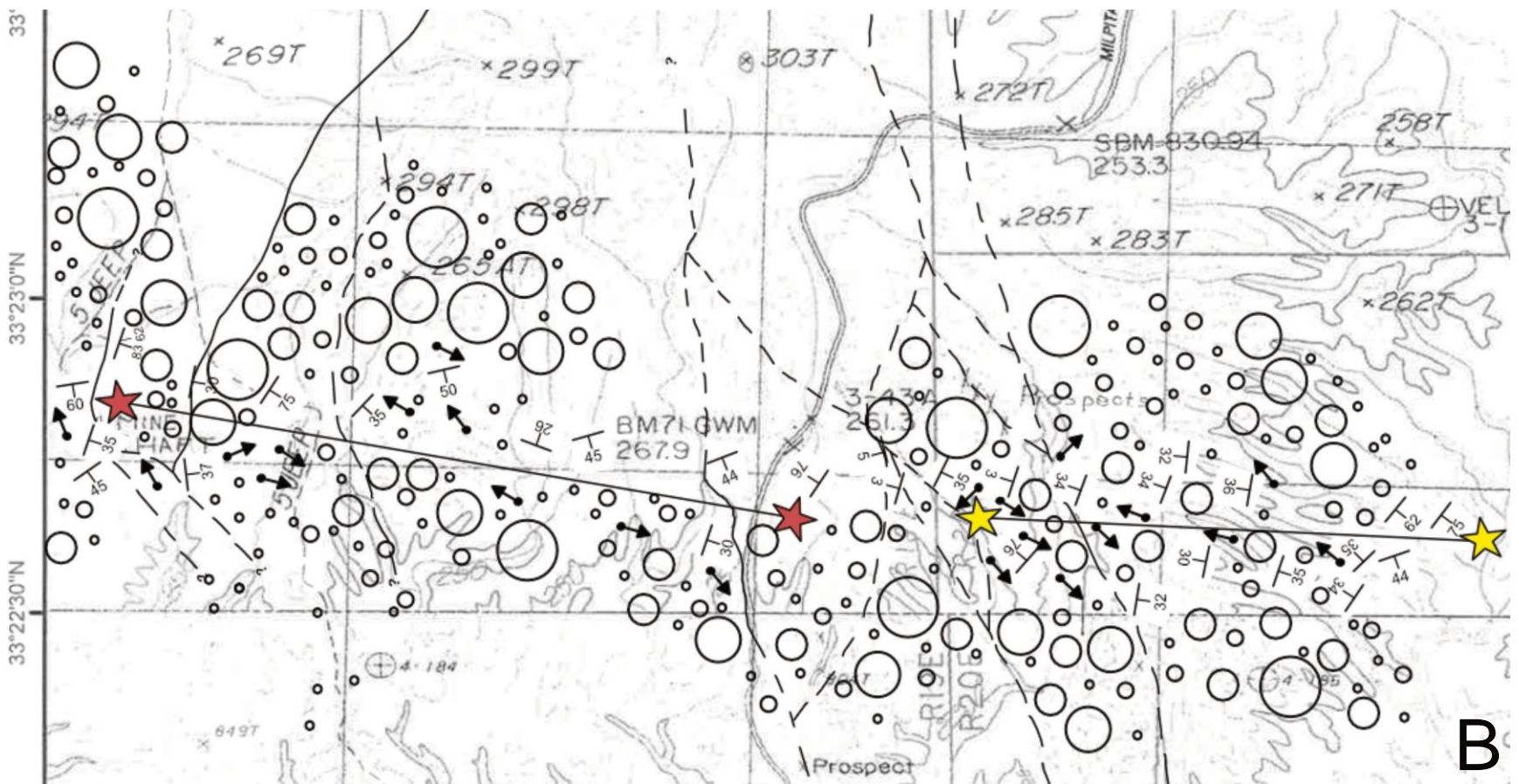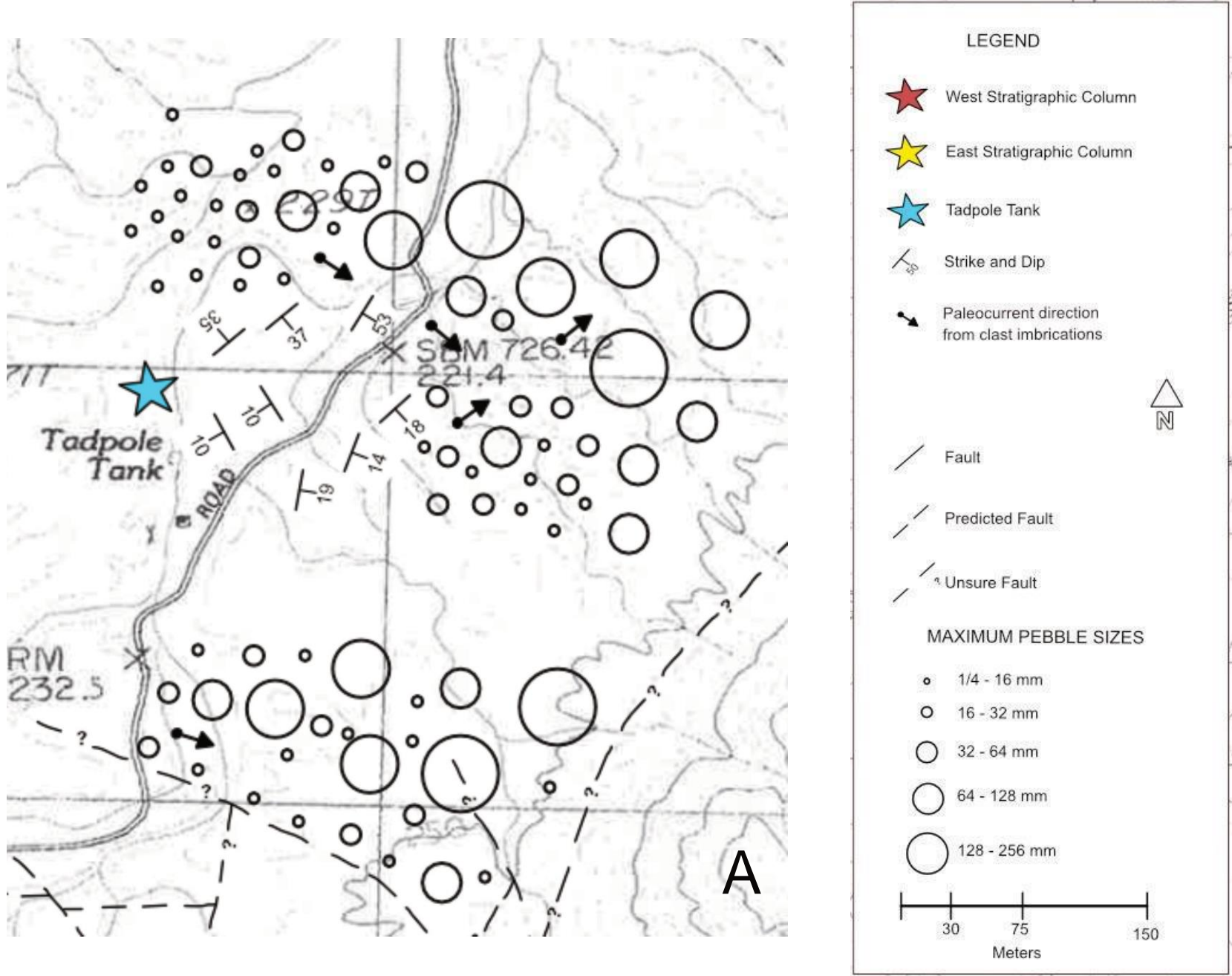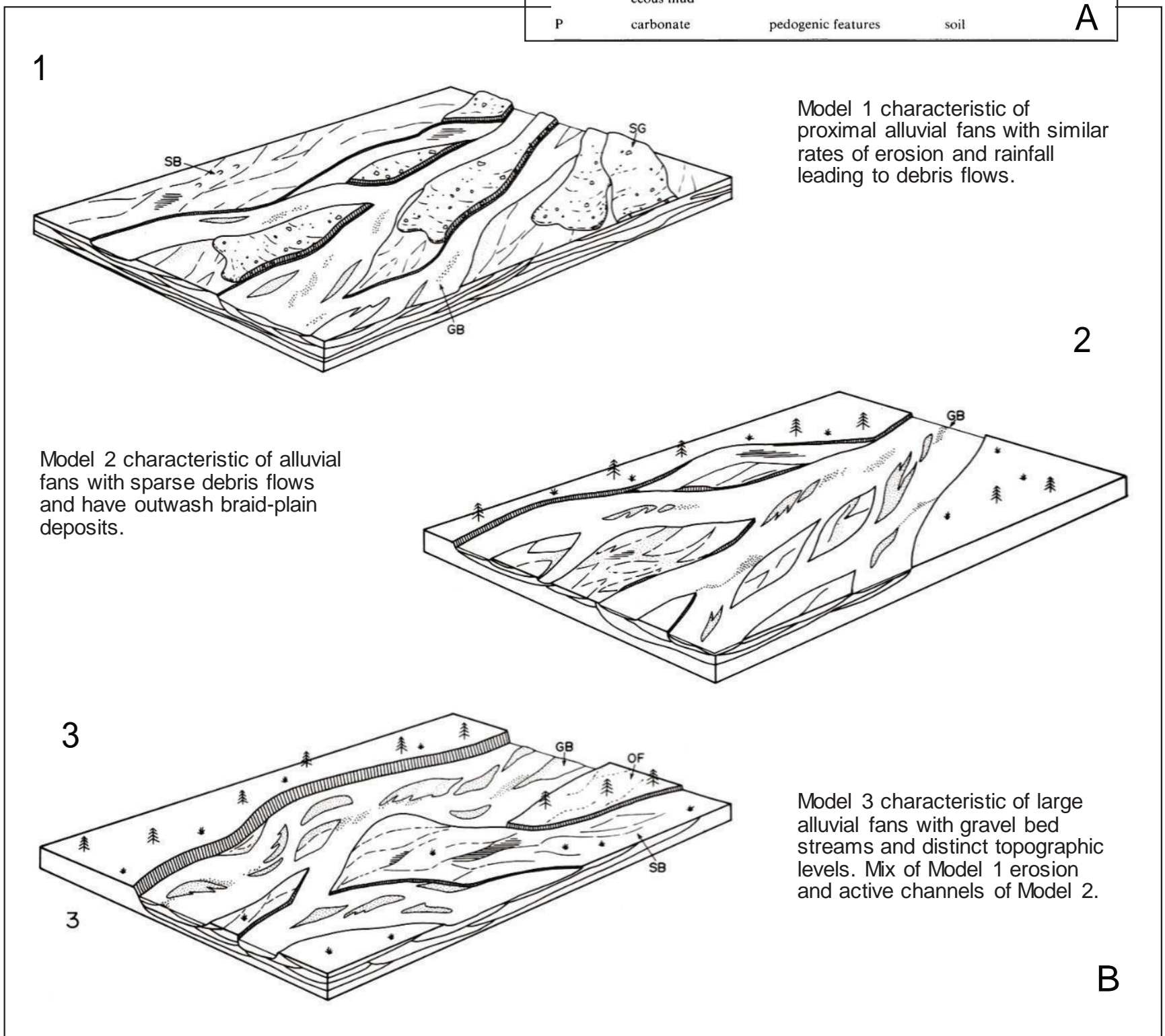 columns (yellow stars). Maps shows direction of paleoflow at (black arrow) coinciding with grain sizes found in each clast count location.

Alluvial Architecture

Figure 19a. Lithofacies classification for alluvial architecture-element model analysis. Taken from Miall (1975). Soledad Rojo formation shows evidence of lithofacies codes Gms, Gm, Gt, Sr, Ss, and Fm (left).

Figure 19b. Lithofacies model examples for alluvial architecture-element model analysis. Taken from Miall (1975). Soledad Rojo formation shows evidence of lithofacies codes Gms, Gm, Gt, Sr, Ss, and Fm, in ranging environments represented in models 1-3 (below).

Lithofacies classification, from Miall (1978)

Facies code	Lithofacies	Sedimentary structures	Interpretation
Gms	massive, matrix supported gravel	grading	debris flow deposits
Gm	massive or crudely bedded gravel	horizontal bedding, imbrication	longitudinal bars, lag deposits, sieve deposits
Gt	gravel, stratified	trough crossbeds	minor channel fills
Gp	gravel, stratified	planar crossbeds	linguoid bars or deltaic growths from older bar remnants
St	sand, medium to v. coarse, may be pebbly	solitary (theta) or grouped (pi) trough crossbeds	dunes (lower flow regime)
Sp	sand, medium to v. coarse, may be pebbly	solitary (alpha) or grouped (omikron) planar crossbeds	linguoid, transverse bars, sand waves (lower flow regime)
Sr	sand, very fine to coarse	ripple marks of all types	ripples (lower flow regime)
Sh	sand, very fine to very coarse, may be pebbly	horizontal lamination, parting or streaming lineation	planar bed flow (l. and u. flow regime)
Sl	sand, fine	low angle (<10°) crossbeds	scour fills, crevasse splays, antidunes
Se	erosional scours with intraclasts	crude cross-bedding	scour fills
Ss	sand, fine to coarse, may be pebbly	broad, shallow scours including eta cross-stratification	scour fills
Fl	sand, silt, mud	fine lamination, very small ripples	overbank or waning flood deposits
Fsc	silt, mud	laminated to massive	backswamp deposits
Fcf	mud	massive, with freshwater molluscs	backswamp pond deposits
Fm	mud, silt	massive, desiccation cracks	overbank or drape deposits
Fr	silt, mud	rootlets	seatearth
C	coal, carbonaceous mud	plants, mud films	swamp deposits
P	carbonate	pedogenic features	soil

A

1

Model 1 characteristic of proximal alluvial fans with similar rates of erosion and rainfall leading to debris flows.

2

Model 2 characteristic of alluvial fans with sparse debris flows and have outwash braid-plain deposits.

3

Model 3 characteristic of large alluvial fans with gravel bed streams and distinct topographic levels. Mix of Model 1 erosion and active channels of Model 2.

B

CHAPTER 5: Paleocurrent Measurements

Paleocurrent measurements were collected from the Soledad Rojo formation in the northern Tadpole Tank region and the two stratigraphic columns to determine potential sediment provenance directions, which suggests primarily southeasterly paleoflow directions into the basin. (Figure 5, Figure 7, and Figure 19). A total of 220 paleoflow measurements from 22 clast imbrication stations were collected from these study sites (Tables 3-7). A general observation of the field site before taking clast imbrication measurements inferred that clasts that are significantly larger, such as a meta-plutonic augen gneisses, which contain large pink feldspar crystals, tended to be more subangular and subrounded and are averagely NE dipping, and imbricated clasts that observationally looked to dip to the north-west were typically more rounded and of volcanic origin.

Total paleocurrent measurements for both stratigraphic columns and the Tadpole Tank region were compiled to establish an overall provenance description of the research basin, all implying multiple sources into the research area. The western stratigraphic column measurements rose diagram showcases the average paleoflow mean vector direction from each of the 10 individual stations collected (Figures 20-21).

Similarly, the eastern stratigraphic column, east of Milpitas Wash Road, overall direction was used from 9 individual station mean vector paleoflow directions (Figure 20 and Figure 22). At the Tadpole Tank, north of the stratigraphic columns along the Milpitas Wash Road, two distinct directions were displayed, with the mean vector averaging a $032.7° \pm 0.94°$ northeast paleoflow directional trend, as well as a large distribution of clasts also being transported southwest. These two opposite paleoflow

directions can be interpreted as provenance sources in the southwest direction, as well as to the northwest (Figure 23).

Paleocurrent data varied significantly per each clast count location on both sides of Milpitas Wash Road and the Tadpole Tank region (Figures 21-23). Clast imbrications corrected for tectonic tilt from the western stratigraphic column infers an average imbrication to be 130.8° ± 11.4° southeasterly for Unit R and 121.2° ± 20.3° southeasterly for Unit L (Figure 20, Tables 3-4). Clast imbrications from the eastern stratigraphic column indicates an average paleocurrent direction to be 121.1° ± 50.2° northsouth easterly for Unit R and 132.0° ± 13.9° southeasterly for Unit L (Figure 20, Tables

5-6). In the Tadpole Tank region (Figure 5), clast imbrication paleocurrent analysis infer an average imbrication and paleoflow direction to be 123.3° ± 24.7° southeast for the orange-red sandstone (ORSS) of Unit R, and an average imbrication and paleoflow direction to be 115.9° ± 38.5° northeasterly for Unit BT (Figure 20, Table 7).

Paleocurrent Measurements Interpretation

Interpretations were made using the Division of Mines Salton Sea geological map (Jennings, 1967) to locate possible provenance sources in the Soledad Rojo formation basin locally, based on the clast imbrication paleoflow measurements collected. The individual northwest paleoflow sterneonets from the western and eastern stratigraphic column clast imbrications and Tadpole Tank region (Figures 21-23) provide a proposed provenance to be in the southeasterly direction of mountains bounding the basin, such as the southern tip of the Palo Verde Mountains, the southern bend of Chocolate Mountains and proposed location of the Chocolate Mountains Anticlinorium (Bennett et al, 2016),

the Midway Mountains, or further east towards the Gila Mountains in the Arizona and

Sonora Desert, along the Mexico border (Figure 2, Figure 30). Individual north east -

south easterly paleoflow clast imbrications taken on the western and eastern column

inferred an overall western provenance direction. The southeasterly paleoflow direction

can be hypothesized as the Mule Mountains, Black Hills Mountains, or Little Chuckwalla

Mountains to the northwest as provenance options if locally sourced, or to the southwest

within the Chocolate Mountains, as interpreted from the north east paloflow measured.

These act as possible sources for tuffaceous rocks and metaplutonic rocks within each of

the stratigraphic columns (Figure 2, Figure 30). This observation may infer deposition

from a gravity flow event, traveling east.

Clast assemblages varied in stereonet directions for Unit L within the western and

eastern stratigraphic columns (Figure 7). Exposed outcrops in the tan conglomeratic

sandstones of Unit L on both sides of Milpitas Wash Road showcased conflicting clast

imbrications with an easterly paleoflow direction, inferring a southwest-westerly

provenance direction, however also showcases with a northwest paleoflow directions

inferring a south easterly provenance source (Figure 2, Figure 30). Clast assemblages and

grain sizes varied in stereonet directions for Unit R on the western and eastern

stratigraphic columns, interpreted as having multiple sources due to the northeast,

southeast, and westerly paleoflow directions measured (Figure 19).

Paleocurrent Measurements - Unit R (West)				
BEDDING	STRIKE	DIP	CLAST COUNT NUMBER	OBSERVATIONS
N25E 55NW	--	--	--	R/Tuff contact
N75E 60SE	S221W	10NW	2	90mm volcanic, WP #14 & WP #15
--	--	--	2	WP #15
--	--	--	2	WP #15
--	N50E	32SE	2	20 mm rhyolite, light tan, subangular
--	N10E	24SE	2	10mm volcanic
--	S221W	10NW	2	90mm volcanic black and white
--	N65E	15SE	2	80mm chert fine grained light gray subangular/ subrounded
--	S190W	25NW	2	40mm volcanic, rounded elongated, black
--	S258W	23NW	2	30mm diorite white subangular crystalline
--	S170E	17SW	2	70mm gneiss subrounded
--	S210W	16NW	2	240mm diorite, black and white crystals, subrounded; WP #16
--	N15E	35SE	2	25mm quartzite, white, subrounded
--	S241W	20NW	2	55mm gneiss, angular; WP #17
--	N8E	68SE	2	20mm red tuff, vesicular
--	S230W	35NW	2	90mm volcanic, red, subangular/angular; WP #18
--	S223W	26NE	2	30mm volcanic, white, subrounded; WP #19
--	N43E	26SE	2	12mm clast, subrounded
S245W 45NW	--	--	3	Brick red sandstone, very fine, matrix supported, rounded/subrounded; WP #27
--	N45E	15SE	3	30mm volcanic
--	S225W	25NW	3	50mm volcanic
--	S193W	36NW	3	75mm basalt, black, subrounded
--	N11E	12SE	3	80mm gneiss
--	S230W	7NW	3	30mm gneiss subrounded
--	N282W	21NE	3	30mm augen gneiss
--	N355W	12NE	3	25mm chert
--	N12E	30SE	3	50mm volcanic
--	S130E	32SW	3	30mm gneiss
S177E 37SW	S200W	20NW	4	60mm augen gneiss, rounded; WP #33
--	S190W	35NW	4	50mm chert, rounded/subrounded; WP #33
--	N66E	17SE	4	30mm volcanic subangular/ subrounded
--	N88E	34SE	4	10mm chert black rounded subrounded
--	S233W	28NW	4	10mm schist subrounded
--	N10E	7NW	4	55mm black volcanic, subangular; WP #33
--	S215W	48NW	4	70mm granodiorite, angular; WP#33
--	N9E	30SE	--	Red sandstone, graded bedding; WP #34
N25E 75SE	N315W	52NE	6	40mm green volcanic, subrounded; WP #36
--	S205W	57NW	6	55mm black tuff
--	N25E	55SE	6	45mm black/white diorite
--	S135E	45SW	6	85mm black pumice, smooth, vesicular
--	N301W	34NE	6	55 mm volcanic
--	S118E	35SE	6	110 granodiorite, black and white; rounded
--	N13E	26SE	6	95mm green basalt
--	N295W	38NE	6	35mm gabbro black
--	S155E	12SW	6	35mm black basalt; rounded
N45E 35SE	S152E	56SW	7	25mm gneiss, subrounded; WP#42
--	S122E	75SW	7	10mm augen gneiss, subangular; WP#42
--	N332W	62NE	7	15mm basalt black rounded
--	N345W	32NE	7	25mm volcanic, rounded; WP#42
--	N272W	10NE	7	12mm pink tuff
N65E 50SE	--	--	8	Red sandstone; WP #48
--	N69E	76SW	8	80mm pink tuff volcanic
--	S205W	50NW	8	100mm gneiss
--	N30E	66SE	8	110mm pink tuff
--	S192W	57NW	8	65mm smooth black tuff
--	S162E	55SW	8	120mm pink tuff
--	N32E	8SE	8	95mm wacke subrounded
--	S178E	32SW	8	60mm augen gneiss
N61E 45SE	N312W	14NE	10	brick red sandstone
--	N11E	71SE	10	80mm schist subangular
--	S118E	15SW	10	110mm augen gneiss
--	S126E	36SW	10	60mm quartzite
--	N342W	22NE	10	15mm wacke

Table 3. Paleocurrent indicators (clast imbrications) of the red sandstones Unit R from the Western Stratigraphic column. All measurements were taken during the construction of clast counts. A Brunton compass was used to measure the clast imbrications.

Paleocurrent Measurements - Unit L (West)				
BEDDING	STRIKE	DIP	CLAST COUNT NUMBER	OBSERVATIONS
N9E 30SE	N320W	20NE	5	10mm brown chert, subangular; WP #32
--	S149E	17SW	5	30mm red rhyolite, subangular; WP #32
--	N32E	16SE	5	10mm black basalt angular
--	N325W	65NE	5	5mm black basalt, subrounded
--	N320W	20NE	5	12mm chert brown, subangular
--	N21E	55SE	5	13mm volcanic
--	N79E	21SE	5	30mm green basalt subrounded
--	N311W	8NE	5	11mm pink volcanic tuff, subrounded; WP #32
--	S110E	21SW	5	10mm augen gneiss, subangular; WP #32
--	S211W	51NE	5	14mm volcanic subangular
--	N85E	30SE	5	15mm chert rounded
--	N280W	12NE	5	25mm chert; subangular; WP #32
--	N15E	30SE	5	10mm augen gneiss
--	N300W	16NE	5	50mm black volcanic, subangular; WP #32
N61E 44SE	N315W	12NE	9	70mm granodiorite black and white, angular; WP #44
--	N24E	37SE	9	80mm gneiss
--	N62E	20SE	9	20mm augen gneiss
--	N302W	11NE	9	110mm pink tuff, rounded; WP #44
--	S162E	24SW	9	90mm gneiss, subangular; WP #44
--	S158E	66SW	9	75mm gneiss
--	N297W	18NE	9	120mm chert black
--	N288W	21NE	9	45mm augen gneiss
--	S125E	32SW	9	95mm volcanic, rounded; WP #44
--	S110E	51SW	9	90mm pink tuff
--	N47E	13SE	9	10mm subrounded gneiss
--	S100E	21SW	9	10mm volcanic, rounded; WP #44
N9E 30SE	N320W	18NE	22	30mm schist
--	N65E	12SE	22	40mm pink tuff
--	S210W	25NW	22	15mm schist
--	S186W	26NW	22	35mm tuff
--	S120E	72SW	22	35mm gneiss
--	N12E	31SE	22	10mm schist
--	N7E	50SE	22	8mm quartzite
--	N297W	16NE	22	55mm black tuff

Table 4. Paleocurrent indicators (clast imbrications) of the tan sandstone Unit L from the Western Stratigraphic column. All measurements were taken during the construction of clast counts. A Brunton compass was used to measure the clast imbrications.

Paleocurrent Measurements - Unit R (East)				
BEDDING	STRIKE	DIP	CLAST COUNT NUMBER	OBSERVATIONS
S215W 76NW	--	--	--	Red sandstone outcrop, hard rock
N350W 5SW	--	--	--	Red sandstone outcrop, white calcite layers
S190W 3NW	--	--	--	Red sandstone, matrix supported
S210W 35NW	--	--	--	Unit R/Unit L contact
S190W 3NW	N15E	10SE	11	155mm schist, subrounded; WP #63
--	S200W	40NW	11	230mm volcanic, rounded; WP #63
--	N5E	30SE	11	50mm granodiorite, black and white, subrounded; WP #63
--	S265W	20NW	11	95mm schist subrounded
--	S302W	24NE	11	65mm pink ignimbrite, subangular/subangular; WP #63
--	N351W	51NE	11	100mm ignimbrite
--	N332W	40NE	11	160mm schist, subangular; WP #63
S215W 76NW	N29E	32SE	12	20mm brown chert; subrounded; WP #64
--	N350W	55NE	12	100mm ignimbrite
--	N24E	66SE	12	15mm schist
--	N5E	43SE	12	80mm andesite
--	N349W	54NE	12	45mm pink ignimbrite, rounded; WP #64
--	N310W	57NE	12	30mm schist subrounded
--	N56E	35SE	12	65mm augen gneiss, subrounded; WP #64
--	N68E	86SE	12	10mm volcanic rounded
--	S210W	45NW	12	95mm chert gray
--	N312W	57NE	12	120mm schist, subrounded; WP #64
S195W 34NW	N310W	47NE	13	55mm gneiss, subrounded; WP #65
--	N345W	52NE	13	35mm schist
--	S105E	74SW	13	15mm ignimbrite
--	N70E	20SE	13	60mm augen gneiss
--	N12E	30SE	13	50mm green basalt
--	S215W	45NW	13	25mm wacke, subrounded; WP #65
S195W 34NW	--	--	15	Red sandstone, grain supported, crumbly matrix
S183W 30NW	--	--	15	Red sandstone, grain supported, crumbly matrix
--	N310W	45NE	15	23mm pink ignimbrite, subrounded
--	S208W	41NW	15	36mm green basalt
--	N315W	45NE	15	55mm schist
--	N355W	28NE	15	80mm schist, subrounded
--	S242E	75NW	15	45mm augen gneiss
--	N77E	12SE	15	90mm schist
--	N56E	30SE	15	75mm augen gneiss
--	N28E	77SE	15	62mm black volcanic, subrounded
S183W 36NW	N280W	32NE	16	13mm augen gneiss, subrounded; WP #67
--	N32E	54SE	16	20mm schist
--	N320W	24NE	16	20mm wacke
--	S182W	21NW	16	18mm schist
--	S260W	25NW	16	20mm schist, subrounded; WP # 67
S183W 32NW	S195W	15NW	17	45mm schist, subangular; WP #68
--	S210W	33NW	17	30mm gneiss
--	N315W	48NE	17	45mm schist
--	N355W	25NE	17	35mm schist
--	S195W	18NW	17	30mm schist
--	S165E	80SW	17	50mm augen gneiss
--	S170E	20SW	17	40mm black, volcanic, rounded; WP #68

Table 5. Paleocurrent indicators (clast imbrications) of the red sandstones Unit R from the Eastern Stratigraphic column. All measurements were taken during the construction of clast counts. A Brunton compass was used to measure the clast imbrications.

Paleocurrent Measurements - Unit L (East)				
BEDDING	STRIKE	DIP	CLAST COUNT NUMBER	OBSERVATIONS
N293W 25NE	--	--	BCC 1	Tan sandstone, pebbles, matrix supported
S190W 45NW	--	--	BCC 1	Tan sandstone, fine grain, matrix supported
S183W 32NW	N280W	30NE	14	30mm black volcanic, subangular; WP #66
--	S117E	18SW	14	75mm schist subangular
--	S170E	45SW	14	80mm augen gneiss, subangular; WP #66
--	N42E	61SE	14	15mm schist subangular
--	N305W	30NE	14	30mm ignimbrite
--	N57E	60SE	14	25mm pink ignimbrite, rounded; WP #66
--	N41E	52SE	14	15mm schist; subangular/subrounded; WP #66
N10E 35SE	N20E	30SE	18	50mm augen gneiss, subrounded; WP #69
--	N35E	10SE	18	30mm schist
--	N290W	32NE	18	42mm pink volcanic
--	N40E	60SE	18	30mm gneiss
--	N320W	30NE	18	35mm black volcanic
--	N322W	25NE	18	30mm green basalt, rounded; WP #69
--	N69E	66SE	18	40mm schist, subrounded; WP #69
--	N355W	82NE	18	45mm black volcanic, rounded; WP #69
S245W 35NW	N12E	40SE	19	190mm gneiss, subangular; WP #72
	N24E	10SE	19	75mm schist subangular
--	S100E	89NW	19	80mm augen gneiss, subangular; WP #72
--	N315W	30NE	19	30mm pink ignimbrite, rounded; WP #72
--	N15E	64SE	19	150mm schist, subangular, WP #72
--	S115E	20SW	19	170mm schist, subangular; WP #72
S240W 34NW	--	--	--	WP# 84
N5E 65SE	N357W	23NE	--	WP #90
--	N41E	24SE	--	
N61E 44SE	N14E	26SE	--	WP #92
--	S98E	18SW	--	WP #93
--	N320W	35NE	--	
--	S137E	72SW	--	
N35E 62SE	N350W	80NE	--	WP #94
--	N66E	64SE	--	
--	N74E	46SE	--	
--	N307W	88NE	--	
--	N55E	55SE	--	
N27E 75SE	S211W	80NW	--	WP #95
--	S198W	29NW	--	
--	N15E	20SE	--	

Table 6. Paleocurrent indicators (clast imbrications) of the tan sandstone Unit L from the Eastern Stratigraphic column. All measurements were taken during the construction of clast counts. A Brunton compass was used to measure the clast imbrications.

Paleocurrent Measurements - Tadpole Tank				
BEDDING	STRIKE	DIP	CLAST COUNT NUMBER	OBSERVATIONS
N42E 37SE	S107E	66SW	BCC 1	65mm black volcanic, rounded
--	N68E	86SE	BCC 1	150mm green volcanic, subrounded
--	N88E	75SE	BCC 1	40mm black and white meta-volcanic, subangular
--	N311W	26NE	BCC 1	120mm black and white meta-volcanic, subrounded
--	N30E	66SE	BCC 1	15mm, pink tuff, smooth, rounded
--	N74E	40SE	BCC 1	80mm black and white meta-volcanic, rounded
--	N55E	73SE	BCC 1	100mm green volcanic, subangular
--	N291W	71NE	BCC 1	200 gneiss, subangular
--	N67E	81SE	BCC 1	150mm tuff, rounded
--	N356W	75NE	BCC 1	75mm volcanic, rounded
--	N321W	62NE	BCC 1	40mm sedimentary, angular/subangular
--	N72E	65SE	BCC 1	80mm black volcanic, rounded
--	N65E	64SE	BCC 1	20mm red sandstone, subangular
--	N32E	85SE	BCC 1	200mm augen gneiss, subangular/subrounded
N20E 53SE	N348W	68NE	1	200mm pink felsic granite, rounded/subrounded
--	S102E	68SW	1	30 mm green basalt/ subrounded / rounded
--	N5E	27SE	1	30mm white volcanic, subrounded/subangular
--	N12E	32SE	1	30mm black and green volcanic, rounded
--	S200W	20NW	1	20mm quartzite/ subrounded/rounded NW orientation
--	N4E	54SE	1	55mm quartzite, rounded/subrounded
--	N322W	35NE	1	40mm augen gneiss, rounded
--	N7E	57SE	1	70mm augen gneiss, rounded
--	N20E	45SE	1	70mm augen gneiss, subrounded
--	N310W	45NE	1	60mm granite, subrounded
--	S174E	28SW	1	100mm augen gneiss, Feldspar 60mm, angular/subangular
--	N355W	26NE	1	20mm black andesite with fine grain matrix 2mm or less
--	S200W	70NW	1	20mm augen gneiss pink and black, crystals around 15mm
--	N28E	77SE	1	60mm black pumice, smooth, round
--	S168E	65SW	1	350mm augen gneiss, Feldspar 15mm, rounded, subrounded
--	N46E	53SE	1	85mm granite, rounded
--	N311W	61SE	1	50mm black volcanic, smooth, round
S213W 35NW	N345W	80NE	--	
--	N310W	45SW	--	
--	S213W	35SE	--	
--	S275W	20NE	--	
N334W 10SW	S215W	78NW	20	95 mm granodiorite WP #78
--	--	--	20	
--	--	--	20	
--	N278W	67NE	20	90mm granodiorite WP #78
--	N348W	14NE	20	190mm andesite scoria red vesicular volcanic WP #78
--	S215W	78NW	20	95mm granodiorite
--	S190W	65NW	20	110mm andesite scoria purple vesicular volcanic WP #78
--	S166E	46SW	20	65mm basalt black vesicular volcanic WP #78
--	N15E	14SW	20	55mm andesite scoria red vesicular volcanic WP #78
--	S164E	46SW	20	45mm basalt black vesicular volcanic WP #78
N334W 10SW	S251E	82NE	21	100mm granodiorite
--	N46E	22SE	21	145mm granodiorite
--	N70E	55SE	21	110mm green basalt vesicular
--	S200W	45NW	21	90mm schist
--	S222W	57NW	21	30mm quartzite
--	S155E	41SW	21	125mm andesite scoria red vesicular
--	N7E	18SE	21	30mm black volcanic

Table 7. Paleocurrent indicators (clast imbrications) from the Tadpole Tank canyon. All measurements were taken during the construction of clast counts. A Brunton compass was used to measure the clast imbrications.

Western Stratigraphic Column
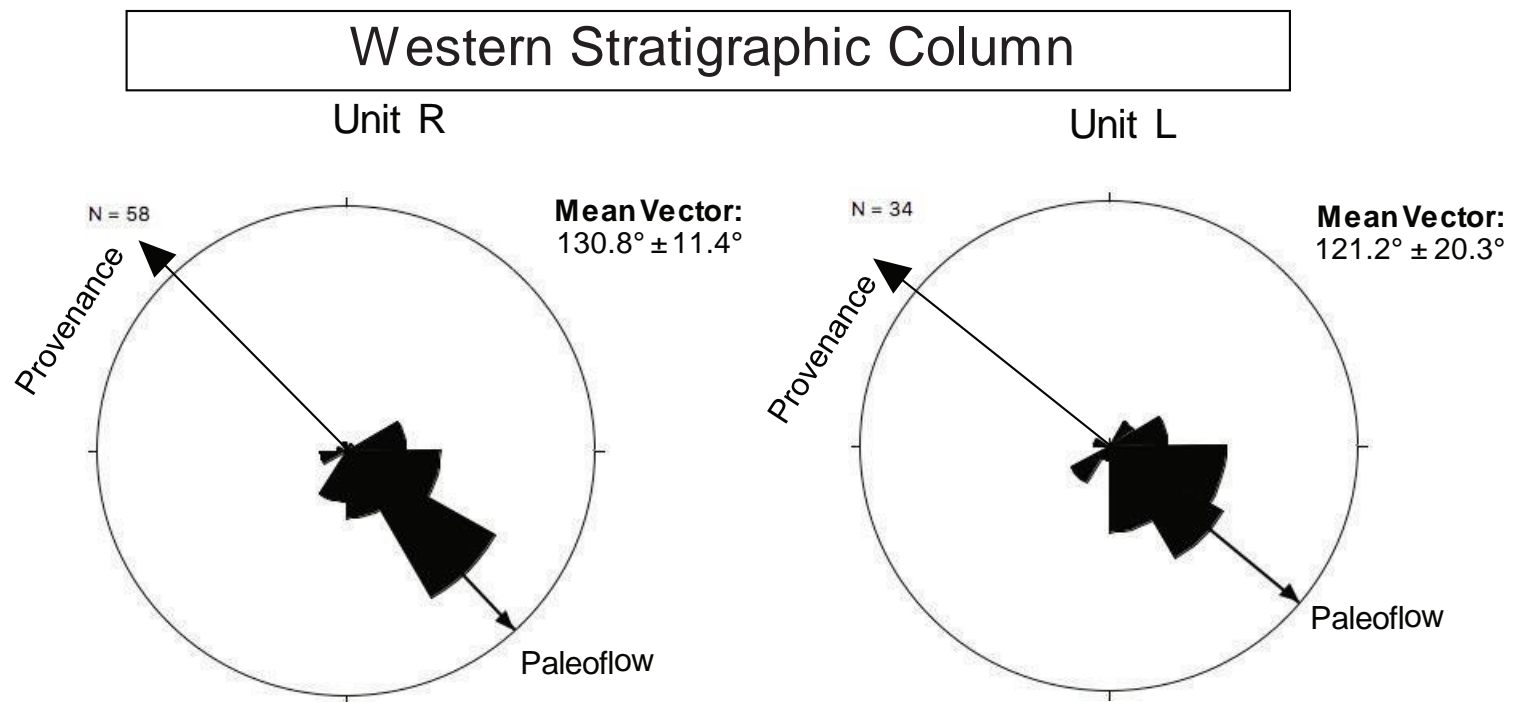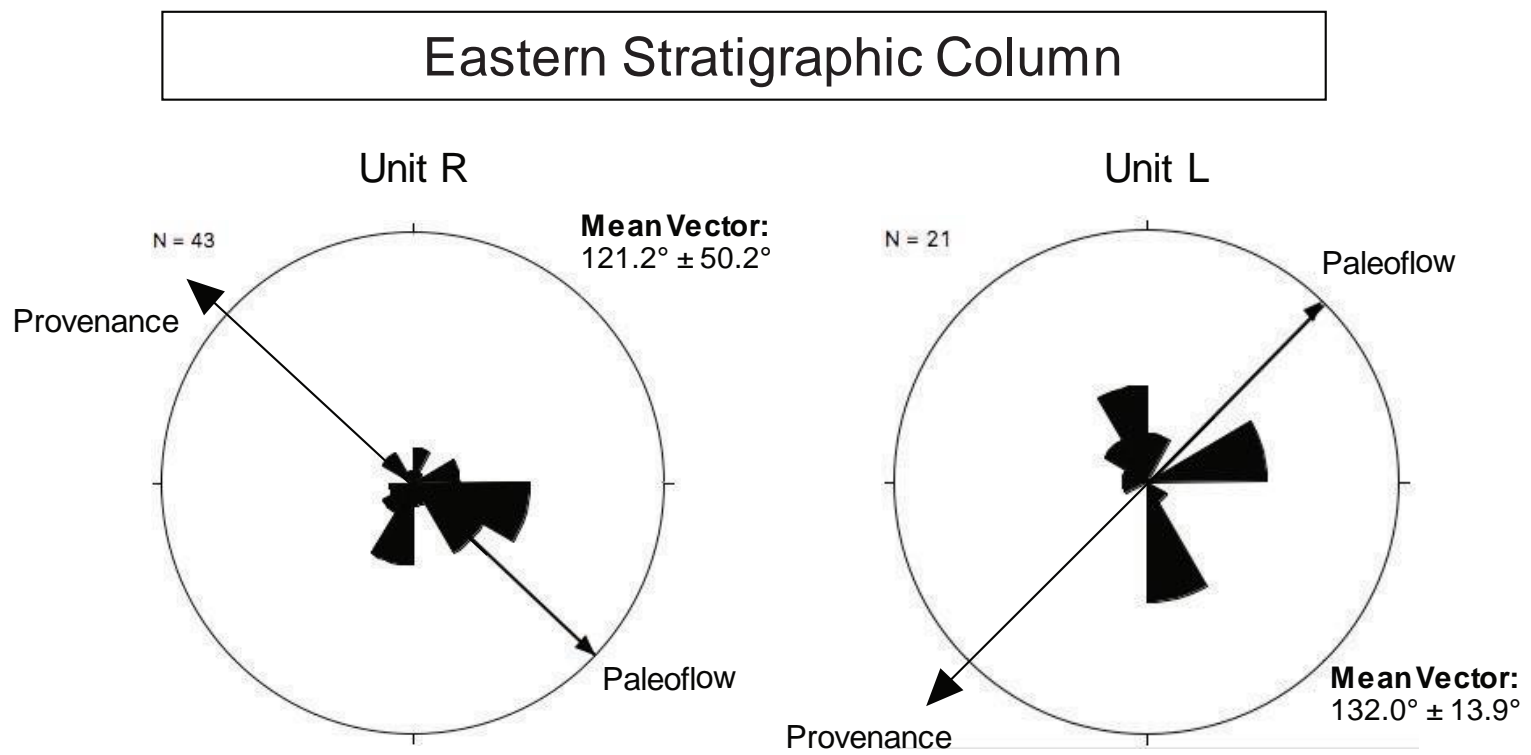
Unit R

Unit L

Figure 20a. Paleocurrent total results from clast imbrication measurements from Unit R and Unit L in the western stratigraphic column. Stereonet for Unit R infer a southeast paleoflow direction; Taken while completing CC2 - CC5, CC6 - CC8 and CC10. The southeast 130.8° ± 11.4° mean vector for Unit R coincides with the measured paleoflow direction determined. Stereonet for Unit L infer a southeast paleoflow direction; Taken while completing CC5, CC9 and CC22. The southeast 121.2° ± 20.3° mean vector for Unit L coincides with the measured paleoflow direction. N represents the number of a determined direction using paleocurrent clast imbrications. Large arrow indicates provenance direction.

Eastern Stratigraphic Column

Unit R

Unit L

Figure 20b. Paleocurrent total results from clast imbrication measurements from Unit R and Unit L in the eastern stratigraphic column. Stereonet for Unit R infer a southeast paleoflow direction; Taken while completing CC11 - CC13 and CC15 - CC17. The southeast 121.2° ± 50.2° mean vector for Unit R coincides with the measured paleoflow direction determined. Stereonet for Unit L infers a southwest paleoflow direction; Taken while completing CC14, CC18 and CC19. The northeast 132.0° ± 13.9° mean vector for Unit L matches with the rose diagram, however does not match with paleoflow direction. N represents the number of determined directions using paleocurrent clast imbrications. Large arrow indicates provenance direction.

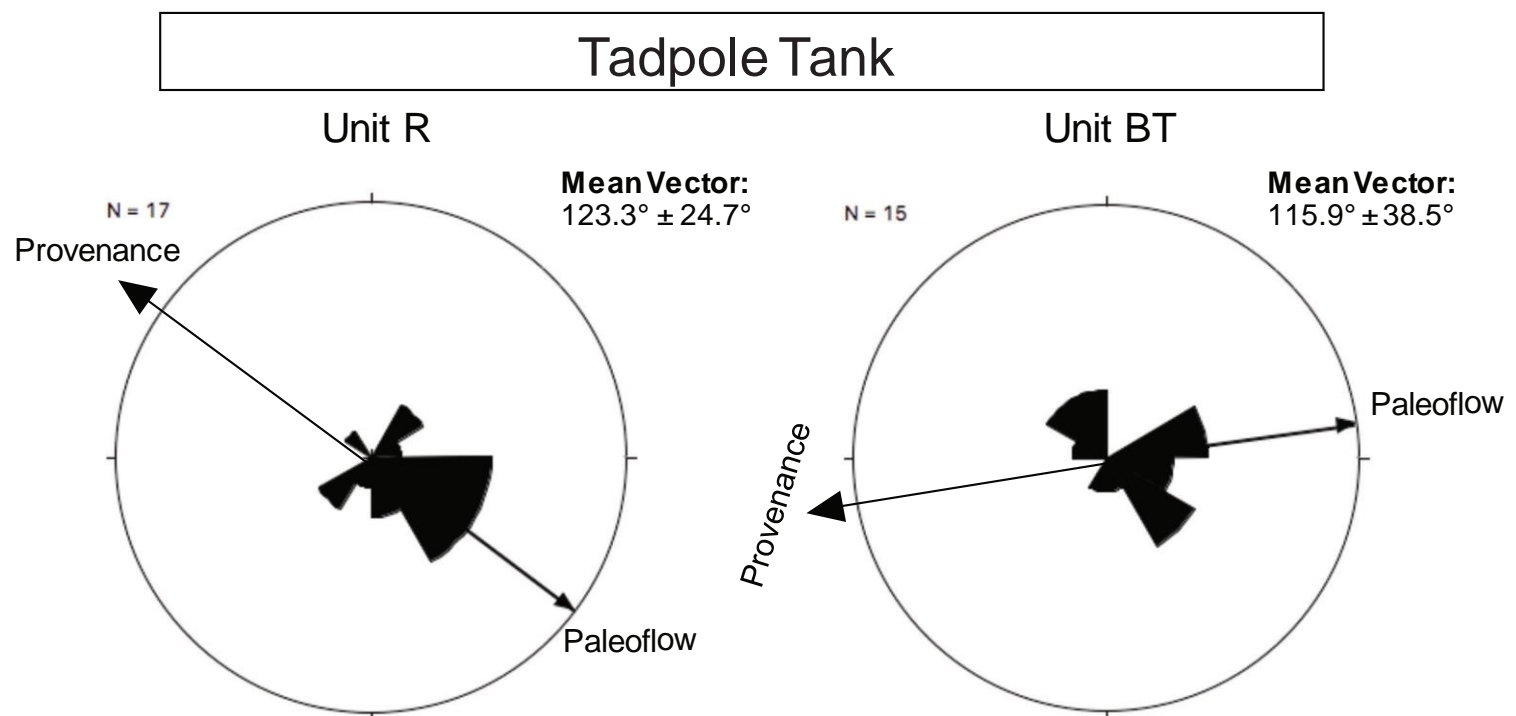## Tadpole Tank

Unit R

Unit BT

Figure 20c. Paleocurrent total results from clast imbrication measurements from Unit R and Unit BT in the Tadpole Tank region. Stereonet for Unit R infer a southeast paleoflow direction; Taken while completing CC1. The southeast 123.3° ± 24.7° mean vector for Unit R coincides with the measured paleoflow direction determined. Stereonet for Unit BT infer a northeast-easterly paleoflow direction; Taken while completing CC20 and CC21. The northeast 115.9° ± 38.5° mean vector coincides with the measured paleo direction determined. N represents the number of a determined direction using paleocurrent clast imbrications. Large arrow indicates provenance direction.
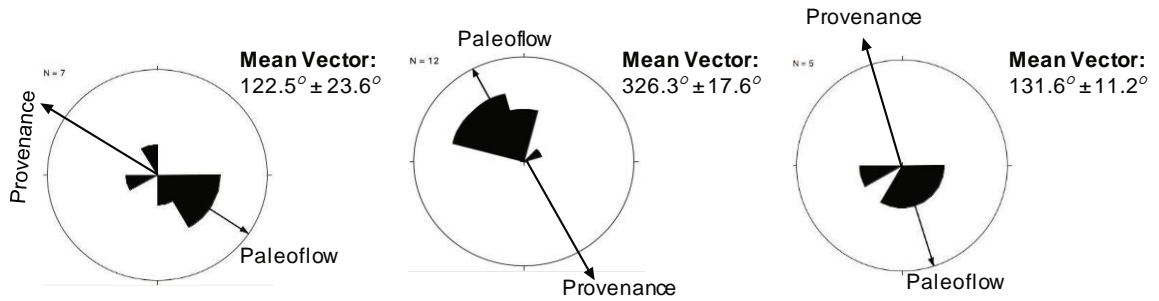
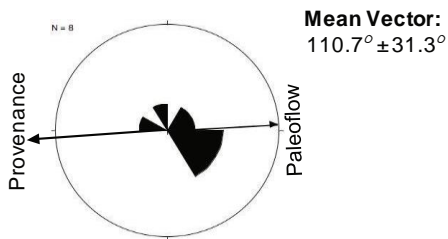## West Stratigraphic Column: Unit L & Unit R: Paleocurrent Measurements
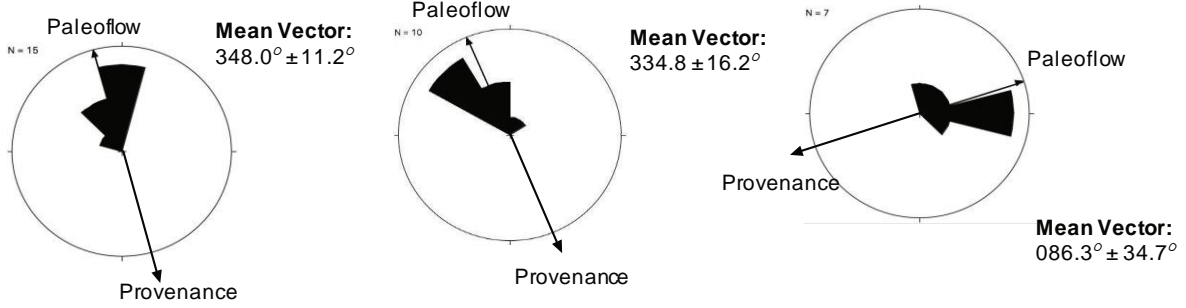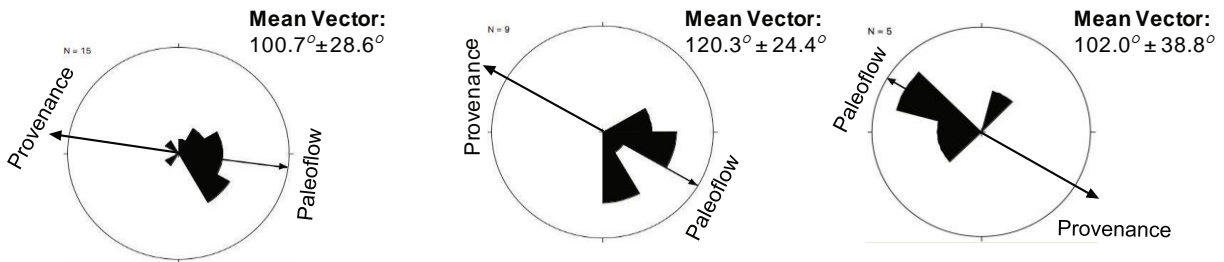
Figure 21. Labeled individual paleocurrent measurements of Unit L and Unit R in the western stratigraphic column (Tables 3-4). N represents the number of a determined direction using paleocurrent clast imbrications. Large arrow indicates provenance direction.

East Stratigraphic Column: Unit L & Unit R: Paleocurrent Measurements

| CC11 UNIT R | CC12 UNIT R | CC13 UNIT R |

| CC14 UNIT L | CC15 UNIT R | CC16 UNIT R |

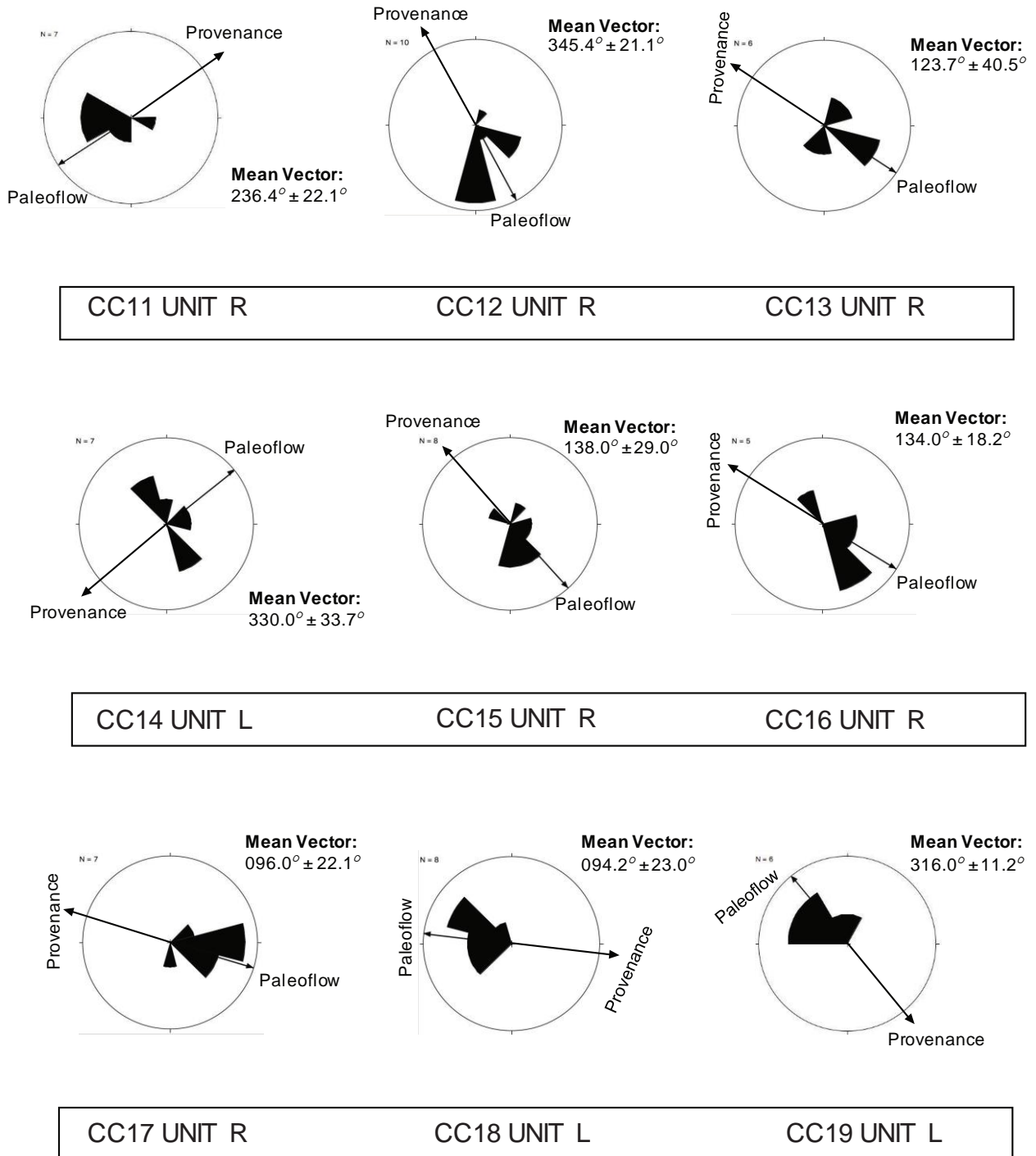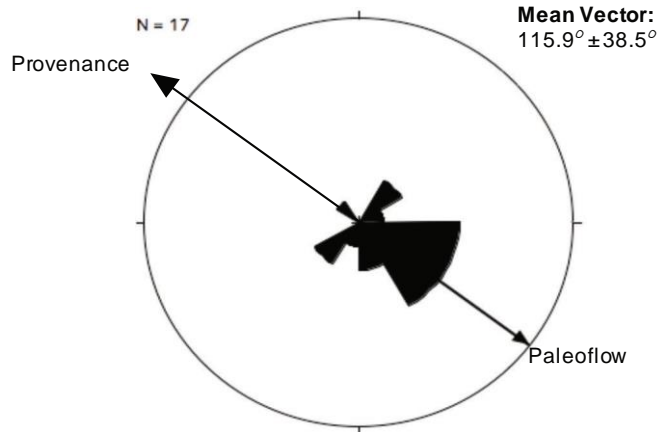| CC17 UNIT R | CC18 UNIT L | CC19 UNIT L |

Figure 22. Labeled individual paleocurrent measurements of Unit L and Unit R in the eastern stratigraphic column (Tables 5-6). N represents the number of a determined direction using paleocurrent clast imbrications. Large arrow indicates provenance direction.

69

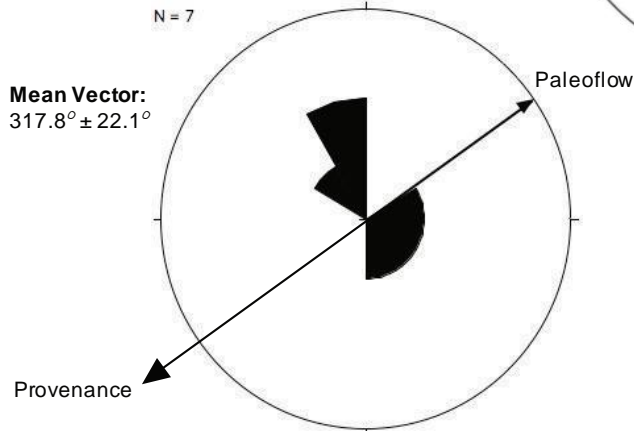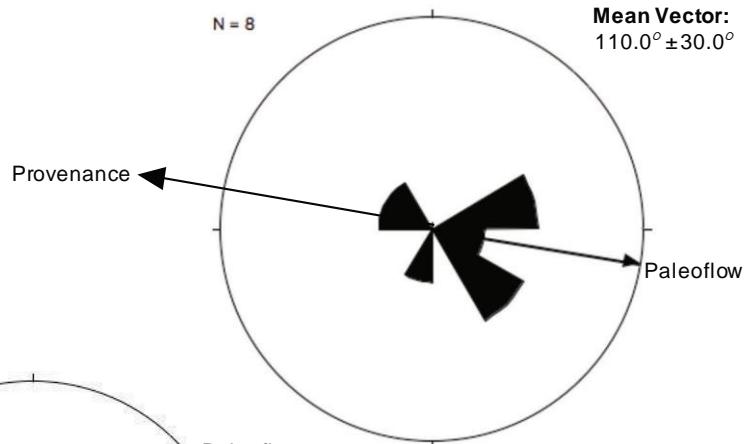# Tadpole Tank Unit BT & Unit R: Paleocurrent Measurements

CC1 UNIT R

CC1 UNIT R (right)

N = 17

Provenance

Mean Vector:
$115.9^o \pm 38.5^o$

Paleoflow

CC20 and CC221 UNIT BT

CC20 UNIT BT (right)

N = 8

Provenance

Mean Vector:
$110.0^o \pm 30.0^o$

Paleoflow

N = 7

Mean Vector:
$317.8^o \pm 22.1^o$

Paleoflow

CC21 UNIT BT (left)

Provenance

Figure 23. Labeled individual paleocurrent measurements taken from clast imbrications of Unit R (23a) and Unit BT (23b, 23c) in the Tadpole Tank (Table 7). N represents the number of a determined direction using paleocurrent clast imbrications. Large arrow indicates provenance direction.

CHAPTER 6: Sediment Grain Size and Composition

A. *Conglomerate Clast Size Counts*

Clast counts at various outcrops were conducted during the measurement of the western and eastern stratigraphic columns to interpret and compare the stratigraphic variations of clast assemblages (Figure 7, Tables 8-12, Appendix A.1-A.22). Collectively, the red conglomeratic sandstone subunits of Unit R on the Western stratigraphic column, west of Milpitas Wash Road, consisted of 162 counted clasts total (Figure 7, Table 8) ranging from 2mm pebbles to 128mm medium sized cobbles. On the Eastern stratigraphic column, east of Milpitas Wash Road, the red conglomeratic sandstone subunits of Unit R (Figure 7) consisted of 151 counted clasts total (Table 10) with clasts ranged from 4mm very coarse sands to 260mm large sized cobbles to small boulders, however a variety of grain sizes were found in the six clast counts completed (Figure 24, Appendix B.1-22).

The tan conglomeratic sandstone of Unit L on the western stratigraphic column (Figure 7) consisted of 44 counted clasts total (Table 9). On average, Unit L was composed of a ¼ mm – ½ mm fine to medium sandy, rounded to subrounded matrix and is primarily clast supported throughout the western stratigraphic column (Figure 24). The clasts size range averaged from conglomerate and very fine pebbles at 4mm to 64mm sized fine cobbles, the largest being a medium cobble at over 150mm, and are composed of angular to sub-angular metaplutonic and volcanic rocks such as biotite and augen gneisses and tuffs. The tan conglomeratic sandstone of Unit L on the eastern stratigraphic column (Figure 7) consisted of 70 counted clasts total (Table 5). Unit L stayed uniform in grain size averagely composed of ½ mm – 1mm fine to coarse sandy, subrounded matrix

71

and is primarily clast supported throughout the eastern stratigraphic column (Figure 24).
The conglomerate clasts range averaged from very fine pebbles at 4 mm to 120mm sized
medium cobbles, the largest being a medium cobble at approximately 200mm, and are
composed of subangular metaplutonic and volcanic rocks such as muscovite schist,
biotite gneiss and augen gneiss, and little to no tuffs present.

At Tadpole Tank, north of the stratigraphic columns, the orange red
conglomeratic sandstone ORSS clast count consisted of 90 counted clasts total. Clast
count one, referenced as CC1, highlighted a 4mm – 9mm fine to medium pebbled,
rounded to subrounded matrix that is primarily matrix supported (Figure 16). The clasts
size range averaged from very fine pebbles to conglomerates at 10mm to 40mm sized, the
largest being a large cobble at over 200mm, and are composed of subangular to
subrounded metaplutonic and volcanic rocks such as biotite, augen gneisses, and tuffs.
Unit BT in the Tadpole Tank location (Figure 5) consisted of 67 counted clasts total
(Table 12). On average, Unit BT was composed of a 30mm – 80mm medium cobbled
clasts with a 5mm sandy, rounded to subrounded matrix, and is primarily clast supported
throughout, however some regions showcased higher matrix amounts (Figure 16). Clast
count twenty and clast count twenty-one from the Tadpole Tank highlighted a 5mm fine
pebbled, rounded to subrounded matrix that is cemented and primarily grain supported.
Both clast counts sizes range averaged from very coarse pebbles to conglomerates at
40mm to 200mm sized, the largest being a large cobble at over 240mm, and are
composed of subrounded to rounded metaplutonic and volcanic rocks such as biotite,
augen gneisses, tuffs, and andesite scoria.

WEST STRATIGRAPHIC COLUMN - LOWER UNIT R

Grain Size and Phi Frequency

Clast Counts	Grain Size Frequency (mm)								
West - Unit R grain sizes	*2 mm VCoarse sand*	*4 mm VFine pebbles*	*8 mm Fine pebbles*	*16 mm Med. pebbles*	*32 mm Coarse pebbles*	*64 mm Fine cobbles*	*128 mm Med. cobbles*	*256 mm Boulder*	
Phi Size	*-1*	*-2*	*-3*	*-4*	*-5*	*-6*	*-7*	*-8*	**Total Clasts**
CC2	3	9	10	9	3	15	5	1	55
CC3	0	0	0	12	14	15	0	0	41
CC4	15	0	12	15	14	14	11	0	81
CC6	19	15	0	0	14	15	18	12	93
CC7	10	9	14	7	7	7	0	0	54
CC8	17	11	0	11	0	19	21	11	90
CC10	15	0	16	12	13	16	13	0	85
								Total	499

Table 8. Western Stratigraphic Column clast counts. Clast Counts showcase grain size and phi frequency for lower Unit R of the Soledad Rojo fm.

WEST STRATIGRAPHIC COLUMN - UPPER UNIT L

Grain Size and Phi Frequency

Clast Counts	Grain Size Frequency (mm)								
West - Unit L Grain Sizes	*2 mm VCoarse sand*	*4 mm VFine pebbles*	*8 mm Fine pebbles*	*16 mm Med. pebbles*	*32 mm Coarse pebbles*	*64 mm Fine cobbles*	*128 mm Med. cobbles*	*256 mm Boulder*	
Phi Size	*-1*	*-2*	*-3*	*-4*	*-5*	*-6*	*-7*	*-8*	**Total Clasts**
CC5	0	14	16	12	12	13	0	0	67
CC9	0	9	12	8	8	14	17	0	68
CC22	0	8	9	10	14	0	0	0	41
								Total	176

Table 9. Western Stratigraphic Column clast counts. Clast Counts showcase grain size and phi frequency table for upper Unit L of the Soledad Rojo fm.

EAST STRATIGRAPHIC COLUMN - LOWER UNIT R

Grain and Phi Size Frequency

Clast Counts	Grain Size Frequency (mm)								
East - Unit R Grain Size	*2 mm VCoarse sand*	*4 mm VFine pebbles*	*8 mm Fine pebbles*	*16 mm Med. pebbles*	*32 mm Coarse pebbles*	*64 mm Fine cobbles*	*128 mm Med. cobbles*	*256 mm Boulder*	
Phi Size	*-1*	*-2*	*-3*	*-4*	*-5*	*-6*	*-7*	*-8*	**Total Clasts**
CC11	14	0	10	10	14	13	22	14	97
CC12	17	13	14	12	21	25	22	0	124
CC13	17	16	18	12	18	11	0	0	92
CC15	8	9	9	9	11	17	7	0	70
CC16	0	27	24	14	0	0	0	0	65
CC17	0	25	7	8	14	0	0	0	54
								Total	502

Table 10. Eastern Stratigraphic Column clast counts. Clast Counts showcase grain size and phi frequency for lower Unit R of the Soledad Rojo fm.

EAST STRATIGRAPHIC COLUMN - UPPER UNIT L

Grain and Phi Size Frequency

Clast Counts	Grain Size Frequency (mm)								
East - Unit L	*2 mm VCoarse sand*	*4 mm VFine pebbles*	*8 mm Fine pebbles*	*16 mm Med. pebbles*	*32 mm Coarse pebbles*	*64 mm Fine cobbles*	*128 mm Med. cobbles*	*256 mm Boulder*	
Phi Size	*-1*	*-2*	*-3*	*-4*	*-5*	*-6*	*-7*	*-8*	**Total Clasts**
CC14	0	16	16	15	13	13	0	0	73
CC18	0	0	0	0	25	0	0	0	25
CC19	0	10	7	9	7	8	11	0	52
								Total	150

Table 11. Eastern Stratigraphic Column clast counts. Clast Counts showcase grain size and phi frequency tables for upper Unit L of the Soledad Rojo fm.

TADPOLE TANK - MIDDLE UNIT R & UNIT BT

Grain and Phi Size Frequency

Clast Counts	Grain Size Frequency (mm)								
Tadpole Tank Grain Size	*2 mm VCoarse sand*	*4 mm VFine pebbles*	*8 mm Fine pebbles*	*16 mm Med. pebbles*	*32 mm Coarse pebbles*	*64 mm Fine cobbles*	*128 mm Med. cobbles*	*256 mm Boulder*	
Phi Size	*-1*	*-2*	*-3*	*-4*	*-5*	*-6*	*-7*	*-8*	**Total Clasts**
CC1	3	24	25	16	8	2	6	1	85
CC20	0	13	0	0	11	14	10	6	54
CC21	0	13	6	7	10	13	12	7	68
								Total	207

Table 12. Tadpole Tank clast counts. Clast Counts showcase grain size and phi size frequency tables for middle Unit BT (CC20, CC21) and lower Unit R orange-red sandstone (CC1).
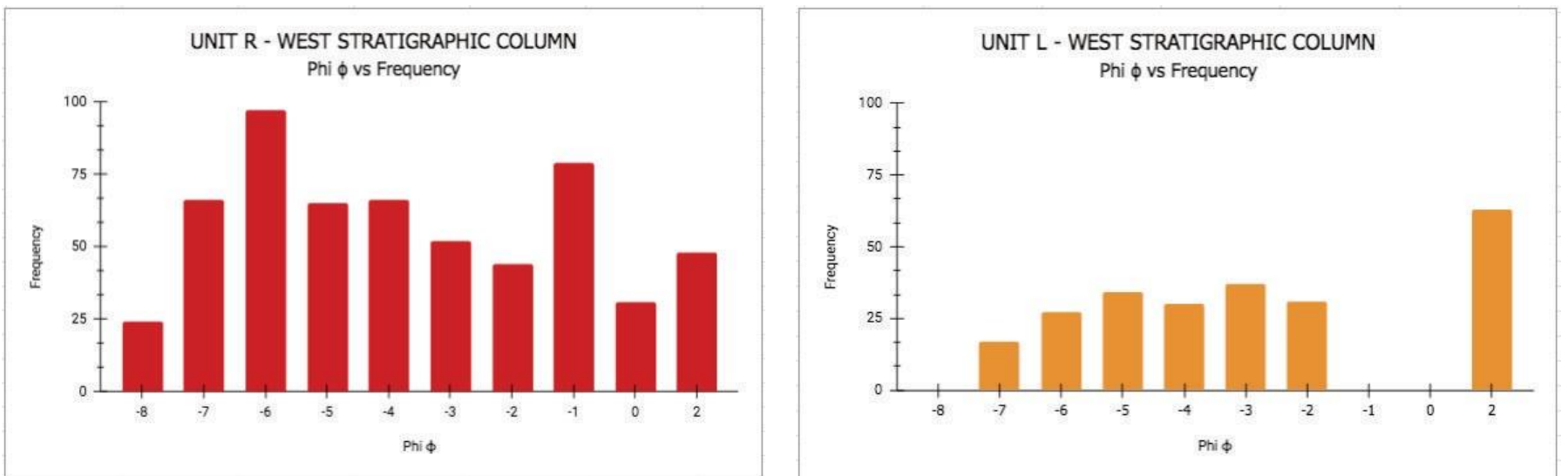
Western Stratigraphic Column

Figure 24a. Phi vs Frequency distribution bar graph for Unit R and Unit L of the western stratigraphic column. Measurements taken from clast counts.
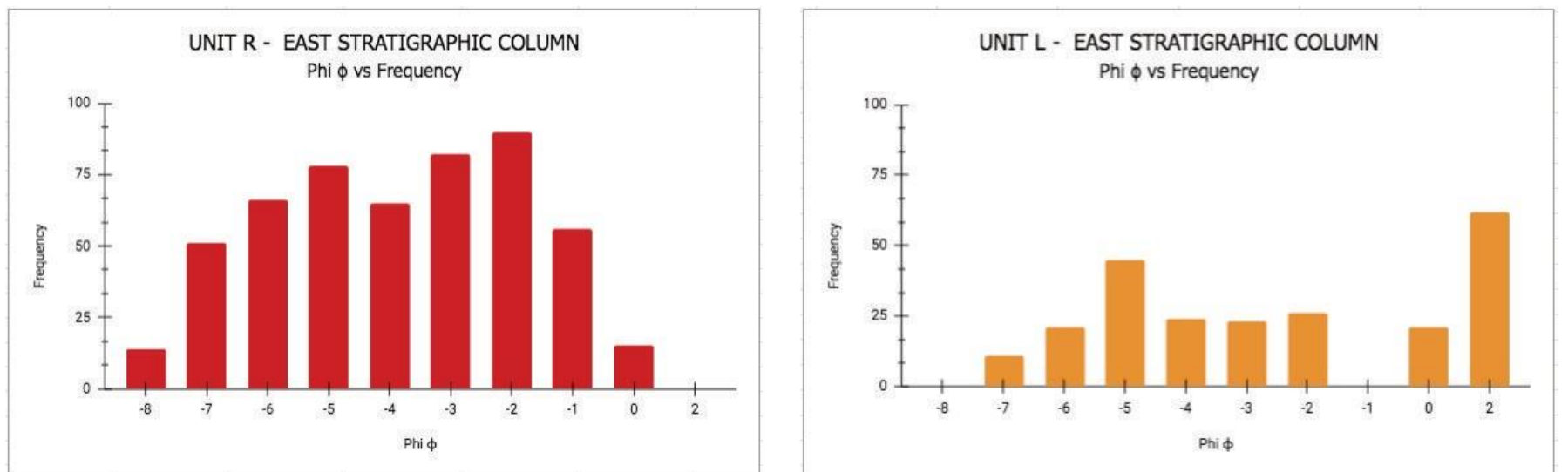
Eastern Stratigraphic Column

Figure 24b. Phi vs Frequency distribution bar graph for Unit R and Unit L of the eastern stratigraphic column. Measurements taken from clast counts.
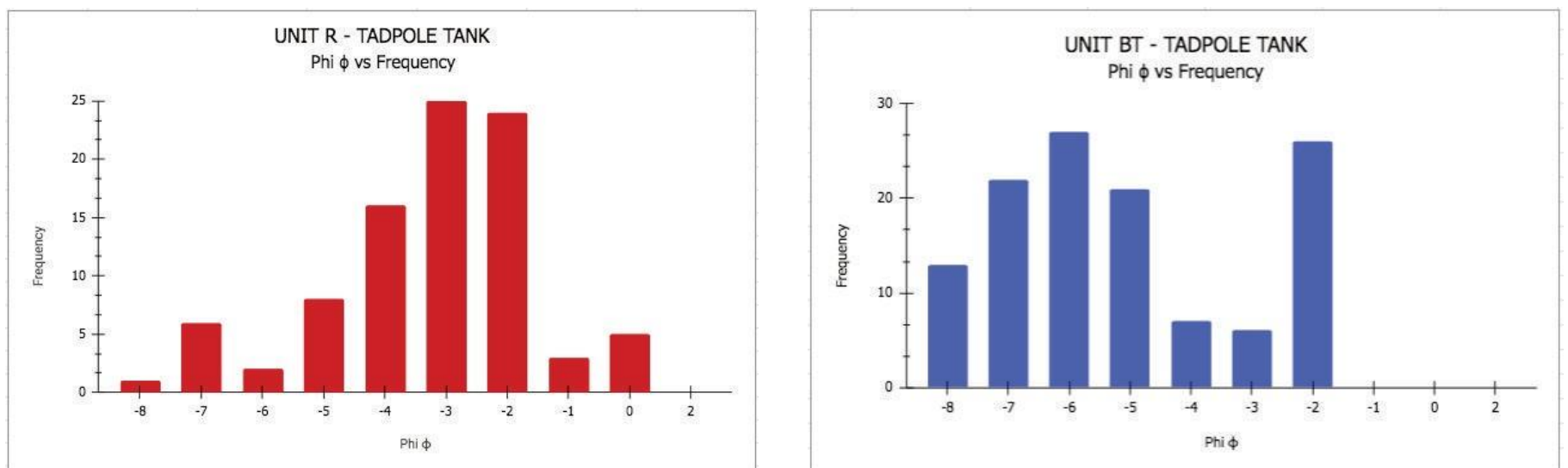
Tadpole Tank

Figure 24c. Phi vs Frequency distribution bar graph for Unit R and Unit BT of the Tadpole Tank region, north of the stratigraphic column. Measurements taken from clast counts.

Clast Size Count Interpretations

Analyzing the differences between the red conglomeratic sandstone Unit R and tan conglomeratic sandstone Unit L, each clast counts roughly had the same amount of clasts collected and compared for each side of Milpitas Wash Road. The two sides of Milpitas Wash Roads show a subtle distinction in clast grain sizes for the red conglomerate sandstone (Figure 7). The eastern column displays larger cobbles to small boulders in sizes, which could be due to the subtle tectonics on the eastern research side, whereas the western column displayed a variety of subunits, hypothesized to have been from separate depositional events during this period, leading to transportation occurring and a variety of grain sizes being deposited on the western research side of the basin. Comparing the tan conglomeratic sandstone Unit L, more clasts were counted on the eastern stratigraphic column overall due to the outcrop availability and clast visibility compared to on the western stratigraphic column. Between the two sides of Milpitas Wash Road, Unit L was consistent with 1/2 mm sized matrix grains and large cobbles up to 200mm in size. However, the western stratigraphic column overall displayed smaller matrix and clasts grain sizes, with the eastern stratigraphic column displaying larger matrix and clast grain sizes (Figure 17). This coincides with the interpretation on the western stratigraphic column having more tectonic activity compared to the eastern stratigraphic column, therefore leading to more transportation occurring and different grain sizes accumulating in the western research side.

Irregular to the other units, Unit BT consisted predominantly of porphyritic volcanic rock heading west exiting the Tadpole Tank canyon and northwest towards the Black Hills Tuffs, but did not contain hardly any tuffaceous material mixed alongside.

76

The matrix grains varied between the orange-red conglomeratic sandstone ORSS and the beige conglomeratic sandstone BSS within the Tadpole Tank canyons but averagely were angular in shape, interpreted as an intense fluvial event causing the conglomerates to weather and become rounded at a rapid period of time. This led to the angular matrix sands that have shed off the canyon walls from freshly eroded sediment and have been transported down the valley further south into the basin where the stratigraphic columns were measured.

B. Conglomerate Clast Count Composition

Based on a simplified inquiry of each clast count analysis from rock fragments of Unit L and Unit R, compositions varied between the three research sites. The western stratigraphic column (Figure 7) displayed approximately twenty-two different identified clast compositions (Figures 25-26, Appendix B.23-32). Clast compositions include but are not limited to: 26.2% unidentified volcanic material, 3.0% quartzite, 8.4% augen gneiss, 11.9% tuffs, 12.9% banded gneisses, 6.4% chert, 5.4% granodiorite, 7.4% muscovite schist, 2.0% wacke, 4.5% green and black basalt, 0.5% felsic granite, 1.5% andesite, 5.9% diorite, 1.0% rhyolite, and 2.5% pumice. The eastern stratigraphic column (Figure 7) displayed approximately fifteen different identified clast compositions (Figures 25-26, Appendix B.33-41). Clast compositions include but are not limited to: 15.7% unidentified volcanic material, 3.7% quartzite, 14.7% augen gneiss, 1.0% tuffs and also has 7.9% pink ignimbrite, 11.5% banded gneisses, 6.8% chert, 4.2% granodiorite, 25.7% muscovite schist, 1.6% wacke, 6.3% green and black basalt, and 1.0% andesite. The Tadpole Tank region displayed approximately nineteen different identified clast
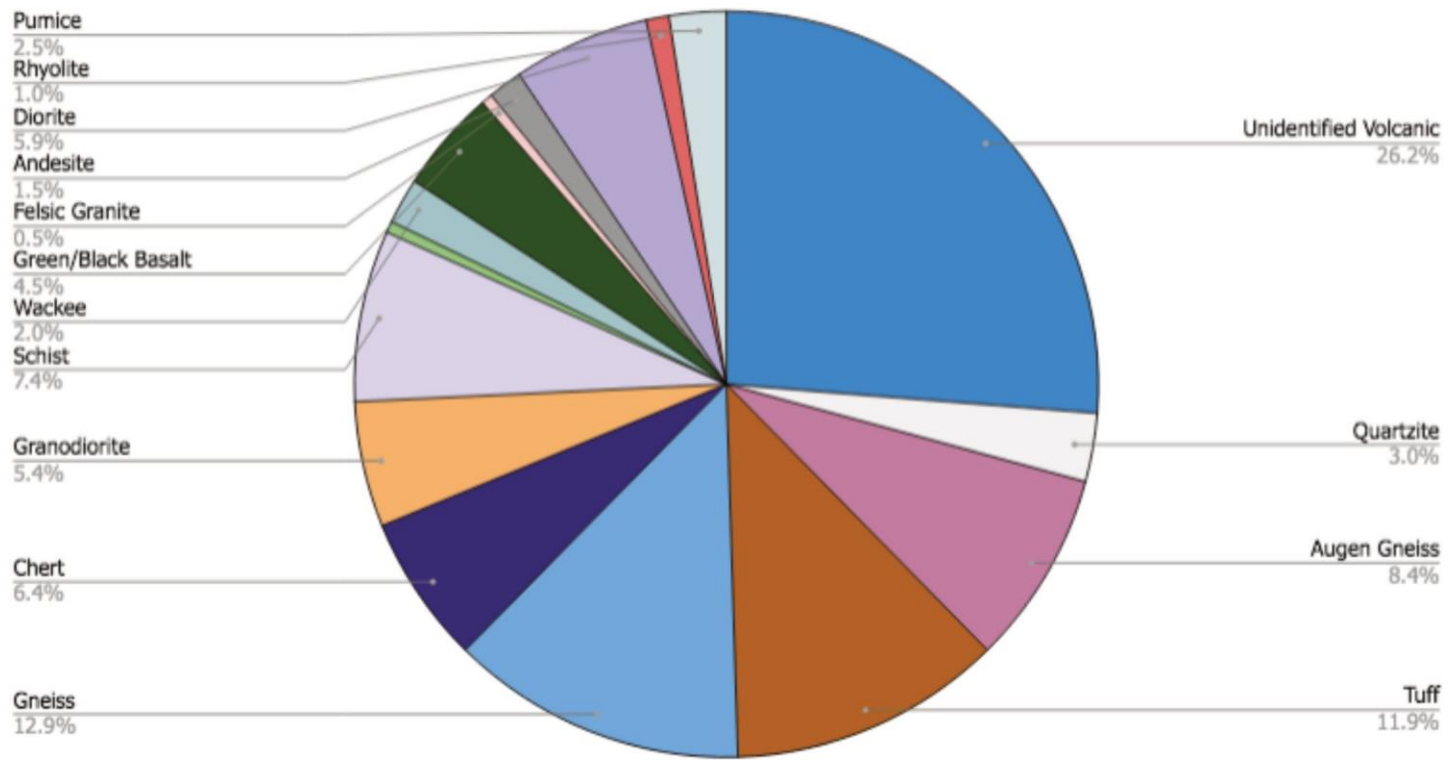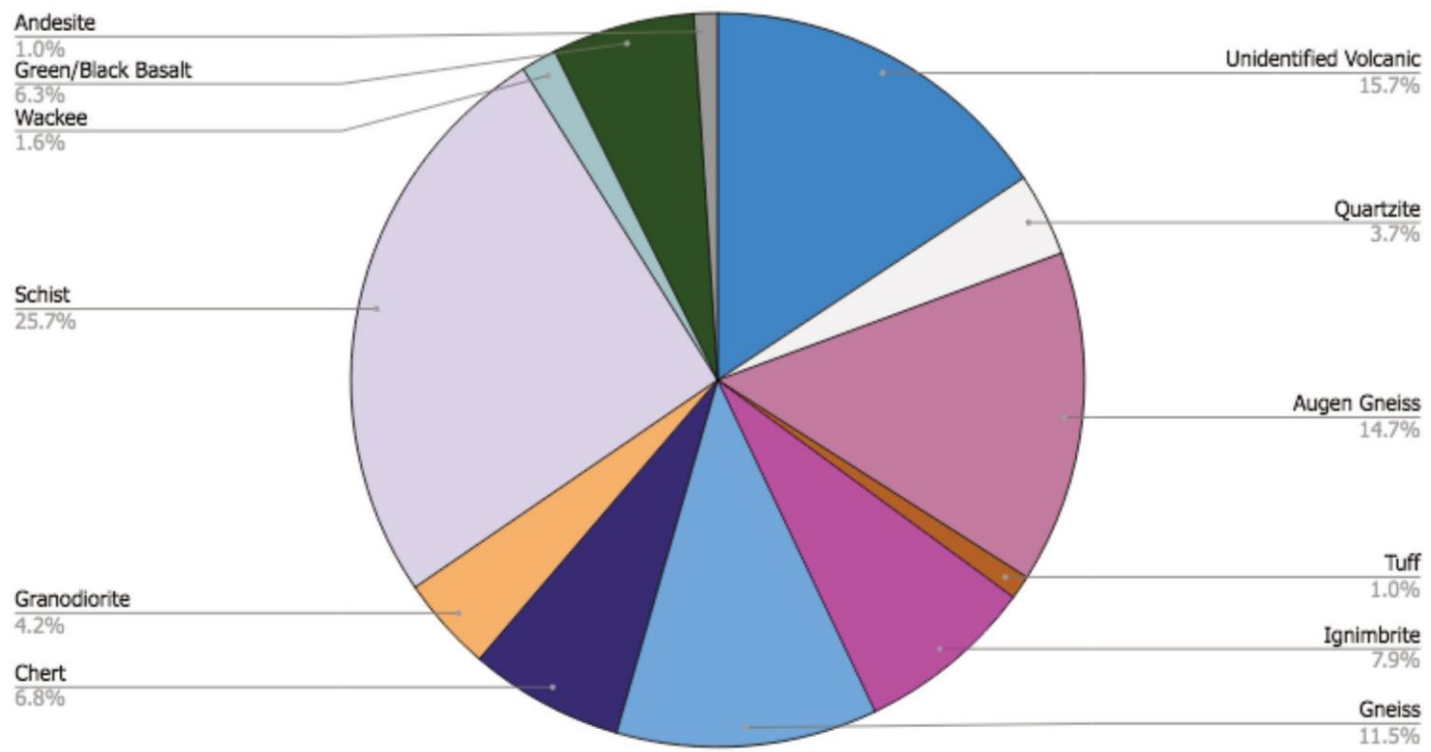
West Stratigraphic Column: Total Composition

Figure 25. Labeled pie chart of total clast count composition analysis from rock fragments of Unit R and Unit L in the western stratigraphic column.

East Stratigraphic Column: Total Composition

Figure 25. Labeled pie chart of total clast count composition analysis from rock fragments of Unit R and Unit L in the eastern stratigraphic column.
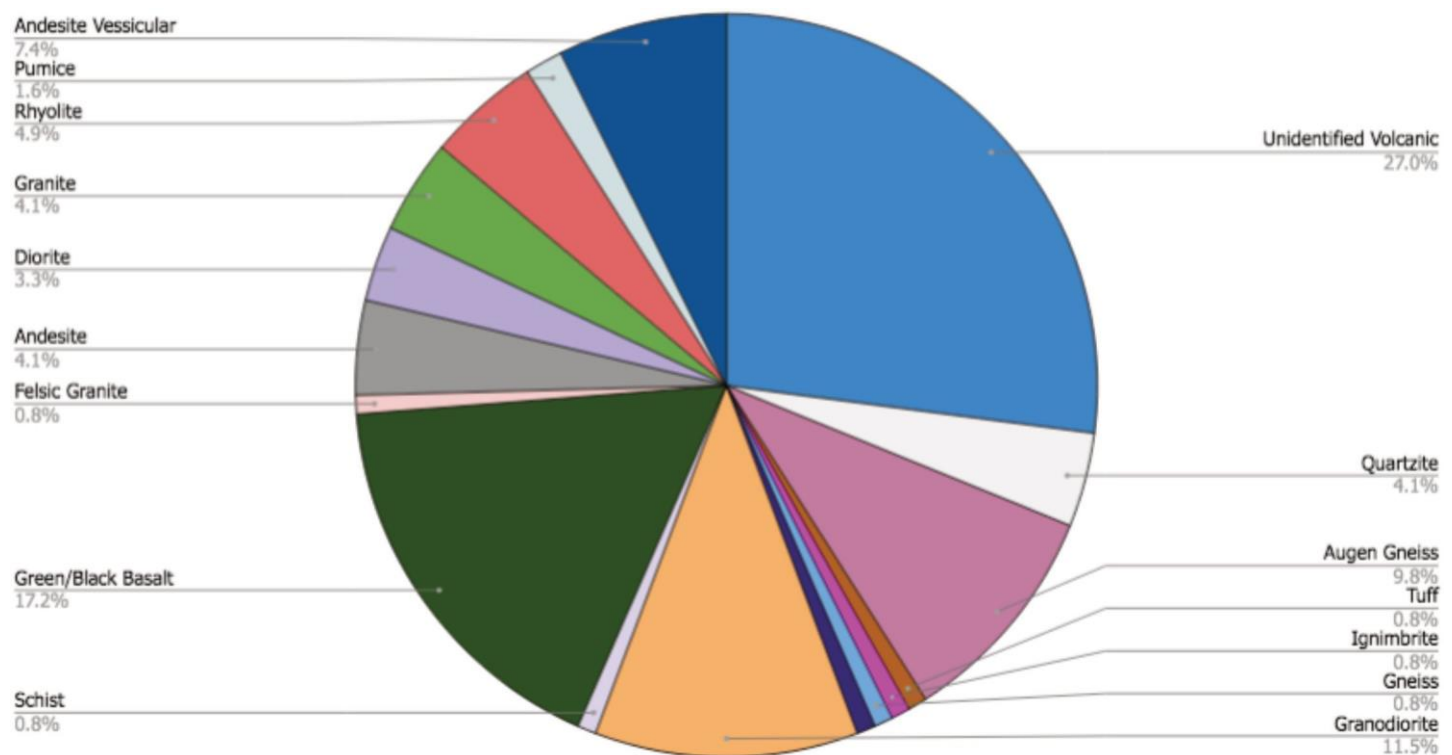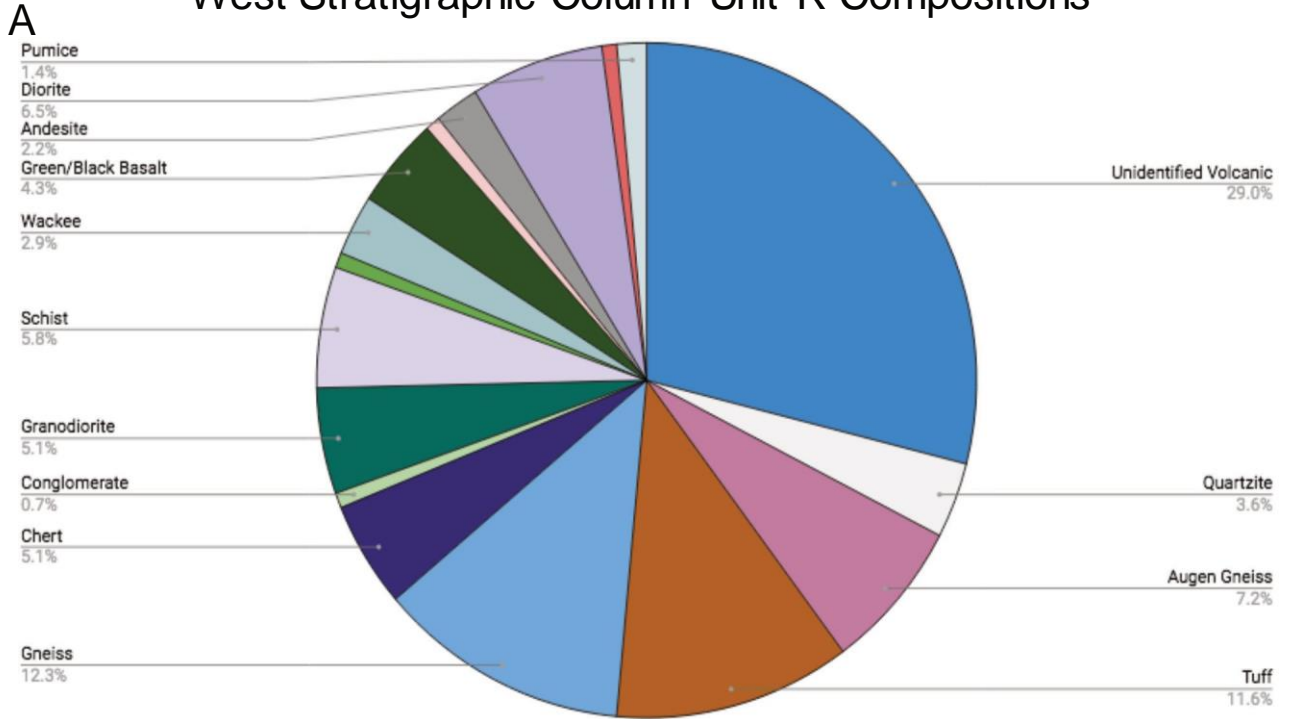
Tadpole Tank: Total Composition

Figure 25. Labeled pie chart of overall clast count composition analysis from rock fragments of Unit BT and Unit R orange red sandstone (ORSS) in the Tadpole Tank.

West Stratigraphic Column Unit R Compositions

A

Pumice 1.4%
Diorite 6.5%
Andesite 2.2%
Green/Black Basalt 4.3%
Wackee 2.9%
Schist 5.8%
Granodiorite 5.1%
Conglomerate 0.7%
Chert 5.1%
Gneiss 12.3%

Unidentified Volcanic 29.0%
Quartzite 3.6%
Augen Gneiss 7.2%
Tuff 11.6%

West Stratigraphic Column Unit L Compositions

B

Pumice 4.6%
Rhyolite 1.5%
Diorite 4.6%
Green/Black Basalt 4.6%
Schist 10.8%
Granodiorite 6.2%
Chert 9.2%
Gneiss 13.8%

Unidentified Volcanic 20.0%
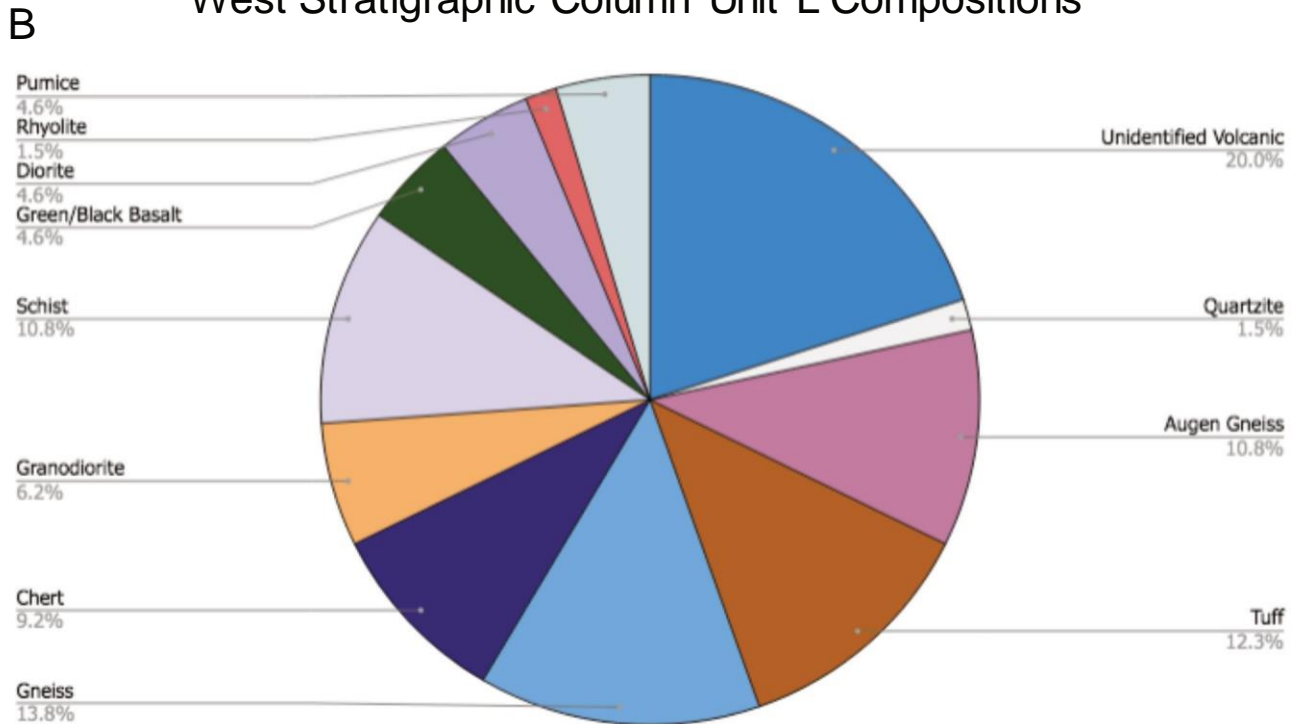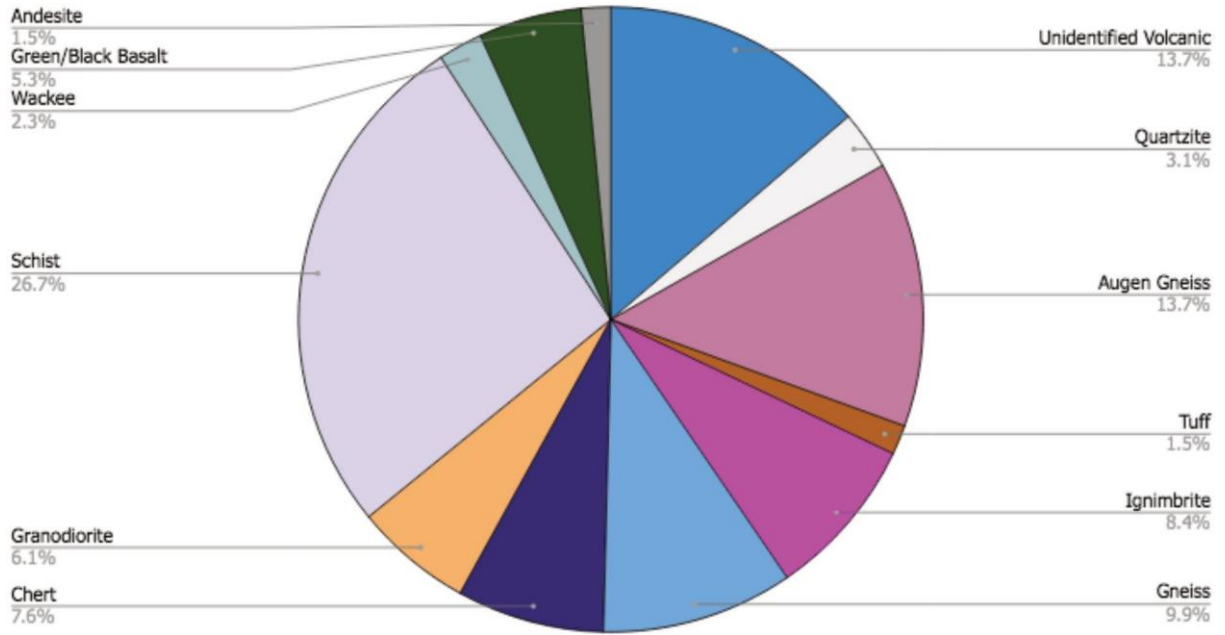Quartzite 1.5%
Augen Gneiss 10.8%
Tuff 12.3%

Figure 26a and Figure 26b. Labeled pie charts of overall clast count composition analysis from rock fragments of Unit R and Unit L in the western stratigraphic column.

East Stratigraphic Column Unit R: Compositions

C

Andesite
1.5%

Green/Black Basalt
5.3%

Wackee
2.3%

Unidentified Volcanic
13.7%

Quartzite
3.1%

Schist
26.7%

Augen Gneiss
13.7%

Tuff
1.5%

Ignimbrite
8.4%

Granodiorite
6.1%

Chert
7.6%

Gneiss
9.9%

East Stratigraphic Column Unit L: Compositions

D

Green/Black Basalt
8.3%

Unidentified Volcanic
20.0%

Schist
23.3%

Quartzite
5.0%

Chert
5.0%

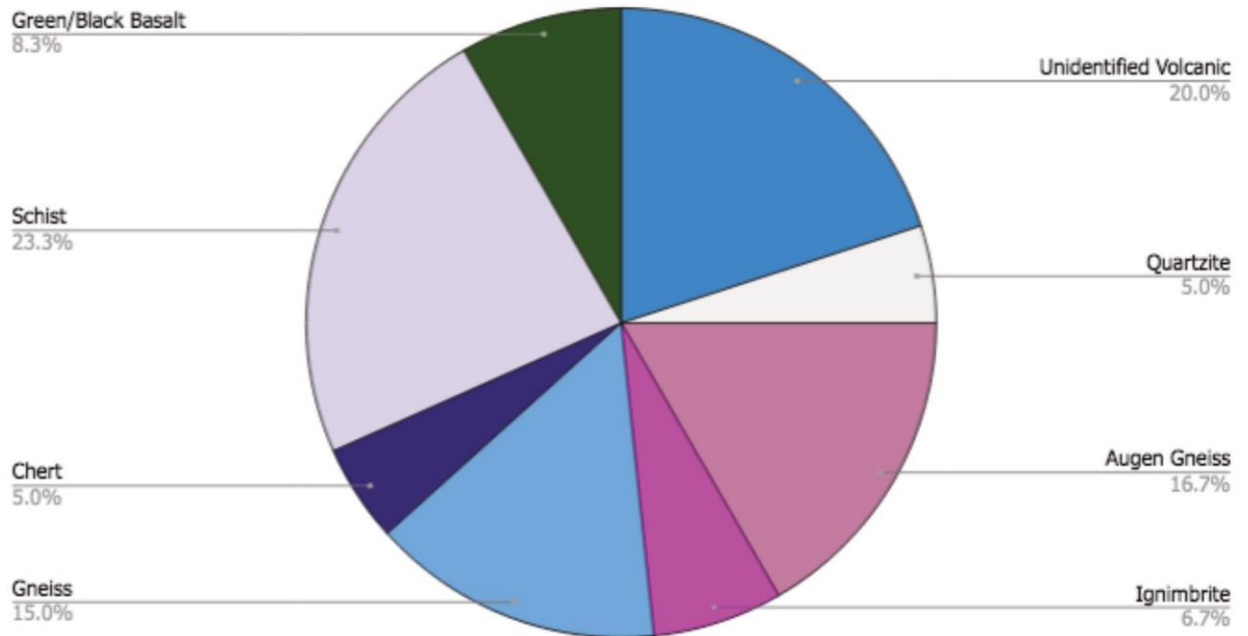Augen Gneiss
16.7%

Gneiss
15.0%

Ignimbrite
6.7%

Figure 26c and Figure 26d. Labeled pie charts of overall clast count composition analysis from rock fragments of Unit R and Unit L in the eastern stratigraphic
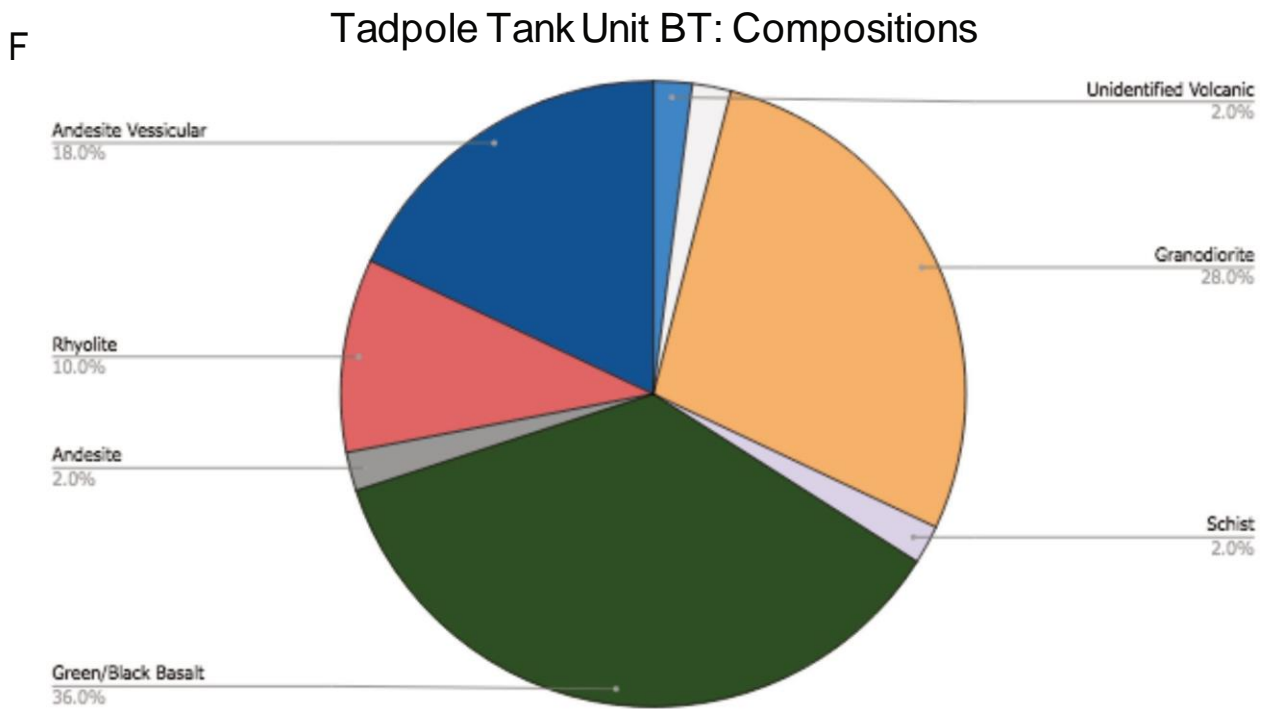
E

Tadpole Tank Unit R: Compositions

Pumice
2.8%
Rhyolite
1.4%
Granite
6.9%
Diorite
5.6%

Andesite
5.6%

Felsic Granite
1.4%

Green/Black Basalt
4.2%
Chert
1.4%
Gneiss
1.4%
Ignimbrite
1.4%
Tuff
1.4%

Augen Gneiss
16.7%

Unidentified Volcanic
44.4%

Quartzite
5.6%

F

Tadpole Tank Unit BT: Compositions

Andesite Vessicular
18.0%

Rhyolite
10.0%

Andesite
2.0%

Green/Black Basalt
36.0%

Unidentified Volcanic
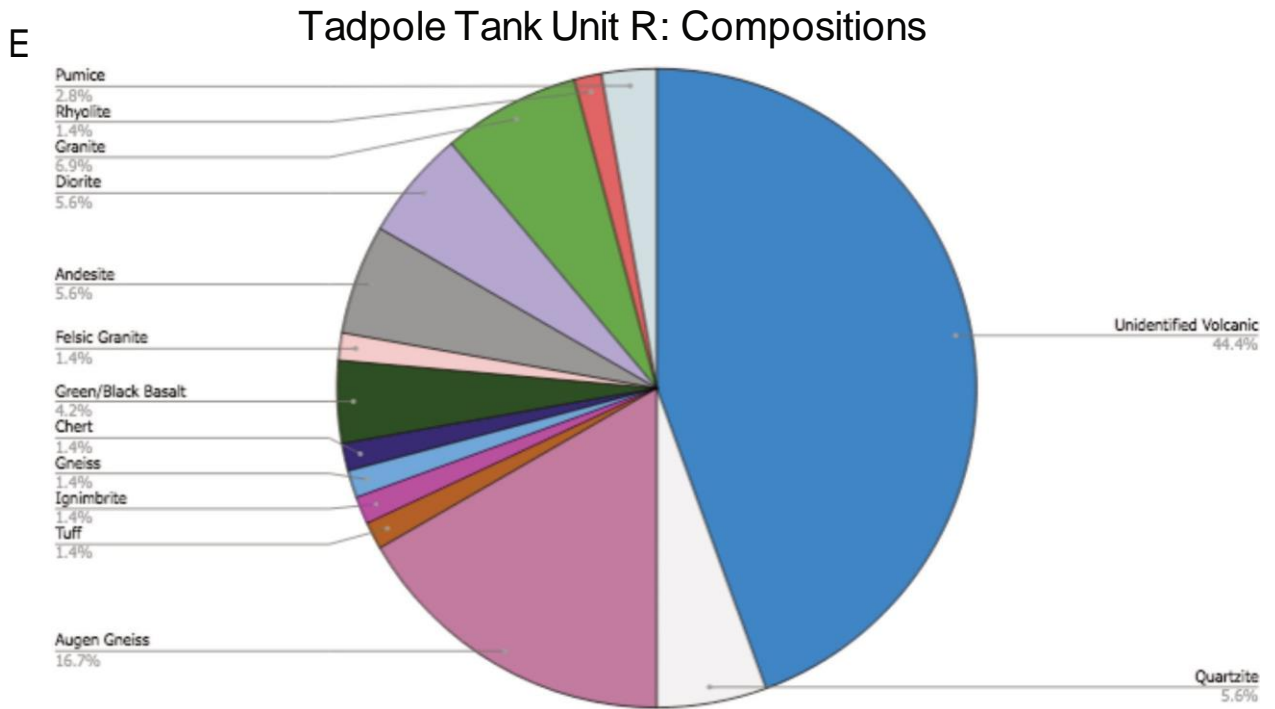2.0%

Granodiorite
28.0%

Schist
2.0%

Figure 26e and Figure 26f. Labeled pie charts of overall clast count composition analysis from rock fragments Unit R orange red sandstone (ORSS) and of Unit BT in the Tadpole Tank.

compositions   (Figure 5, Figures 25-26, Appendix B.42-44) Clast compositions include but are not limited to: 27.0% unidentified volcanic material, 4.1% quartzite, 9.8% augen gneiss, 0.8% for tufts, schists, felsic granite, ignimbrites, chert and banded gneisses separately, 11.5% granodiorite,   17.2% green and black basalt, 4.1% andesite, 3.3% diorite, 4.1% granite, 4.9% rhyolite, 1.6% pumice, and 7.4% vesicular andesite.

Clast Count Composition Interpretations

Each of the three study sites within the Soledad Rojo formation displayed similar clast compositions, including tuffs, augen and biotite gneisses, as well as muscovite schists, with varying compositions in others such as sedimentary lithics including wackes and cherts, as well as ignimbrite lithics found east of Milpitas Wash Road. Overall, the western stratigraphic column showcased larger amounts of volcanic compositions,   such as an increase in unidentified volcanics and tuffaceous rocks compared to the eastern stratigraphic column and Tadpole Tank region. (Figure 25). These results coincide with the working hypothesis that a primarily   local volcanic rock source, such as those within the surrounding Black Hills and Chocolate Mountains, is closer in proximity   to the western stratigraphic column compared to the metaplutonic rock source further east. The eastern stratigraphic column displayed larger amounts of metamorphic compositions such as an increase in muscovite mica schist, and an increase in banded and augen gneisses compared to the western stratigraphic column and Tadpole Tank research area (Figure 25). These percentages infer a metamorphic rock source, such as those within the Palo Verde Mountains, is closer in proximity   to the eastern stratigraphic column compared to the volcanic rock source in the west and may be a provenance source. The northern

82

Tadpole Tank study area displayed a larger variety of compositions collectively compared to both stratigraphic columns, interpreted to be because of the fluvial fed environment within this part of the basin.

C.   *Sandstone Point Counts*

Collected inside of the Tadpole Tank region within the Unit R orange red conglomeratic sandstone ORSS, thin sections SR-1, SR-2 and SR-4 vary amongst each other based on compositions, mineral sizes and cement amounts (Figure 5). Sample SR-1 (Figure 27) was taken the closest to the entrance to Tadpole Tank on the western side from Milpitas Wash Road, which is the most northern location of the three point counting hand samples and part of the orange red conglomeratic sandstone ORSS of Unit R. This sample is predominantly composed of a coarse grained cemented sandstone with grain supported, subangular to subrounded monolithic quartz that produced undulose extinction, alongside microcline feldspar grains with cross-hatched twinning. Sample SR-2 (Figure 27) was taken directly south of SR-1 along the Tadpole Tank canyon on the western side, deeper into Unit R. There is a similarity of grain types to SR-1 but has finer, well sorted and rounded grains with monolithic quartz, microcline feldspar, as well as plagioclase with albite twinning, sanidine feldspar, muscovite mica, zircons and volcanic lithic materials. Sample SR-4 (Figure 27) continued into Tadpole Tank, being the most southwestern thin section hand sample taken from Unit R. Sample SR-4 is also similar to the previous samples, however, it has a higher porosity and showcases grains that are moderately sorted with subrounded-subangular textures and includes more metamorphic lithic materials.

Point Count data: SR-1, SR-2, SR-4

|		Sample					
Unit	Description	SR-1 Point Counts	SR-1 %	SR-2 Point Counts	SR-2 %	SR-4 Point Counts	SR-4 %
Qm	Monocrystalline Q	113	22.6	100	20	86	17.2
Qp	Polycrystalline Q	104	20.8	65	13	49	9.8
K	Potassium Feldspar	22	4.4	47	9.4	85	17
P	Plagioclase Feldspar	30	6	60	12	65	13
Ls	Sedimentary lithics	17	3.4	34	6.8	24	4.8
Lm	Metamorphic lithics	71	14.2	76	15.2	51	10.2
Lv	Volcanic lithics	37	7.4	58	11.6	91	18.2
mica	Muscovite Mica	2	0.4	12	2.4	9	1.8
pore	Pore spaces	1	0.2	7	1.4	12	2.4
other	Zircons etc	7	1.4	9	1.8	2	0.4
cement	Cement %	96	19.2	32	6.4	26	5.2
matrix	Matrix %	0	0	0	0	0	0
		500 Points Total	100%	500 Points Total	100%	500 Points Total	100%

Table 13. Recorded point count data measured from thin sections of samples SR-1, SR-2 and SR-4.

Normalized QFL percentages from SR-1, SR-2, SR-4

		Sample					
Unit	Description	SR-1 Point Counts	Normalized SR-1 %	SR-2 Point Counts	Normalized SR-2 %	SR-4 Point Counts	Normalized SR-4 %
Qt	Total framework Q (Qt = Qp + Qm)	217	55.1	165	37.5	135	29.9
F	Total framework feldspars (F = K+P)	52	13.2	107	24.3	150	33.3
L	Framework lithics fragments (L = Ls+Lv+Lm)	125	31.7	168	38.2	166	36.8
Lt	Total framework lithic fragments (Lt = L + Qp)	229	--	228	--	215	--
Qt+F+L	Total framework	394	--	440	--	451	--
Qm+F+Lt	Total framework	394	--	435	--	451	--
Lm+Ls+Lv	Total lithic framework	125	--	168	--	166	--
Qm	Recalculated QmFLt %	--	28.7	--	23.0	--	19.1
F	Recalculated QmFLt %	--	13.2	--	24.6	--	33.3
Lt	Recalculated QmFLt %	--	58.1	--	52.4	--	47.6
Lm	Recalculated LmLsLv %	--	56.8	--	45.2	--	30.5
Ls	Recalculated LmLsLv %	--	13.6	--	20.2	--	14.5
Lv	Recalculated LmLsLv %	--	29.6	--	34.6	--	55.0
			100%		100%		100%

Table 14. Normalized QFL percentages from thin sections of samples SR-1, SR-2 and SR-4.

Tadpole Tank: Point Counting Compositions
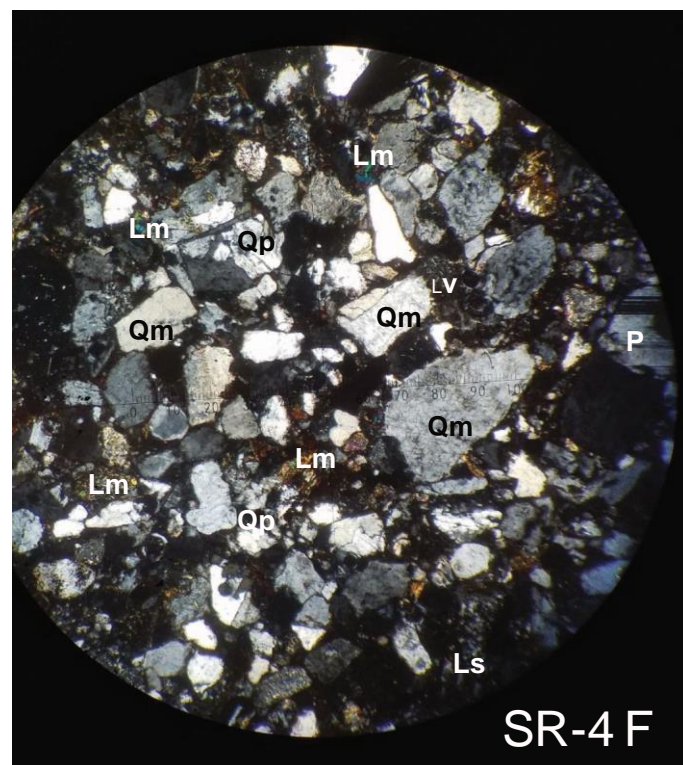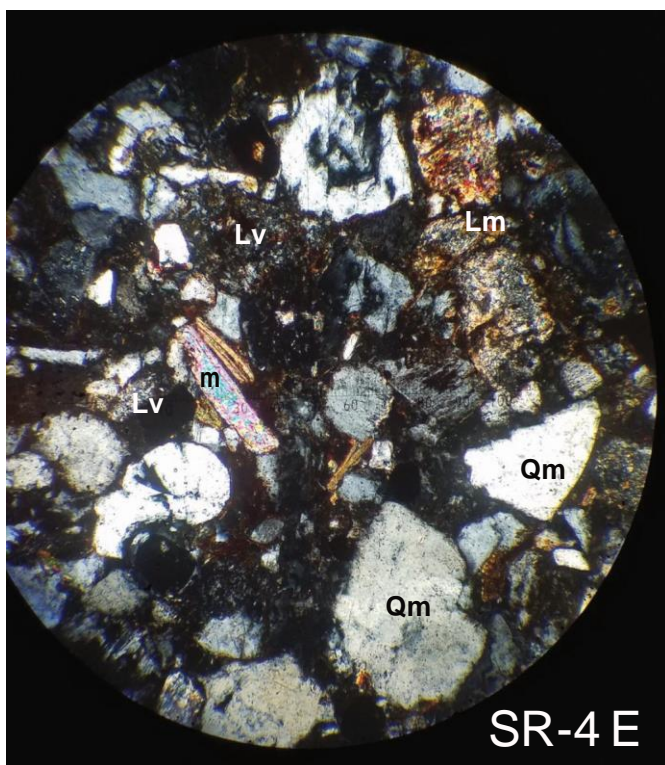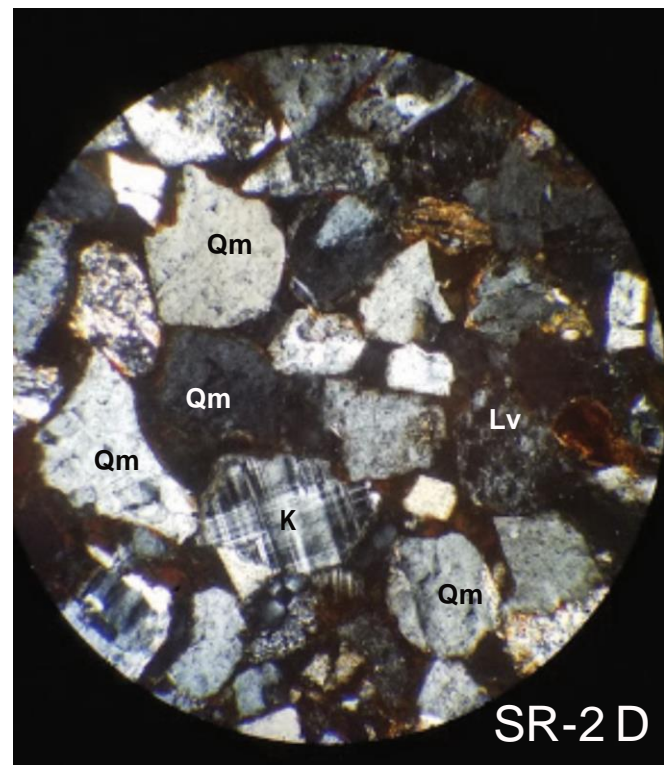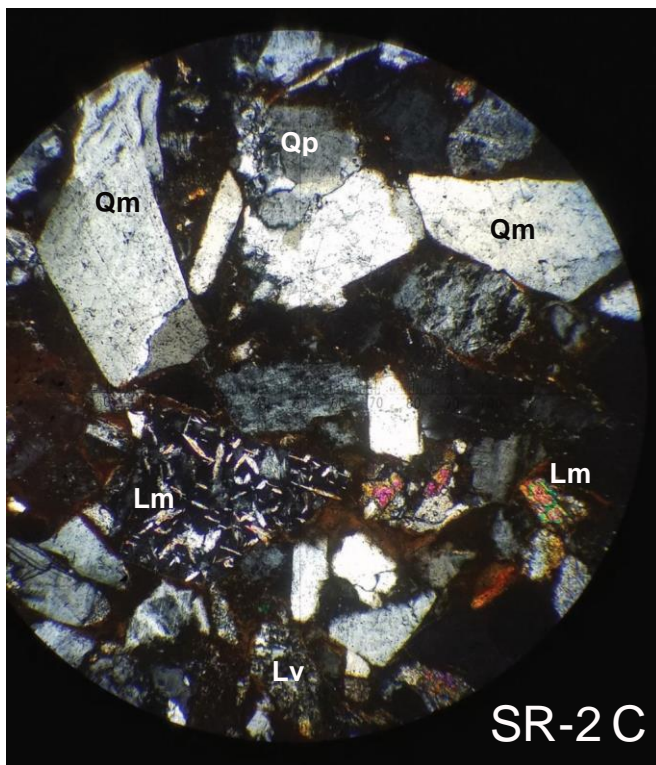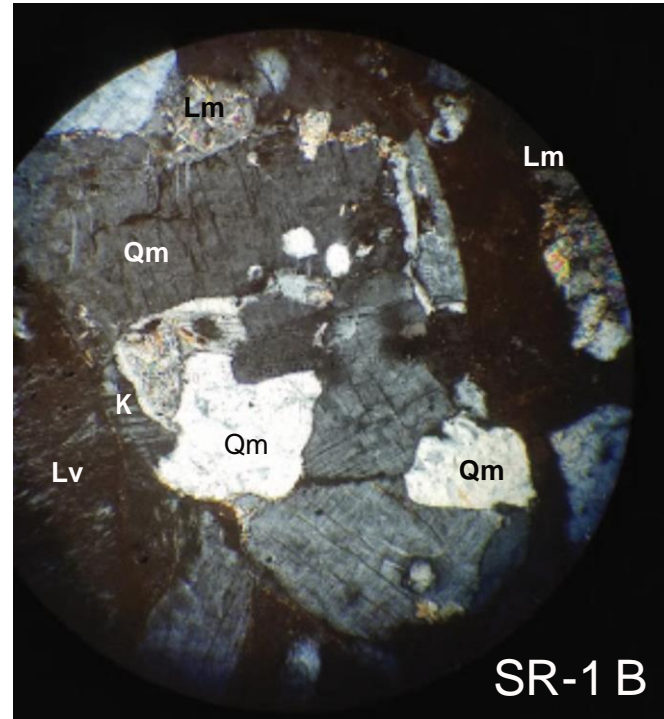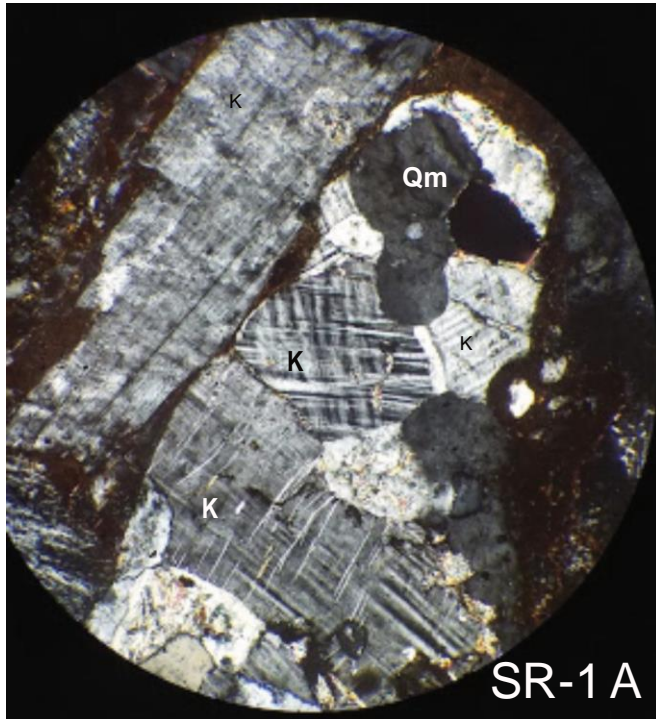
Figures 27a - 27f. Pictures taken during point counting analysis and are in XPL. SR-1 thin sections shown in pictures A and B. Picture A shows evidence of twinning feldspar, microcline and microcrystalline quartz, picture B shows evidence of metamorphic lithic and microcrystalline quartz. SR-2 thin section shown in pictures C and D. Picture C shows evidence of volcanic and metamorphic lithic and microcrystalline quartz, picture D shows evidence of lithics, microcline extinction, microcrystalline quartz and moderately well sorting of grains overall. SR-4 thin sections shown in picture E and F. Picture E shows evidence of volcanic and metamorphic lithic, muscovite mica and microcrystalline quartz, picture F shows evidence of feldspars, microcline extinction, microcrystalline quartz and moderately well sorting. Qm = Microcrystalline Quartz. Qp = Polycrystalline Quartz. K = Potassium Feldspar. P = Plagioclase Feldspar. Ls = Sedimentary Lithics. Lm = Metamorphic Lithics. Lv = Volcanic Lithics. m = Muscovite mica.
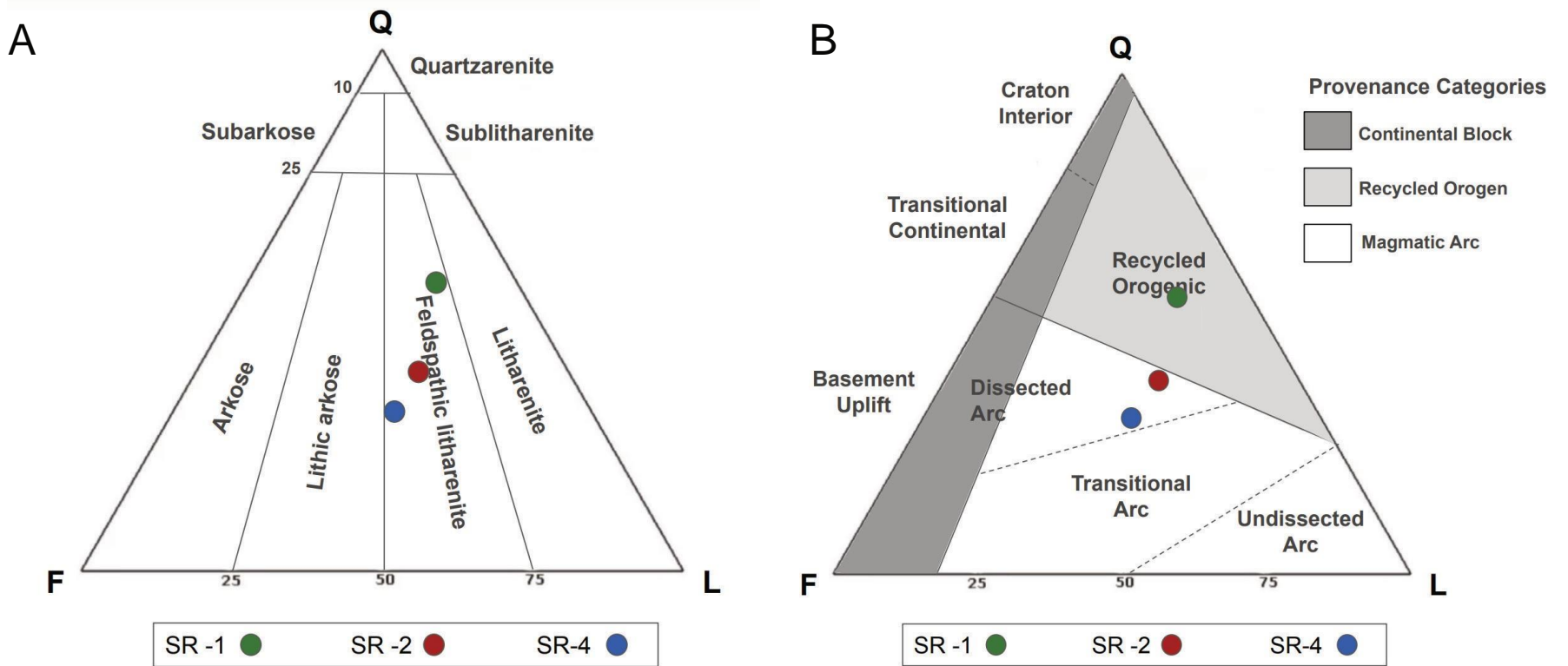
Ternary Diagrams

Figure 28a displays a QFL Lithology plot. Green represents sample SR-1. Red represents sample SR-2. Blue represents SR-4. Measurements taken from point counting analysis. Modified from Folk, 1980.

Figure 28b displays a QFL Provenance plot. Green represents sample SR-1. Red represents sample SR-2. Blue represents SR-4. Measurements taken from point counting analysis. Modified from Dickinson, 1988
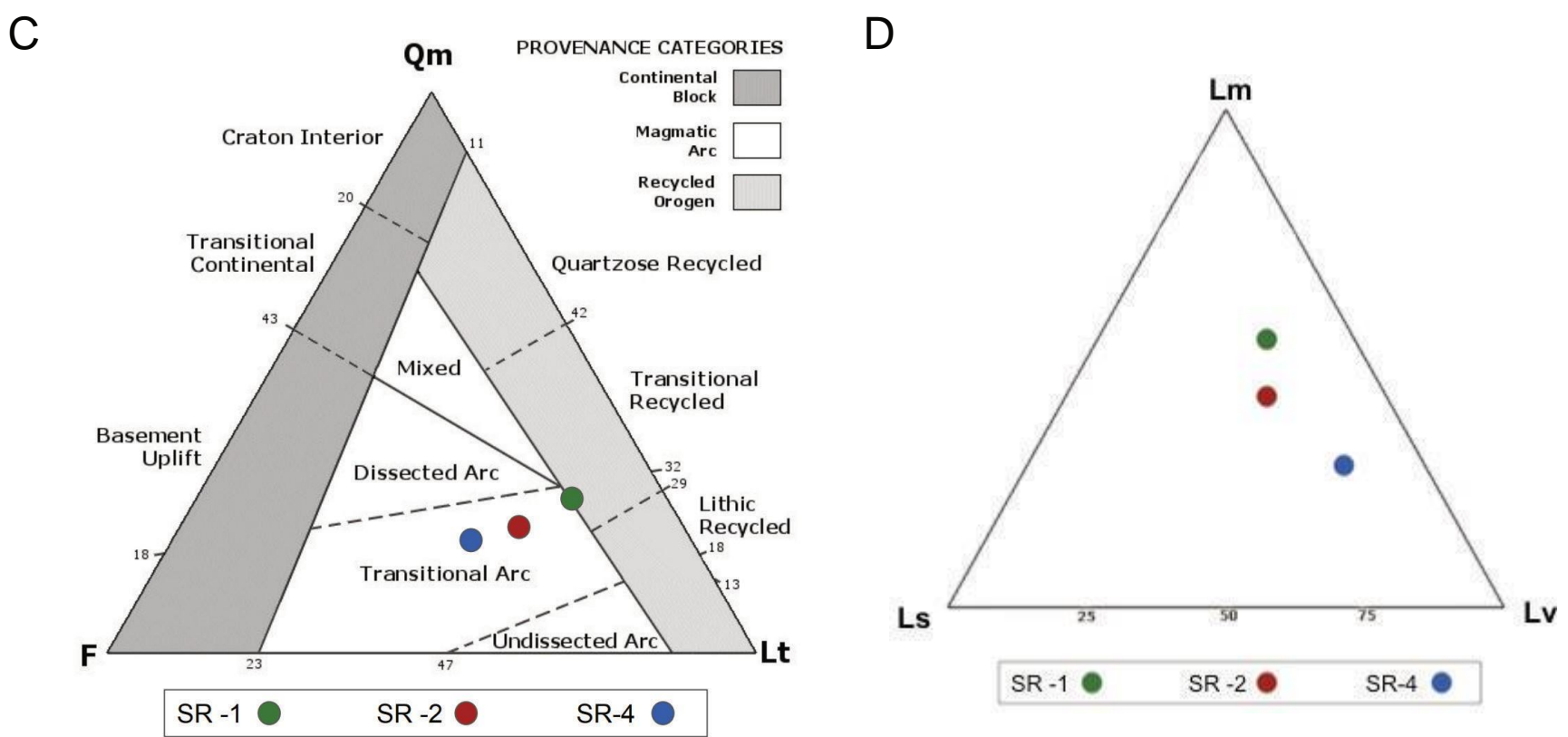
Figure 28c displays a Qm/F/Lt Ternary Provenance plot. Green represents sample SR-1. Red represents sample SR-2. Blue represents SR-4. Measurements taken from point counting analysis. Modified from Dickinson, 1988.

Figure 28d displays a Lm/Ls/Lv Lithic plot. Green represents sample SR-1. Red represents sample SR-2. Blue represents SR-4. Measurements taken from point counting analysis.

The composition of these three conglomeratic sandstones were plotted on QFL ternary diagrams, a QmFLt provenance ternary diagram and a Lm/Ls/Lv lithic ternary diagram (Figure 28, Tables 13-14) and all plot within different compositional lithologies based on the QFL lithology ternary plot that was created from visual interpretation. Though all plotted differently, all samples are a feldspathic lithic sandstone containing more than 20% of lithic fragments (Figures 28). Thin section SR-1 plotted under feldspathic litharenite, containing at least 10% feldspar, 43% quartz, 25% lithics, 20% cement and 2% of micas, zircons and pore spaces. Thin section SR-2 also plotted as a feldspathic litharenite, consisting of roughly 21% feldspars, 33% quartz, 34% lithics, 6% cement and 6% of micas, zircons and pore spaces. Thin section SR-4 plotted as a feldspathic litharenite consisting of roughly 30% feldspars, 27% quartz, 33% lithics, 5% cement and 5% of micas, zircons and pore spaces.

Normalized QFL percentages on the provenance ternary diagram (Dickenson and Suczek, 1979) (Figure 28), for SR-2 and SR-4 both plot within the dissected magmatic arc block, indicative of a forearc basin, whereas SR-1 plotted in the recycled orogenic provenance, exhibiting collision orogen or uplifted forarcs. The QFL provenance diagram focuses on mechanical and chemical weathering stability of a grain, as it changes along with its depositional environment, such as a quartz or a feldspar. To further categorize the provenance, the QmFLt diagram highlights the source of conglomerates by their tectonic setting. By normalizing percentages focusing on the QmFLt ternary diagram (Figure 28), all three thin sections plotted within a transitional magmatic arc. On the normalized Lm/Ls/Lv lithic ternary diagram (Figure 28d), SR-1 plots as having more metamorphic

lithics, SR-2 plots as having a mixture of conglomerates from all three: metamorphic, volcanic and sandstone lithics, and SR-4 has more sandstone lithics present.

Sandstone Point Counts Interpretations

Rock fragments in thin sections SR-1, SR-2 and SR-4 are distinctly characteristic to each other in terms of composition and all plot within a similar category of a transitional arc based on the Qm/F/Lt provenance ternary plot that was created from visual interpretation (Figure 28). This ternary diagram differs from the QFL provenance diagram, as it normalizes the monocrystalline quartz crystals specifically found in the thin sections to verify if from volcanic source such as granite, as opposed to all of the quartz crystals collectively, including the polycrystalline quartz which is commonly sourced from metamorphic sheared rock. Each thin section displayed a slight variance in the type of clasts collected during sedimentation of the unit. On the Lm/Ls/Lv lithic ternary diagram (Figure 28), SR-1 plots as having more metamorphic conglomerates, such as schists, as well as banded gneisses and augen gneisses containing large feldspar crystals, inferring close proximity to the source. Thin section SR-2 plots closer to the center of the ternary plot compared to SR-1 and SR-4, indicating a mix of volcanic lithics, metamorphic lithics and sandstone lithics. Thin section SR-4's hand sample, however, was taken the furthest southwest of the three and has the highest amount of sandstone lithics of the three samples taken, inferring a different depositional environment the further south away from the Tadpole Tank region. Compared to the clast count compositions found during the construction of the two stratigraphic columns and Tadpole Tank observations, the sandstone point counting samples contained similar

mineral compositions that would be likely found based on the identified rocks in the clast count compositional analysis. All three samples, SR-1, SR-2 and SR-3 showcased a set of minerals that were commonly found throughout the basin, including the two different quartz' monocrystalline and polycrystalline, as well as plagioclase and potassium feldspars. All four minerals are commonly found in rock fragments found within the Soledad Rojo formation such as granites and different gneisses. It is interpreted that the polycrystalline quartz and metamorphic minerals identified originated from conglomerates that have metamorphic and plutonic lithic sources such as those in the eastern stratigraphic column, southeast of Tadpole Tank, as well as the more plagioclase and volcanic minerals observed originated from volcanic conglomerates that are more commonly found in the western stratigraphic column, southwest of Tadpole Tank.

CHAPTER 7: Discussion

Sedimentology and Stratigraphy

A detailed sedimentological study of the Soledad Rojo formation led to the identification of multiple sources entering the basin. Compositionally, the subunits identify as locally sourced alluvial fan deposits from the Black Hills Mountains to the west consisting of welded tuffaceous rocks, and the Palo Verde Mountains to the east which consist of muscovite schist and biotite rich gneisses. Both the western and eastern stratigraphic columns are representative of each side's bounding mountain composition. The Soledad Rojo formation represents a series of time periods of deposition that experienced tectonic activity, as well as continuous fluvial events overtime. Shown best in Unit R and Unit BT of the Tadpole Tank region, sedimentary structures such as: channel scours, horizontal bedding, thin granule-pebble conglomeratic lenses, graded bedding and trough cross-bedding infer series of various strong fluvial environments that came into the basin and repeated over periods of time. The soft sediment deformation found within the Tadpole Tank region symbolizes the inability for the Unit R and Unit BT to become lithified before a new layer was deposited, coinciding that repeated deposition occurred regionally. On the eastern edge of the Soledad Rojo formation, east of Milpitas Wash Road, the late Oligocene - Miocene metaplutonic Palo Verde Mountains bounds the formation with a northeast striking, shallow northwest dipping normal fault. The faulted unconformity between the Oligocene Volcanic Black Hills Tuff and the Soledad Rojo formation on the western side of Milpitas Wash Road displays steep southeast dips interpreted to be the southeast sources entering the basin (Figure 4b).

Paleocurrent Implications for Provenance

Paleocurrent indicators for the measured sections of the Soledad Rojo formation demonstrated a change in average flow directions during different periods of deposition. Prior research, completed by Jorgensen (Jorgensen et al, 1982) averaged an imbrication in the western Palo Verde Mountains to be east-south easterly plus or minus roughly 30 degrees. Concurring with this research, his analysis of the Soledad Rojo formation demonstrates multiple source directions, with an average $132.0° \pm 13.9°$ east-south easterly paleoflow direction throughout the research site, indicating a northwest provenance direction. Compared to grain sizes observed along both stratigraphic columns, paleoflow directions coincide with the indication of larger clasts becoming finer in the direction of paleoflow, as well as being larger when inferring the direction of provenance based on the map created (Figure 24). Locations of previously mapped fault locations highlighted areas of larger clasts collectively, with alternating paleoflow directions. The western and eastern stratigraphic columns showed similar grain fining based on sediment sizes found decreasing heading into the Soledad Rojo formation (Figure 24). This observation infers that the transported sediments entering the basin have already begun to be eroded and rounded, coinciding with the average subrounded matrix and clasts grains, however, the Tadpole Tank region displayed larger grains throughout.

To the north-west, the Northern Chocolate Mountains, Chuckwalla Mountains, Black Hills Mountain welded tuff or areas within the Eastern California Shear Zone (Bennett et al., 2016, Langenheim et al., 2009) are thought to be sources of volcanic and pyroclastic rock fragments in the Soledad Rojo sandstone, which have a southeasterly paleoflow (Figure 1, Figure 29). For the other individual paleoflow directions recorded,

multiple provenance sources were explored to better understand the dynamics of the basin. To the north-east, the Mule Mountains, McCoy Mountains and Riverside Mountains showcase similar Mesozoic manganese ore deposits, augen gneiss rocks, red fanglomerate units and Triassic granitoids that are found in both the western and eastern stratigraphic columns and note a southwesterly paleoflow (Figure 1, Figure 29). Triassic granitoids also appear in the west within the Northern Chocolate Mountains and Chuckwalla Mountains due to their location in the upper plates of localized thrust faults (Barth et al., 1990) and could be interpreted as a possible source. Due to augen gneiss not being commonly found, observing it in large amounts throughout the Soledad Rojo formation implies a local provenance, such as the Mule Mountains, as a possible source for deposition of this lithic, however the source for the augen gneiss is still unknown. To the south-east, the Palo Verde Mountains stretches into the distance until hitting the most southern part of the Chocolate Mountains which includes outcrops of a Miocene non-marine gray cemented fanglomerate with angular muscovite schists, as well as subangular biotite and augen gneisses, interpreted as another possible source for the specific augen gneiss lithics displaying an overall northwest paleoflow direction (Figure 1, Figure 29). Prior to transtensional and transrotational deformation of the Eastern Transverse Ranges and Eastern California Shear Zone to the northwest, the Palo Verde Mountains location was further southeast. Further sources southeast, including the Gila Mountains and northwestern Sonoran Desert of Mexico, displays Tertiary boulder-cobble conglomerates, biotite granites, biotite rich granodiorites, Tertiary andesite lava flows, as well as augen gneisses, diabase rock from dikes intrusions and Tertiary red sandstones (Premo and Nourse, 2007; Figure 29), all of which can be identified in the Soledad Rojo formation.

The Palo Verde basin is recognized by Fauld's to have old gravel beds which include arkosic rocks and he suspects could have come from Precambrian rocks from the Basin and Range province locally (Fauld's, 1990). This provenance hypothesis is supported by directions of south-easterly source determined clast imbrications, where a Precambrian unit is noted in the southern Chocolate Mountains and Peter Kane Mountains. With the Palo Verdes Mountains previous placement more southeasterly before right lateral growth-strata extension took place, the Mule Mountains, Riverside Mountains and Big Maria Mountains in the northeast all contain a Precambrian unit that may have eroded and flowed down into the Palo Verde Mountains via an ancient fluvial processes. The interplay of far travelled arkosic gravels along with locally derived gravels indicate repeated and temporary interruptions of drainage in these developed washes. Conglomerates within the Soledad Rojo formation subunits were concluded to be derived from surrounding mountains in the Colorado desert region, such as the Black Hills Mountains and Palo Verde Mountains, due to the large grain sizes, subangular to subrounded textures, as well as the volcanic and metaplutonic clast compositions within the arkosic matrix, all which suggest a relatively short distance of travel after erosion occurred.

Clast Counts

Clast counts were compared for lithic interpretations at all three research sites within the Soledad Rojo formation. On average, subrounded rock fragment grains alongside a fine to medium sized sandy grain-supported matrix were characteristically observed on both sides of the Milpitas Wash Road. However, on the eastern stratigraphic

column (Figure 7) by the Palo Verde Mountains, subangular muscovite schists were more commonly observed when compared to the western stratigraphic column near the Black Hills Mountains which showcased more welded tuffs. The wide range in grain sizes of Unit L leads to the anticipation of an ancient alluvial debris flow with a local provenance source due to the medium cobbles that still reside on the surface (Figure 24). However, a further source is possible from the sub-rounded clasts and rounded fine matrix sands implying this tan conglomeratic sandstone Unit L of the Soledad Rojo formation may have traveled a distance before its final deposition into this basin. The red conglomeratic sandstones of Unit R also demonstrated an alluvial debris flow revealing a large variety of grain supported and matrix supported layers with ranging rock fragment sizes depending on the sub-unit lithofacies. Though the beds are presumed to be the same unit, deposited roughly around 25 million years ago during the Tertiary period, the red conglomeratic sandstone strata layers varied from a bountiful of subtle color differences, but averagely contained subangular volcanic and metaplutonic clasts on both stratigraphic columns and a subrounded matrix. The subangular shapes of the clasts infer that the source of the conglomerates has not traveled a long distance, however the matrix could have been transported from a further distance, later deposited in the Palo Verde basin and was reworked during an alluvial debris event that occurred at a later time. The western stratigraphic column displayed a wider distribution of grain sizes and finer matrix supported sections (Figure 7), whereas the eastern stratigraphic column has less variety and a denser amount of finer pebbles overall and contains a coarser matrix in most areas representative of two separate depositional environments within the Soledad Rojo formation basin.

Another hypothesis theorizes that the tectonics on the western side created fluvial fed valleys, changing the depositional environment and allowing for further reworking of the sediments on the western side of the Soledad Rojo formation basin. These processes further alter the lithofacies making Unit L on the western stratigraphic column slightly different than on the eastern stratigraphic column. Each research side contained conglomerates that ranged in sizes from 4mm to 128mm, but the western stratigraphic column displayed a wider even distribution of grain sizes (Figure 17), whereas the eastern stratigraphic column has less variety and a larger amount of coarse pebbles on average and contains a coarser matrix collectively. Thorough clast counts analysis showcased that measured imbricated clasts on the eastern stratigraphic column have been unaltered compared to the western stratigraphic column and exhibit a different depositional setting, presumed to be due to the theorized tectonic framework of the western side of Milpitas Wash Road. Due to the size of the varying conglomerate layers throughout each unit, the presumption is that tectonic activity in the basin has occurred alongside multiple flash flooding events tracing back to the Tertiary period which has led to the deposition, diagenesis and compaction of distinct smaller and larger scale red conglomeratic sandstone Unit R subunits and the tan conglomeratic sandstone Unit L depositional layers' overtime.

Clast Count Compositions

The compositions of visible lithics from the three separate research sites provided insight into the type of rocks found locally within the basin. Clast count ten had the largest amount of augen gneisses compositionally overall for the western stratigraphic column (Figure 7). Both units, Unit L and Unit R, contained high amounts of unidentified volcanics and tuffaceous rock, indicative of the bounding Black Hills Mountains of the western stratigraphic column (Figures 25-27). Due to the Tadpole Tank region being directly north of the stratigraphic columns along the Milpitas wash and in the direct path of a southerly paleoflow of grains, Unit L and Unit R in the western stratigraphic column has a larger variety of compositions compared to the eastern stratigraphic column (Figures 25-27). Clast count eleven CC11 and clast count twelve CC12 on the eastern stratigraphic column (Figure 7) have the highest amounts of pink ignimbrite due to the close proximity to locations of local ignimbrite flare ups. While heading east on the eastern stratigraphic column, the presence of ignimbrites becomes inexistent, further inferring the source was near the beginning of the column. Augen gneiss composition amounts stabilize at roughly between 5-10% continuing east on the eastern stratigraphic column (Figures 25-27). Upon arrival near where clast count nineteen CC19 was taken closer to the mountain front, large amounts of augen gneisses are displayed. This is indicative of closer proximity to the Palo Verde Mountains.

Hand Sample Compositions

The compositional data from the Soledad Rojo formation sandstones and conglomerates provided further insight into the evolution of the Basin and Range

Province. Each hand sample in the Tadpole Tank region, as well as on the western and eastern stratigraphic columns were characteristically different, creating a visual map on transport and depositional processes occurring in the basin (Figure 20). Frequent conglomerate clasts found throughout the Soledad Rojo formation consisted predominantly of rounded to subrounded tuffaceous rocks and other volcanic material in a variety of colors possibly derived from the Black Hills Tuff in the western stratigraphic column, as well as predominantly muscovite schist, and biotite gneisses from the Palo Verde Mountains in the eastern stratigraphic column.

Sandstone Point Counts

The individual study of the Soledad Rojo formation using point counting data helped for a better understanding of the multiple factors that could have led to deposition. Described by Suttner, compositions of detrital sediments are controlled by four different factors that are working collectively together including provenance, transportation, depositional and diagenesis (Suttner, 1974). By using the Gazzi-Dickinson Point counting method, this allowed for an analysis on the source rock based on the modal composition of sand in the Soledad Rojo conglomeratic sandstone units. Regions that have a higher rate of tectonism, the sediment composition can be more easily defined from the source rock. However, in regions of relatively average rates of tectonism, such as in the Soledad Rojo formation, the sediments display the different paleoclimates and ancient depositional environments of the region more easily, due to the source rocks being in constant supply.

A transition from a dissected magmatic arc basin to a recycled orogen provenance, identified on the QFL provenance ternary diagram (Figure 28), is interpreted that the basin once experienced uplift, subduction and possibly plate collision, which may have initiated a new process of generating various sediment sources into the basin, further inferring a predicted trend for the conglomerate sandstone composition. Comparing the provenance results, SR-1 represented a recycled orogen provenance typical of plate collision, inferring the possibility of rapid deposition of this unit is valid. The same is observed alongside SR-2 which is compositionally mostly quartz and indicative of basement uplift of the continental block. Tectonically, the observed lithology percentages are characteristic with different depositional environments typically found in active margins, containing either fluvial or alluvial rock fragments (Dickinson and Suczek, 1979). The change from dissected magmatic arc and recycled origin indicates a source change from plutonic to metamorphic clasts, as presented in the ternary diagrams.

Alongside sandstone modal plots and clast compositions from point counting and visual interpretations, all provided confirmation that the Black Hills and Palo Verde Mountains served as a possible source of the Soledad Rojo clastic basin debris, however based on contradicting paleoflow directions, sources for the sediment are interpreted to have entered the basin from all directions. Another hypothesis for the Soledad Rojo formation questions the possibility for the red conglomeratic sandstone Unit R to be from a further source that transported the Tertiary red fanglomerate, possibly from the Riverside Mountains - northeast of the Soledad Rojo formation, via fluvial events and was fed into the basin, further creating Unit R, the first layer of deposition in this sequence. Clast imbrications corrected for tectonic tilt from the red conglomeratic

sandstone on both stratigraphic columns infers an average paleoflow direction to be $130.8° \pm 11.4°$ southeasterly, coinciding with this hypothesis as a possible north east or north west provenance source.

History of Basin

Characteristics of the three subunit beds of the Soledad Rojo formation showcase mostly Tertiary volcanic rocks that are found to have originated from the Palo Verde Mountains to the east and the Oligocene tuffs from the Black Hills to the west. After further analysis, however, various other surrounding mountains, such as those further south east near the Mexico border region (Figure 29), have shown to be possible sources for the rock fragments that have also entered this basin.

Historically, prior to the formation of the Soledad Rojo formation, the Precambrian (Neoproterozoic) igneous and metamorphic Chuckwalla Complex was found regionally and is the base rock to the adjacent mountains such as the Little Chuckwalla Mountains, Mule Mountains, Palo Verde Mountains, Chocolate Mountains, Riverside Mountains and Big Maria Mountains (Bennett et al., 2016). The Chuckwalla Complex is composed of schists, augen gneisses and crystallized basement rock. A granitic rock sequence from the Mule Mountains and McCoy Mountains to the northeast containing granodiorite and manganese barite ore deposits in brecciated zones were formed during the Mesozoic and are similar to those found throughout the Palo Verde basin, likely formed during the same period (Barth, 1990). In the late Mesozoic, during the Cretaceous period roughly 88-112 Ma, a brick red fanglomerate was deposited northeast in the Riverside Mountains mineralized with manganese ores, multicolored

volcanic rocks and siltstones that filled fault fissures throughout (Bennett et al., 2016).

Before solidification could take place, a fluvial event is inferred to have transported

debris from the red fanglomerate unit and deposited it during the Tertiary into this Palo

Verde basin (Unit R). Tertiary basaltic, andesitic and rhyolitic flows from the Chocolate

Mountains to the southwest/northwest followed next, indicating a southeasterly

paleoflow, adding intrusive alkalic compositions such as calcite into fault fissures of the

red fanglomerate (Barth, 1990). This continued with pyroclastic flows into the Tertiary-

Oligocene period. A direct result of the Oligocene pyroclastic flows, roughly 17-27 Ma,

is the Black Hills Mountain (Black Hills Tuff) consisting of welded tufts, tuffaceous

breccia, as well as interbedded flows throughout fault fissures that exploded over the still

solidifying red sandstone unit. The intermixing of the far travelled red-arkosic gravels

along with locally derived Black Hills gravels indicate repeated and temporary

interruptions of drainage in the well-developed washes throughout the Tertiary, with

continued basaltic, andesitic and rhyolitic flows entering the basin from the surrounding

Black Hills, Palo Verde, Palen and Chocolate Mountains. Sediments within this bed

formation continued to be well indurated overtime and evidence of wet winters caused

further debris flows with pulsating sediment erosion. During the Miocene, a nonmarine

fanglomerate was deposited consisting of a cemented gray gravel, alongside brown to

reddish Tertiary rocks and was overlaid atop the welded tuffaceous rock material and red

fanglomerate from the Riverside Mountains (Unit BT). This unit, however, is recognized

to possibly be of older origin, based on the detrital zircon U-Pb analysis showcasing

Precambrian-Neoproterozoic clasts compositions, as observed by Murray et al. (2019).

Though the timing and deposition of the three subunits in the Soledad Rojo

formation is difficult to constrain, recent ^{40}Ar/^{39}Ar and U-Pb geochronological dating in

the basin indicated rock fragments within the lower red-bed unit of Unit R were deposited

during the late Oligocene to early Miocene (ca. 23.5 to 25 Ma), as well as sediment from

the middle units of Unit BT and Unit R age peaks reveal deposition to be during the

Cretaceous (ca. 88-112 Ma) (Murray et al., 2019 and Al-kaabi 2021). This time constraint

concurs with the hypothesis that a major fluvial event transported debris, possibly from

the red fanglomerate unit located to the north east by the Riverside mountains, and

deposited sediments into this Palo Verde basin at a later time. During the Oligocene,

pyroclastic flows, roughly 17-27 Ma, created the Black Hills Tuff and deposited rock

fragments into the non-solidified red fanglomerate unit that just recently entered the

basin. Sediments within this bed formation have continued to be well imbricated

overtime and show evidence of wet winters causing further debris flows into the basin.
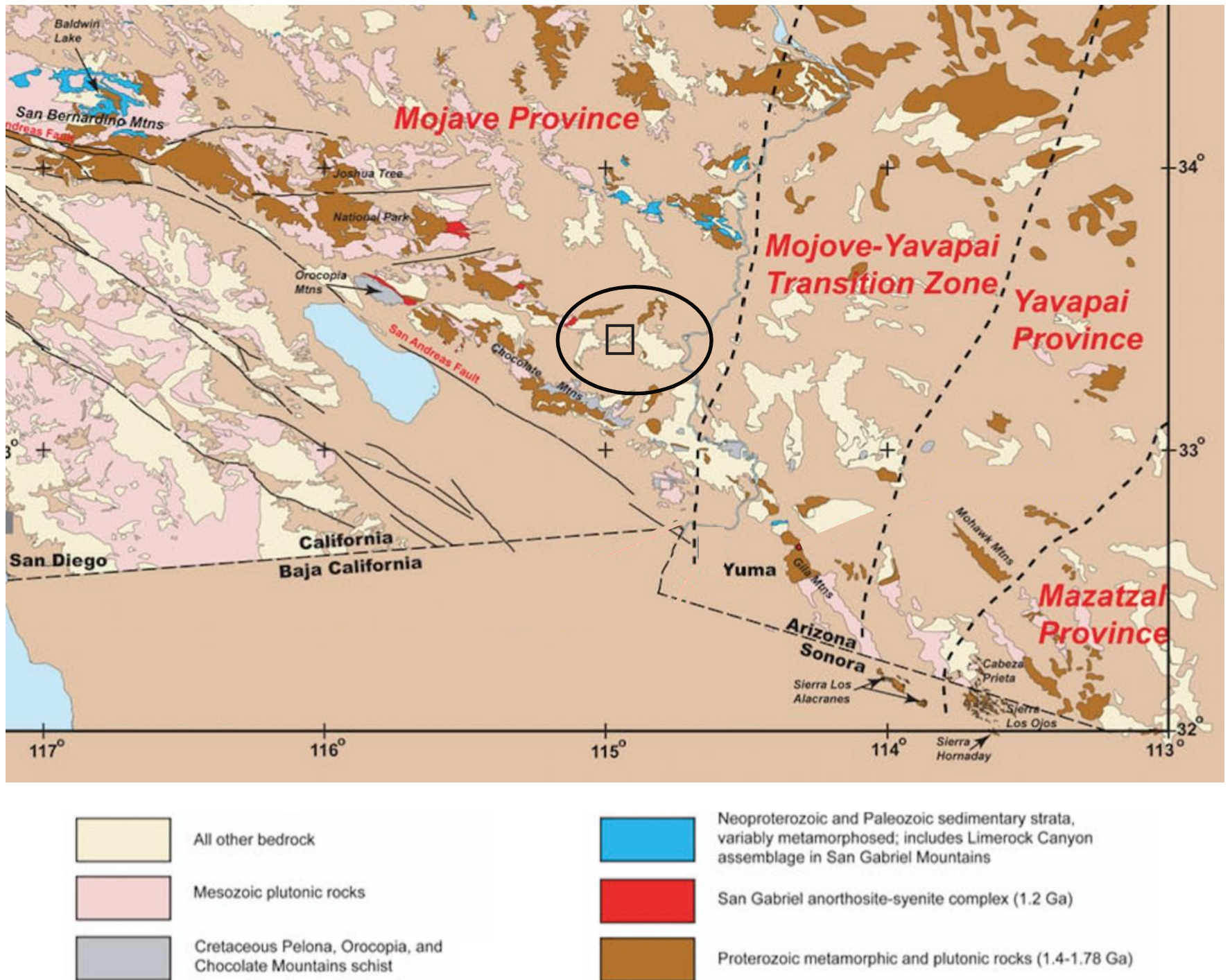
Sediment Provenance

Figure 29. Geologic map previously created of southwestern United Stated and northwestern Mexico. Local bounding mountains and general research area shown in black circle. Location of Soledad Rojo formation shown in black square. Map is used to show possible sediment sources for the Soledad Rojo formation from the southeast direction interpreted from the stereonets throughout the basin (Figures 20 - 23, Tables 3-7). (afterPremo and Nourse, 2007.). Sediment sources inside the research are shown in the black circle include bedrockin tan, Mesozoic plutonic rocks shown in pink, Cretaceous Pelona, Orocopia and Chocolate Mountains schist shown in gray, the San Gabriel anorthosite-syenite complex dated 1.2 Ga in red, and Proterozoic metamorphic and plutonic rocks dating 1.4-1.78 Ga in brown. The San Andreas northwest right lateral fault shown in black lines, highlighted in red. Easterly left lateral faults near Joshua Tree National Park shown in black lines.

CHAPTER 8: Conclusions

This new stratigraphic, paleocurrent, and compositional data from the Soledad Rojo formation further subdivided the previously described three distinct units of variable lithofacies and clast compositions into a series of multiple subunits and lithologically different strata layers. The Soledad Rojo formation is characterized by different depositional environments, including the presumed alternating alluvial debris flow, as well as the fluvial flow deposition in the northern Tadpole Tank. Representative of repetitive events of deposition and erosion, the Soledad Rojo formation collectively displays changes in sediment provenance and different depositional environments during the history of the basin. A sequence is repeated in the facies, alternating between brick red (BRSS), dark red (DRSS) to tan conglomeratic sandstones (Figure 5 and Figure 7), interrupted by north-south trending faults while going upsection on the western stratigraphic column, as well as periodic changes in deposition throughout the Soledad Rojo formation on both sides of Milpitas Wash Road.

Paleocurrent and stereonet analysis using clast imbrication measurements from this analysis infer an average imbrication for the source of sediment supply into the basin to be $121.2° \pm 20.3$ southeasterly, however an array of individual paleoflow directions were determined in specific regions throughout all three research sites, implying northwest, northeast and southeast paleoflow as well. Compositionally from clast counts and sandstone point counting, the subunits coincide with the paleocurrent clast imbrication data identifying as locally sourced deposits from the Black Hills Mountains to the west consisting of welded tuffaceous rocks and monocrystalline quartz, as well as the Palo Verde Mountains to the east which consist of observed metaplutonic lithics,

likely from the muscovite schist and biotite rich gneisses found locally within the Soledad Rojo formation.

All three research sites that were observed are interpreted to have relatively average rates of tectonism based on the recognized constant supply of sediment grains throughout the basin. Having a regular supply of sediments is interpreted to be indicative of different paleoclimates at work, further impacting the distribution of sediments throughout. This observation was identified throughout the stratigraphic columns, alternating between alluvial debris flows to fluvial debris flows, however more so within the Tadpole Tank region. The underlying welded tuff on the western stratigraphic column was not exposed; however, displays a southwest dipping faulted unconformity on the western side of Milpitas Wash Road, confirming a southeast source. On the eastern stratigraphic column, the base of the ignimbrite is not exposed, however it is hypothesized to be the same welded tuff from the western stratigraphic column and continues east to underlie the eastern stratigraphic column. It is proposed that an overlying Quaternary brecciated unconformity may exist within the Soledad Rojo formation and requires further investigation to conclude.

REFERENCES

Al-kaabi, A., and Murray, B.P., 2018, New Geochronology and Stratigraphic Interpretations of the Mid-Tertiary Soledad Rojo formation in the Lower Colorado River Extensional Corridor, Western Palo Verde Mountains, SE California, Department of Geological Sciences, California State Polytechnic University.

Allmendinger, R., Cardozo, N., & Fisher, D., 2012, Structural Geology Algorithms: Vectors and Tensors in Structural Geology: New York, Cambridge University Press, p. 304.

Armstrong, R. L. and Ward, P., 1991, Evolving geographic patterns of Cenozoic magmatism in the North American Cordillera: The temporal and spatial association of magmatism and metamorphic core complexes: Journal of Geophysical Research, v. 96, p. 13,201-13,224.

Barth, A. P., Tosdale, R., Wooden, J. L., 1990, A petrologic comparison of Triassic plutonism in the San Gabriel and Mule Mountains, southern California, Journal of Geophysical Research Atmospheres. P. 20,075 - 20,096.

Bennett, S. K., Darin, M. H., Dorsey, R. J., Skinner, L. A., Umhoefer, P.J., and Oskin, Me. E., 2016, Animated Tectonic Reconstruction of the Lower Colorado River Region: Implications for Late Miocene to Present Deformation. P. 73-86.

Bluck, B.J., 1994, Sedimentation of an alluvial fan in southern Nevada. Journal Sediment and Petroleum 34, p. 395 - 400.

Brown, R. D., 1991, Quaternary Deformation, The San Andreas Fault System, CA, U.S. Geological Survey Professional Paper 1515, p. 83–113.

Cardozo, N. and Allmendinger, R.W., 201, Spherical projections with OSX Stereonet. Computers & Geosciences, v.51, pp.193–205.

Dickinson, W. R., 2002, The Basin and Range province as a composite extensional domain: International Geology Review, v. 44, no. 1, p. 1–38.

Dickinson, W. R. and Suczek, C.A., 1979, Plate tectonics and sandstone compositions: American Association of Petroleum Geologists Bulletin, v. 63, p. 2164-2182.

Dickinson, W. R., 1988, Provenance and Sediment Dispersal in Relation to Paleotectonics and Paleogeography of Sedimentary Basins. In New Perspectives in Basin Analysis, p. 3-25.

Ducea, M. N., 2015, The Architecture, Chemistry and Evolution of Continental Magmatic Arcs, Continental Arc: A Synthesis, p. 1-33.

Elliot, W. J., and Marshall, M., 2011, In search of Colorado River "B" gravel, northeastern Imperial County, California, with notes on Early Tertiary red beds in Wirths, T.A., ed., Picacho and the Cargo Muchachos: gold, guns, and geology of eastern Imperial County, California, 2nd edition: San Diego Association of Geologists, p. 183-193.

[1 SEP]

Faulds, J. E., Geissman, J. W., and Mawer, C. K., 1990, Structural development of a major extensional accommodation zone in the Basin and Range Province, northwestern Arizona and southern Nevada; Implications for kinematic models of continental extension: Geological Society of America Memoir 176, p. 37-76.

Faulds, J. E., Miller, M. F., Smith, E. I., 2001, Cenozoic evolution of the Northern Colorado River Extensional Corridor, southern Nevada and northwestern Arizona. Utah Geological Association Publication 30 - Pacific Section American Association of Petroleum Geologists Publication GB78. p. 239 - 271.

Folk, R. L., 1980, Petrology of Sedimentary Rocks., Hemphill Publishing Company, Austin, p. 184.

Hadley, J. B., 1942, Manganese Deposits in the (Eastern) Paymaster Mining District – Imperial County, California; United States Geological Survey Bulletin 931-S, p.459-473.

House, K. P., Peartree, Phillip, A., Perkins, M. E., 2008, Stratigraphic Evidence for the Role of Lake Spillover in the Inception of the Lower Colorado River in Southern Nevada and Western Arizona. Special Paper 439: Late Cenozoic Drainage History of the Southwestern Great Basin and Lower Colorado River Region: Geologic and Biotic Perspectives, 2008, pp. 335–353.

Howard, 1994, A guide to Miocene Extension and Magmatism in the Lower Colorado River Region, Nevada, Arizona and California. United States Geological Survey Series number 94-246, p. 1-56.

Humphreys, E.D., 1995, Post-Laramide removal of the Farallon slab, western United States: Geology, v. 23, Geosphere, December 200, p. 987–990.

Irwin, W. P., 1991, Geology and Plate-Tectonic Development, The San Andreas Fault System, CA, U.S. Geological Survey Professional Paper 1515, p. 61-80.

Jennings, C. W., 1967, Geologic Map of California: Salton Sea Sheet. US Geological Society, California Division of Mines and Geology, 1967.

Jorgensen, M. R., Natenstedt, C, J, and Trunbly, P.N., 1982, Possible Relationship between Miocene Crustal Extension/Detachment Faulting and the Deposition of the Tolbard Fanglomerate in the Midway and Western Palo Verde Mountains, Imperial County California. Department of Geological Sciences, San Diego State University.

Langenheim, V.E., and Powell, R.E., 2009, Basin geometry and cumulative offsets in the Eastern Transverse Ranges, southern California: Implications for transrotational deformation along the San Andreas fault system. Geosphere. 5. P. 1-22.

MacKenzie, W. S. & Adams, A. E., & Brodie, K. H., 2017, Rocks and Minerals in Thin Section, Second Edition: A Colour Atlas.

McQuarrie, N., Wernicke, B. P., 2005, An animated tectonic reconstruction of southwestern North America since 36 Ma, Division of Geological and Planetary Sciences, MS 100-23, California Institute of Technology, Pasadena, California 91125, USA.

Morris, R. S., 1993, Tertiary Basin Structure Revealed in Seismic Reflection Profiles from Milpitas Wash, Southeastern California, U.S. Geological Survey Bulletin 2053, p. 217-221.

Murray, B. P. and Al-kaabi, A., 2018, Preliminary stratigraphic interpretations of the Soledad Rojo formation in the lower Colorado River Extensional Corridor, western Palo Verde Mountains, southeastern California, Department of Geological Sciences, California State Polytechnic University.

Murray, B. P., House, B. J., Al-Kaabi, A. and HAMES, W. E., (1) New Geochronology and stratigraphic interpretations of the mid-Tertiary Soledad Rojo Formation in the Lower Colorado Extensional Corridor, Western Palo Verde Mountains, SE California, Department of Geological Sciences, California State Polytechnic University, Pomona, 3801 W Temple Ave, Pomona, CA 91768, (2) Department of Geosciences, Auburn University, South College Street, Auburn, AL 36849.

Nourse, J. A., Premo, W. R., Iriondo, Alexander, Stahl Erin R., 2005, Contrasting Proterzoic basement complexes near the truncated margin of Laurentia, northwestern Sonora-Arizona international border region., Geological Society of America Special Paper 393, p. 123 - 182.

Pettijohn, F.J., 1975. Sedimentary Rocks. Harper and Row, 3rd edn.

Pettijohn, F. J., et al., 1987, "Sand and Sandstone." doi:10.1007/978-1-4612-1066-5.

Premo, W. R., Nourse, J. A., Pedro Castineiras, and Kellogg, K. S., 2007, New Shrimp-RG U-Pb Zircon Ages and Sm-Nd Analyses of Proterozoic Metamorphic Rocks of the San Gabriel Mountains: Keys for Laurentian Crustal Reconstruction? USGS Southern California Aerial Mapping Project (SCAMP) Conference Poster.

Sherrod, D. R., and Tosdal, R. M., 1991, Geologic setting and Tertiary structural evolution of southwestern Arizona and southeastern California: Journal of Geophysical Research, v. 96, no. B7, p. 12407-12423.

Suttner, L. J., 1974, Sedimentary petrographic provinces: an evaluation: Soc. Econ. Paleontologist Mineralogist Special Publ. 21, p. 75-84.

Wadell, H., 1933, Sphericity and Roundness of Rock Particles. The Journal of Geology, 41(3), p. 310-331.

Wallace, R. E., ed., 1990, The San Andreas fault system, California: U.S. Geological Survey, Professional Paper 1515, p. 283.

Wentworth, C. K., 1992, A Scale of Grade and Class Terms for Clastic Sediments. The Journal of Geology 30. p. 377-392.